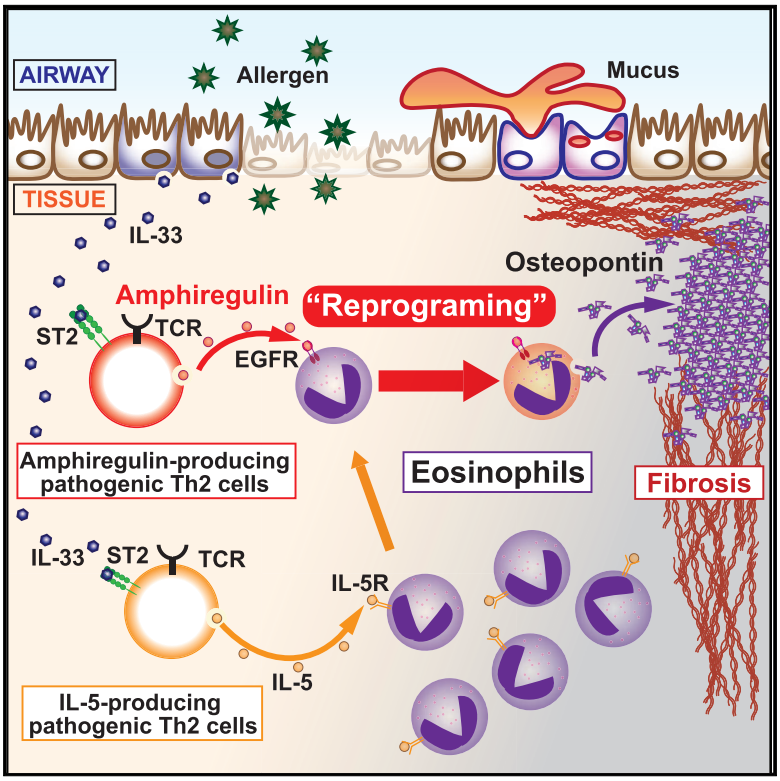
Article

Immunity

Amphiregulin-Producing Pathogenic Memory T Helper 2 Cells Instruct Eosinophils to Secrete Osteopontin and Facilitate Airway Fibrosis

Graphical Abstract



Highlights

- Pathogenic memory Th2 cells induce amphiregulin (Areg) via IL-33
- Areg reprograms the transcriptome of eosinophils toward an inflammatory state
- Areg-reprogramed eosinophils produce osteopontin to trigger airway fibrosis
- Areg^{+} Th2 cells and osteopontin^{+} eosinophils co-localize in fibrotic ECRS polyps

Authors

Yuki Morimoto, Kiyoshi Hirahara, Masahiro Kiuchi, ..., Daiju Sakurai, Yoshitaka Okamoto, Toshinori Nakayama

Correspondence

tnakayama@faculty.chiba-u.jp

In Brief

Asthma is a chronic allergic inflammatory disease with airway remodeling including fibrotic changes. Morimoto and colleagues find that the IL-33-ST2-amphiregulin-EGRF-osteopontin axis directs fibrotic responses in chronic allergic inflammation with the involvement of airway epithelial cells, pathogenic memory Th2 cells, and inflammatory eosinophils in both mouse and human.

Morimoto et al., 2018, Immunity *49*, 1–17
July 17, 2018 © 2018 Elsevier Inc.
https://doi.org/10.1016/j.immuni.2018.04.023

CellPress

Please cite this article in press as: Morimoto et al., Amphiregulin-Producing Pathogenic Memory T Helper 2 Cells Instruct Eosinophils to Secrete Osteopontin and Facilitate Airway Fibrosis, Immunity (2018), https://doi.org/10.1016/j.immuni.2018.04.023

CellPress

Amphiregulin-Producing Pathogenic Memory T Helper 2 Cells Instruct Eosinophils to Secrete Osteopontin and Facilitate Airway Fibrosis

Yuki Morimoto,[1,2,6] Kiyoshi Hirahara,[1,3,6] Masahiro Kiuchi,[1] Tomoko Wada,[1] Tomomi Ichikawa,[1] Toshio Kanno,[1] Mikiko Okano,[1] Kota Kokubo,[1] Atsushi Onodera,[1,4] Daiju Sakurai,[2] Yoshitaka Okamoto,[2] and Toshinori Nakayama[1,5,7,*]
[1]Department of Immunology, Graduate School of Medicine, Chiba University, 1-8-1 Inohana, Chuo-ku, Chiba 260-8670, Japan
[2]Department of Otorhinolaryngology, Head and Neck Surgery, Graduate School of Medicine, Chiba University, 1-8-1 Inohana, Chuo-ku, Chiba 260-8670, Japan
[3]AMED-PRIME, AMED, 1-8-1 Inohana, Chuo-ku, Chiba 260-8670, Japan
[4]Institute for Global Prominent Research, Chiba University, 1-8-1 Inohana, Chuo-ku, Chiba 260-8670, Japan
[5]AMED-CREST, AMED, 1-8-1 Inohana, Chuo-ku, Chiba 260-8670, Japan
[6]These authors contributed equally
[7]Lead Contact
*Correspondence: tnakayama@faculty.chiba-u.jp
https://doi.org/10.1016/j.immuni.2018.04.023

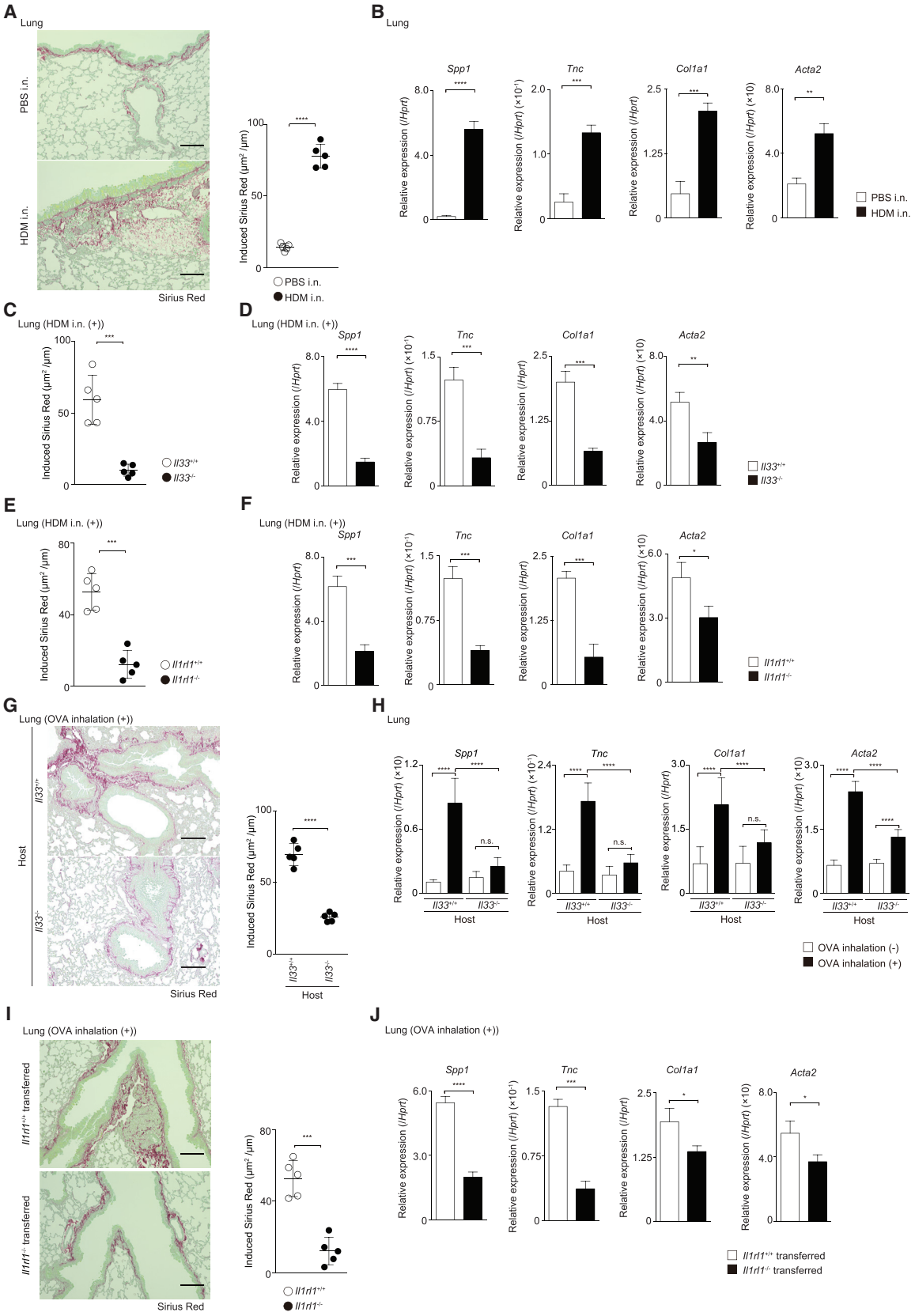
SUMMARY

Memory T cells provide long-lasting protective immunity, and distinct subpopulations of memory T cells drive chronic inflammatory diseases such as asthma. Asthma is a chronic allergic inflammatory disease with airway remodeling including fibrotic changes. The immunological mechanisms that induce airway fibrotic changes remain unknown. We found that interleukin-33 (IL-33) enhanced amphiregulin production by the IL-33 receptor, ST2^{hi} memory T helper 2 (Th2) cells. Amphiregulin-epidermal growth factor receptor (EGFR)-mediated signaling directly reprogramed eosinophils to an inflammatory state with enhanced production of osteopontin, a key profibrotic immunomodulatory protein. IL-5-producing memory Th2 cells and amphiregulin-producing memory Th2 cells appeared to cooperate to establish lung fibrosis. The analysis of polyps from patients with eosinophilic chronic rhinosinusitis revealed fibrosis with accumulation of amphiregulin-producing CRTH2^{hi}CD161^{hi}CD45RO^{+}CD4^{+} Th2 cells and osteopontin-producing eosinophils. Thus, the IL-33-amphiregulin-osteopontin axis directs fibrotic responses in eosinophilic airway inflammation and is a potential target for the treatment of fibrosis induced by chronic allergic disorders.

INTRODUCTION

Asthma is characterized by chronic airway inflammation, mucus hyperproduction, airway hyper-responsiveness (AHR), and variable airway obstruction (Busse and Lemanske, 2001; Kim et al., 2010). Airway remodeling, structural alterations of the airway wall such as subepithelial thickening, vascular changes, and fibrosis are central to the irreversible pathology of asthma (Al-Muhsen et al., 2011; Foster et al., 2017; Lambrecht and Hammad, 2012). Airway remodeling causes AHR, persistent airflow limitation, and a decrease in lung function. Corticosteroids are a key medicine used for the treatment of asthma. Clinical studies regarding the therapeutic effects of corticosteroids on airway remodeling have led to controversial results (Adcock et al., 2008; Durrani et al., 2011; Hansbro et al., 2017). About 5%–10% of asthmatics are refractory to corticosteroid treatment and often need to be hospitalized, and the degree of airway remodeling in asthmatics correlates with disease severity (Lambrecht and Hammad, 2015; Martinez and Vercelli, 2013).

Fibrosis consists of excessive deposition of collagenous and noncollagenous extracellular matrix (ECM) components in lung parenchyma as a consequence of proliferation and activation of fibroblasts, myofibroblasts, and immune cells (Wick et al., 2013). Fibrosis develops as a result of long-lasting inflammation such as occurs in asthma. Both innate and adaptive immunity are involved in the pathogenesis of fibrotic responses during allergic inflammation (Wick et al., 2013). T helper 2 (Th2) cells are a central population in the pathogenesis of allergic airway inflammation and fibrosis (Gieseck et al., 2018; Nakayama et al., 2017; Wick et al., 2013). Interleukin-5 (IL-5) is a key cytokine for the development, recruitment to inflammatory sites, and activation of eosinophils (Rosenberg et al., 2013). Local inflammation causes recruitment of eosinophils with inflammatory features (Mesnil et al., 2016). Eosinophil-induced inflammatory mediators such as reactive oxygen species (ROS), cytokines, and lipid mediators damage airway epithelial cells and nerves and induce asthmatic inflammation together with AHR (Rosenberg et al., 2013; Rothenberg and Hogan, 2006). Eosinophils are also involved in the pathogenesis of airway remodeling characterized by collagen fibril deposition (Humbles et al., 2004), but the molecular mechanisms through which eosinophils induce the fibrotic changes remain uncertain. Recently, pathogenic memory Th2 cells producing high amounts of IL-5 have been shown to direct eosinophilic inflammation (Nakayama et al., 2017). They show high expression of the ST2 receptor,



(legend on next page)

are selectively induced by IL-33 (the ligand of the ST2 receptor), and play critical role in the pathogenesis of chronic eosinophilic inflammation both in human and mouse systems (Endo et al., 2011, 2015; Nakayama et al., 2017). Similar pathogenic Th2 cells producing high amounts of IL-5 have been reported in the skin of patients with atopic dermatitis (Islam et al., 2011) and in the peripheral blood of patients with eosinophilic gastrointestinal disease and asthma (Mitson-Salazar et al., 2016; Seumois et al., 2016; Wambre et al., 2017). However, the pathogenic Th2 cell subpopulation shaping the pathology of fibrosis remains unclear.

Chronic rhinosinusitis (CRS) is a multifactorial disease associated with chronic inflammation and characteristic cytokine and airway remodeling patterns (Ball et al., 2016). Based on diagnostic histological changes, CRS with polyps is classified as either eosinophilic CRS (ECRS) or non-eosinophilic CRS (NECRS) (Hamilos, 2015). Patients with ECRS often present with asthma and their polyps exhibit eosinophilic infiltration, suggesting that aberrant type 2 immune responses are involved in the pathogenesis of ECRS (Hamilos, 2015). The pathogenesis of asthma and ECRS appear to be closely related (Kobayashi et al., 2015). Histological analysis of ECRS shows basement membrane thickening that is the result of a severe fibrotic response typified by accumulation of fibronectin and type I, III, and V collagens (Ball et al., 2016; Pawankar and Nonaka, 2007). A high proportion of patients with ECRS are refractory to current conventional pharmacologic therapy such as corticosteroid treatment and suffer frequent disease recurrence. The precise cellular and molecular mechanisms that cause the type of persistent sino-nasal type 2 inflammation that leads to fibrosis remain unclear.

Herein, we investigated the cellular and molecular mechanisms that control the pathogenesis of airway fibrosis during chronic allergic inflammation. We found that an epithelial cytokine IL-33 drives lung fibrotic responses during antigen-induced Th2 cell-dependent allergic airway inflammation. IL-33 induced amphiregulin production by $ST2^{hi}$ memory-type pathogenic Th2 cells. Amphiregulin reprogrammed the transcriptome of eosinophils toward an inflammatory state that included enhanced production of osteopontin. Amphiregulin-producing $ST2^{hi}$ memory Th2 cells and IL-5-producing $ST2^{hi}$ memory Th2 cells appeared to be distinct subpopulations, and cooperate to establish airway fibrosis during eosinophilic inflammation. Analysis of nasal polyps of ECRS patients revealed increased infiltration of amphiregulin-producing $CD161^{+}CRTH2^{+}$ memory-type $CD4^{+}$ T cells and osteopontin-producing eosinophils accompanied by dense fibrotic responses. Pharmacological blockade of epidermal growth factor receptor (EGFR) signaling resulted in attenuated expression of *Spp1*, which encodes osteopontin in mouse and human eosinophils. Thus, the IL-33-amphiregulin-osteopontin axis directs fibrotic responses in chronic allergic inflammation in both mouse and human systems, and these molecules may be potential therapeutic targets for intractable chronic eosinophilic inflammatory disorders.

RESULTS

Lung Fibrotic Responses Are Induced by Antigen-Induced Type 2 Inflammation via the IL-33-ST2 Axis

Repetitive exposure of house dust mite (HDM) to mice induced a significant increase in collagen deposition around the respiratory tract as detected by Sirius red staining accompanied by increased expression of *Il33*, *Il25*, and *Tslp* in inflamed lungs (Figures S1A, S1B, and 1A; Doherty et al., 2011). In addition, the expression of molecules relevant to fibrotic responses such as *Spp1* (which encodes osteopontin), *Tenascin C* (*Tnc*), *Collagen type 1 alpha 1* (*Col1a1*), and *Actin alpha 2 smooth muscle aorta* (*Acta2*) was significantly enhanced in the lungs of mice with HDM exposure (Figure 1B). Genetic deletion of *Il33* or *Il1rl1*, which encodes ST2 (a component of the IL-33 receptor), resulted in significantly reduced expression of fibrosis-related genes in the lungs together with decreased collagen deposition (Figures 1C–1F, S1C, and S1D). Mice that had received

Figure 1. IL-33 Signaling Induces Lung Fibrotic Changes

(A) Representative histology of lungs of mice with HDM or PBS exposure (Figure S1A), fixed and stained with Sirius red (left) from three experiments. Scale bars, 100 μm. Shown are ratios of areas of randomly selected regions stained with Sirius red surrounding bronchi versus the areas of associated basement membranes (right). More than three mice per group were analyzed.

(B, D, and F) Quantitative RT-PCR analysis of the indicated genes in the lungs of wild-type mice with or without HDM exposure (n = 3 mice per group) (B), the lungs of $Il33^{+/+}$ and $Il33^{-/-}$ mice with HDM exposure (n = 3 mice per group) (D), and the lungs of $Il1rl1^{+/+}$ and $Il1rl1^{-/-}$ mice with HDM exposure (n = 3 mice per group) (F). Three independent experiments were performed with similar results.

(C and E) Shown are ratios of areas of randomly selected regions stained with Sirius red surrounding bronchi versus the areas of associated basement membranes in the lungs of $Il33^{+/+}$ and $Il33^{-/-}$ mice with HDM exposure (C) or the lungs of $Il1rl1^{+/+}$ and $Il1rl1^{-/-}$ mice with HDM exposure (E). More than three mice per group were analyzed.

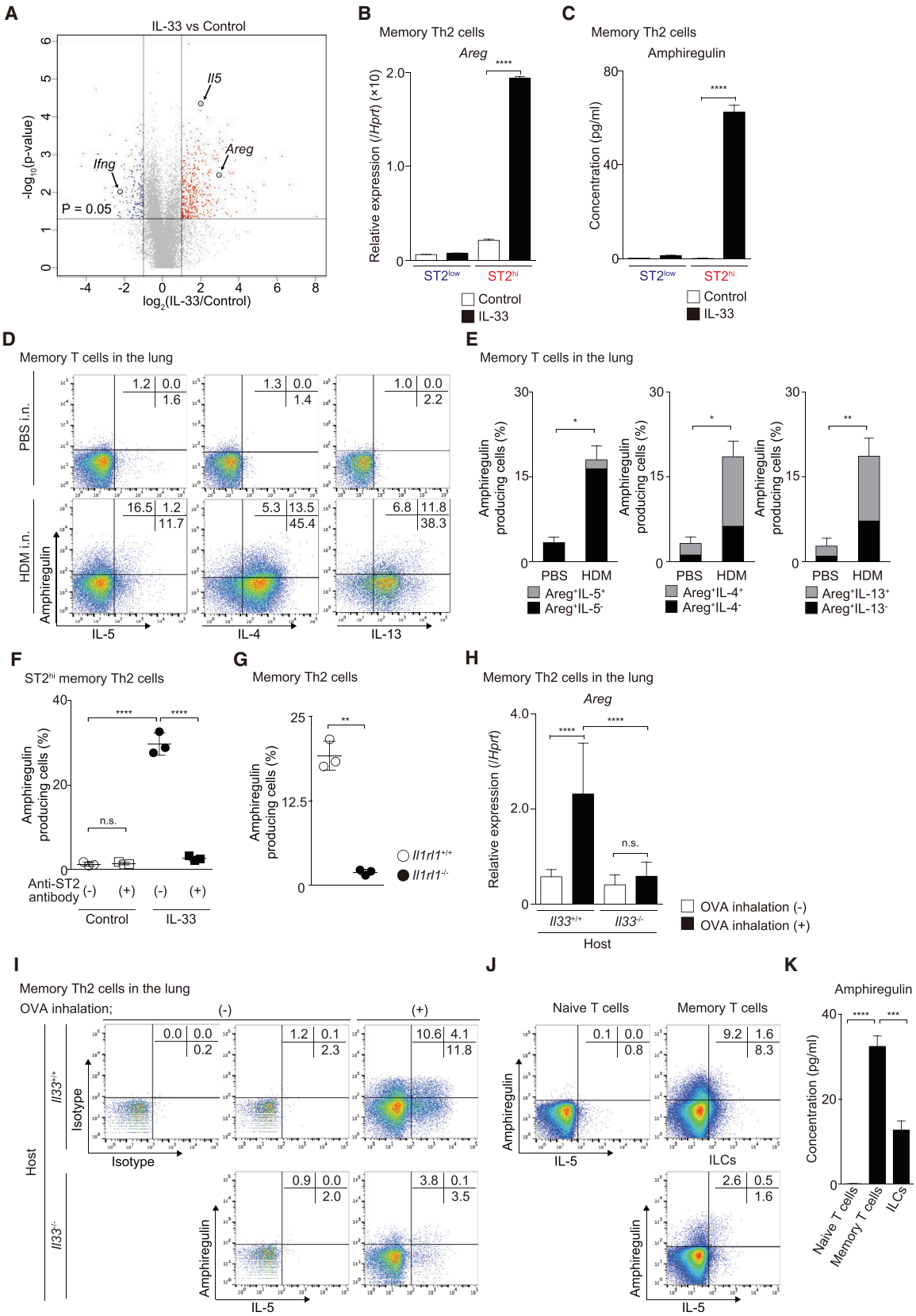
(G) OVA-specific memory Th2 cells (3×10^6 cells) were transferred i.v. into $Il33^{+/+}$ and $Il33^{-/-}$ mice that were subsequently challenged with OVA as indicated in Figure S1E. Shown is a representative confocal micrograph of lung tissue stained with Sirius red from an $Il33^{+/+}$ and an $Il33^{-/-}$ mouse (left) from four experiments. Scale bars represent 100 μm. Shown are ratios of areas of randomly selected regions stained with Sirius red surrounding bronchi versus the areas of associated basement membranes (right). More than three mice per group were analyzed.

(H) Quantitative RT-PCR analysis of gene expression in the lungs of $Il33^{+/+}$ (upper) and $Il33^{-/-}$ (lower) mice challenged with or without OVA inhalation (n = 6 mice per group).

(I) $Il1rl1^{+/+}$ and $Il1rl1^{-/-}$ OVA-specific memory Th2 cells (3×10^6 cells) were transferred i.v. into BALB/c mice that were subsequently challenged with OVA as indicated in Figure S1E. Shown is a representative confocal micrograph of lung tissue stained with Sirius red from an $Il1rl1^{+/+}$ and an $Il1rl1^{-/-}$ memory Th2 cell-transferred mouse (left) from three experiments. Scale bars represent 100 μm. Shown are ratios of areas of randomly selected regions stained with Sirius red surrounding bronchi versus the areas of associated basement membranes (right). More than three mice per group were analyzed.

(J) Quantitative RT-PCR analysis of the indicated genes in the lungs from $Il1rl1^{+/+}$ and $Il1rl1^{-/-}$ memory Th2 cell-transferred mice challenged with OVA inhalation (n = 3 mice per group).

Data are the mean ± SD. *p < 0.05, **p < 0.01, ***p < 0.001, ****p < 0.0001; n.s., not significant; by unpaired t test or one-way analysis of variance (ANOVA). Please see also Figure S1.



(legend on next page)

OVA-specific memory Th2 cells followed by multiple antigen challenges also exhibited a significant increase in fibrotic changes together with increased expression of *Il33* and *Il25* but not *Tslp* in the lungs (Figures S1E–S1H). *Il33*$^{-/-}$ mice that had received OVA-specific memory Th2 cells exhibited significantly decreased collagen deposition in the lungs (Figure 1G). The fibrosis-related genes *Spp1*, *Tnc*, *Col1a1*, and *Acta2* were less induced by OVA inhalation in the lungs of *Il33*$^{-/-}$ mice as compared to those of *Il33*$^{+/+}$ mice (Figure 1H). The ameliorated fibrotic changes in *Il33*$^{-/-}$ mice were reversed by intratracheal administration of IL-33 (Figures S1I–S1K). Mice that had received *Il1rl1*$^{-/-}$ memory Th2 cells also showed significant decrease in fibrotic changes (Figures 1I and 1J). We next immunized *Il1rl1*$^{+/+}$ or *Il1rl1*$^{-/-}$ mice with OVA and Alum twice followed by a series of OVA inhalations (Figure S1L). Collagen deposition together with the expression of fibrosis-related genes in the lungs were significantly decreased in *Il1rl1*$^{-/-}$ mice (Figures S1M and S1N). Thus, the IL-33-ST2 axis plays a critical role in the induction of lung fibrotic responses in our *in vivo* experimental settings.

IL-33 Induces Amphiregulin Production by ST2^{hi} Memory Th2 Cells Both *In Vitro* and *In Vivo*

To explore the molecules expressed in ST2^{hi} memory Th2 cells that are critical for the induction of lung fibrotic responses, we assessed changes in global gene expression in ST2^{hi} OVA-specific memory Th2 cells following 3 days of *in vitro* IL-33 stimulation (Figures S2A–S2C). 745 genes exhibited a >2-fold change between control and IL-33-stimulated ST2^{hi} memory Th2 cells (Figure 2A). One of the genes exhibiting elevated expression in IL-33-stimulated cells was *Areg*, encoding amphiregulin, a key molecule for tissue repair (Figures 2A and S2D; Stoll et al., 1997). Quantitative RT-PCR confirmed selective induction of *Areg* in IL-33-stimulated ST2^{hi} memory Th2 cells (Figures 2B and S2E). Consistent with this, IL-33 stimulation induced amphiregulin protein production by ST2^{hi} memory Th2 cells (Figure 2C). IL-33-stimulated ST2^{hi} memory Th2 cells also exhibited enhanced expression of *Il5* and *Il13* (Figure S2F) but not *Il4* or *Ifng*. IL-33-induced amphiregulin expression correlated with the chromatin status such as increased H3-K4 trimethylation and reduced H3-K27 trimethylation at the *Areg* locus (data not shown). Flow cytometric analysis revealed that the majority of amphiregulin-positive cells did not produce IL-5 (Figures S2G and S2H). In contrast, the majority of amphiregulin-producing cells also produced IL-4 and IL-13 (Figure S2H). To characterize the amphiregulin-producing memory Th2 cells and the IL-5-producing memory Th2 cells, we performed flow cytometric analyses with various antibodies. The expression of CD147, a member of the immunoglobulin superfamily, was significantly lower on amphiregulin-producing memory Th2 cells as compared to IL-5-producing memory Th2 cells (Figure S2I). Amphiregulin-producing memory CD4$^+$ T cells induced by HDM exposure *in vivo* did not overlap with IL-5-producing memory CD4$^+$ T cells (Figures 2D and 2E). IL-33 did not induce amphiregulin production in other types of cells such as naive CD4$^+$ T cells, effector Th2 cells, peripheral regulatory T cells, and activated CD8$^+$ T cells (data not shown).

IL-25 or thymic stromal lymphopoietin (TSLP) stimulation also induced amphiregulin-producing memory Th2 cells, although induction was not as efficient as with IL-33 stimulation (Figure S2J). Blockade of the IL-33-ST2 axis by treatment with anti-ST2 antibody or genetic deletion of *Il1rl1* diminished amphiregulin-producing memory Th2 cells *in vitro* (Figures 2F, 2G, and S2K). Memory Th2 cells under IL-33-sufficient conditions exhibited significantly increased production of amphiregulin after OVA inhalation *in vivo*, while memory Th2 cells in IL-33-deficient conditions failed to produce significant amounts of amphiregulin (Figures 2H, 2I, and S2L). The expression of *Il5* and *Il13* but not *Il4* or *Ifng* was induced in memory Th2 cells in wild-type but not *Il33*$^{-/-}$ mice (Figure S2M). Furthermore, memory CD4$^+$ T cells in the lungs of *Il1rl1*$^{-/-}$ mice treated with OVA and Alum twice followed by a series of OVA inhalations (Figure S1L) showed significant reduction of amphiregulin-producing memory CD4$^+$ T cells (Figure S2N). ILCs from inflamed lungs also

Figure 2. IL-33 Induces Amphiregulin Production from ST2^{hi} Memory Th2 Cells Both *In Vitro* and *In Vivo*

(A) OVA-specific ST2^{hi} memory Th2 cells were cultured with or without IL-33 for 72 hr. RNA-seq data were computed as FPKM (fragments per kilobase of transcript per million mapped reads). Arrows indicate *Areg*, *Il5*, and *Ifng* expression. Volcano plot depicts differential gene expression induced by IL-33 compared to control.

(B) Quantitative RT-PCR analysis of *Areg* in ST2^{lo} or ST2^{hi} memory Th2 cells. Four independent experiments were performed with similar results.

(C) Protein expression of amphiregulin from ST2^{lo} or ST2^{hi} memory Th2 cells. Three independent experiments were performed with similar results.

(D) Shown are intracellular-staining profiles of amphiregulin together with IL-5 (left), IL-4 (middle), and IL-13 (right) in memory CD4$^+$ T cells from the lungs of mice with HDM exposure.

(E) Shown are the percentages of amphiregulin-producing memory CD4$^+$ T cells in the lungs of mice with HDM exposure. Amphiregulin single producers (Areg$^+$IL-5$^-$, Areg$^+$IL-4$^-$, and Areg$^+$IL-13$^-$) are shown in black, and amphiregulin and indicated cytokines double producers (Areg$^+$IL-5$^+$, Areg$^+$IL-4$^+$, and Areg$^+$IL-13$^+$) are shown in gray.

(F) Shown are the percentages of amphiregulin-producing ST2^{hi} memory Th2 cells with (square) or without (circle) neutralizing anti-ST2 antibody followed by IL-33 stimulation (black) or control stimulation (white).

(G) Shown are the percentages of amphiregulin-producing memory Th2 cells derived from *Il1rl1*$^{+/+}$ and *Il1rl1*$^{-/-}$ mice with IL-33 stimulation.

(H) Quantitative RT-PCR analysis of *Areg* in the lung memory Th2 cells from *Il33*$^{+/+}$ and *Il33*$^{-/-}$ recipients challenged with or without OVA (n = 6 mice per group).

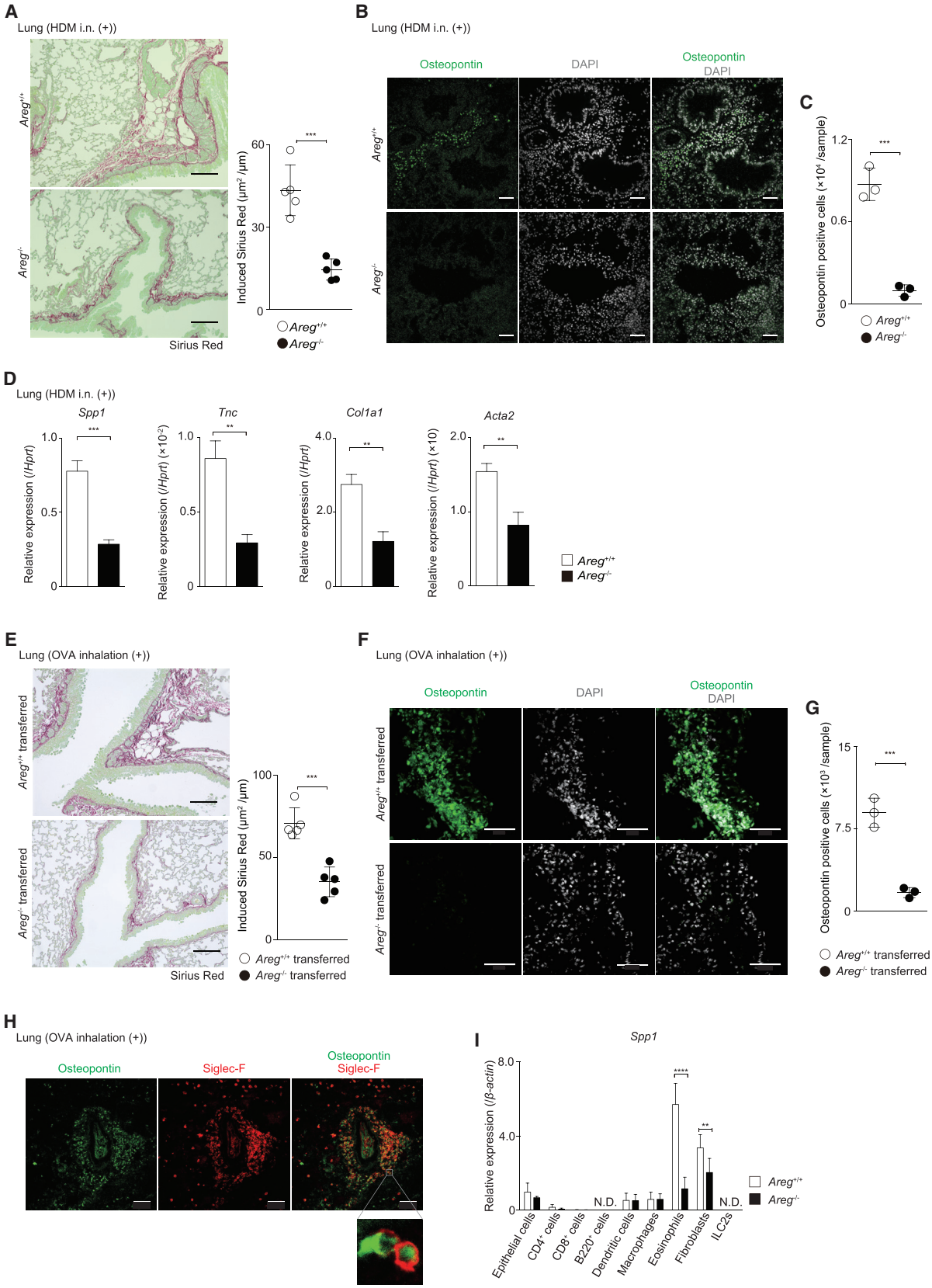
(I) Shown are intracellular-staining profiles of amphiregulin and IL-5 with isotype controls in the lung memory Th2 cells from *Il33*$^{+/+}$ and *Il33*$^{-/-}$ recipients. Six independent experiments were performed with similar results.

(J) Shown are intracellular-staining profiles of amphiregulin and IL-5 in memory CD4$^+$ T cells and ILCs from the lungs of mice with OVA and Alum twice followed by a series of OVA inhalations (Figure S1L).

(K) Protein expression of amphiregulin from naive CD4$^+$ T cells, memory CD4$^+$ T cells, and ILCs. Three independent experiments were performed with similar results.

Data are the mean ± SD. *$p < 0.05$, **$p < 0.01$, ***$p < 0.001$, ****$p < 0.0001$; n.s., not significant; by unpaired t test or one-way analysis of variance (ANOVA). Please see also Figure S2.

Please cite this article in press as: Morimoto et al., Amphiregulin-Producing Pathogenic Memory T Helper 2 Cells Instruct Eosinophils to Secrete Osteopontin and Facilitate Airway Fibrosis, Immunity (2018), https://doi.org/10.1016/j.immuni.2018.04.023



(legend on next page)

produced amphiregulin, but more than 70% reduction compared to that produced by memory $CD4^+$ T cells (Figures 2J, 2K, and S2O). These results indicate that both *in vitro* and *in vivo* IL-33 stimulation is essential for the induction of amphiregulin production by memory Th2 cells.

Amphiregulin Produced by Memory Th2 Cells Induces Lung Fibrotic Responses during Type 2 Inflammation *In Vivo*

Next, we wanted to identify the role of amphiregulin in lung fibrotic responses during allergic inflammation. Deletion of *Areg* resulted in the amelioration of HDM-induced fibrotic changes in the lung (Figures 3A–3D). Collagen deposition in the lung was also significantly decreased in $Areg^{-/-}$ mice treated with OVA and Alum twice followed by a series of OVA inhalations (Figures S3A and S3B). However, expression of *Il33*, *Il5*, and *Il13*, inflammatory cell infiltration in the lung parenchyma, were comparable between $Areg^{+/+}$ and $Areg^{-/-}$ mice (Figures S3C and S3D). $Areg^{+/+}$ and $Areg^{-/-}$ lung memory-type ($CD44^+CD62L^{lo}$) $CD4^+$ T cells also exhibited similar expression of *Il5* and *Il13* (Figure S3E). Molecules relevant to fibrosis exhibited decreased expression in the lungs of $Areg^{-/-}$ mice (Figure S3F). These results indicate that amphiregulin is critical for induction of the lung fibrotic response during allergic airway inflammation. In addition, amphiregulin appeared to be a major downstream target of IL-33 in the induction of lung fibrotic responses.

Next, to determine whether amphiregulin produced by memory Th2 cells was physiologically relevant to the induction of lung fibrotic responses *in vivo*, we transferred OVA-specific memory Th2 cells from $Areg^{+/+}$ mice or $Areg^{-/-}$ mice to wild-type mice and then performed antigen challenge (Figure S1E). Transferred $Areg^{+/+}$ and $Areg^{-/-}$ memory Th2 cells exhibited similar production of IL-5 and IL-13 (Figure S3G). However, lung collagen deposition was diminished in recipients of $Areg^{-/-}$ as compared to $Areg^{+/+}$ memory Th2 cells (Figure 3E). Recipients of $Areg^{-/-}$ as compared to $Areg^{+/+}$ memory Th2 cells also exhibited decreased lung osteopontin deposition accompanied by decreased expression of fibrosis-related genes (Figures 3F, 3G, S3H, and S3I). These results indicated that amphiregulin produced by memory Th2 cells was relevant to the induction of lung fibrotic responses. Thus, Th2 cells play a crucial role in lung fibrotic responses induced by the IL-33-amphiregulin axis during allergen-induced allergic airway inflammation.

Amphiregulin Stimulates Eosinophils to Produce Osteopontin via EGF Receptor Signaling

We next explored the major cellular source of osteopontin in our experimental settings. Histological analysis of inflamed lungs in mice that received OVA-specific memory Th2 cells followed by antigen challenge (Figure S1E) revealed that collagen was deposited adjacent to infiltrating eosinophils (Figure S3J). The majority of osteopontin-stained cells in the asthmatic lung were co-localized with Siglec-F^+ cells (Figure 3H). $B220^+$ cells, $CD4^+$ cells, MHC class II^+ cells, $CD11c^+$ cells, and $F4/80^+$ cells also found in asthmatic lungs were not co-localized with osteopontin-stained cells (Figures S3K and S3L). Amphiregulin belongs to the epidermal growth factor (EGF)-like protein family, which interacts with EGFR to transmit signals into target cells (Shoyab et al., 1989). Compared to airway epithelial cells, bone marrow-derived eosinophils exhibited moderate expression of *Egfr* (Figures S3M and S3N). Deletion of *Areg* resulted in reduced *Spp1* expression from eosinophils of inflamed lungs *in vivo* (Figure 3I). Thus, amphiregulin-stimulated eosinophils are the main cellular source of osteopontin in lungs undergoing allergic inflammatory fibrotic responses.

Amphiregulin Induced Transcriptional Reprogramming of Eosinophils via EGF Receptor Signaling

To determine the consequence of amphiregulin stimulation in eosinophils, we examined the global gene expression profile of eosinophils after stimulation with amphiregulin for 3 days. Amphiregulin stimulation had no obvious effect on expressions of CCR3 and Siglec-F nor on the survival of eosinophils (Figures S4A and S4B). Principle component analysis revealed that amphiregulin dramatically altered the eosinophil transcriptome (Figure S4C). Substantial numbers of genes were upregulated in eosinophils after amphiregulin stimulation (Figure S4D). Gene Ontology enrichment analysis of 10,899 genes indicated that amphiregulin stimulation upregulated genes related to cell activation, cell cycle processes, RNA metabolic processes,

Figure 3. Amphiregulin by Memory Th2 Cells Induces Fibrotic Changes Accompanied by Osteopontin-Positive Eosinophils

(A) Shown is a representative confocal micrograph of lung tissue stained with Sirius red from an $Areg^{+/+}$ and an $Areg^{-/-}$ mouse with HDM exposure (left) from three experiments. Scale bars represent 100 μm. Shown are ratios of areas of randomly selected regions stained with Sirius red surrounding bronchi versus the areas of associated basement membranes (right). More than three mice per group were analyzed.

(B and C) Shown is a representative confocal micrograph of lung tissue stained with anti-osteopontin (green) and DAPI (white) from an $Areg^{+/+}$ and an $Areg^{-/-}$ mouse from three experiments (scale bars represent 50 μm) (B). Shown is the absolute number of ostepontin-positive cells in randomly selected lung tissue slices (C). Three mice per group were analyzed.

(D) Quantitative RT-PCR analysis of the indicated genes in the lungs of $Areg^{+/+}$ and $Areg^{-/-}$ mice with HDM exposure (n = 3 mice per group).

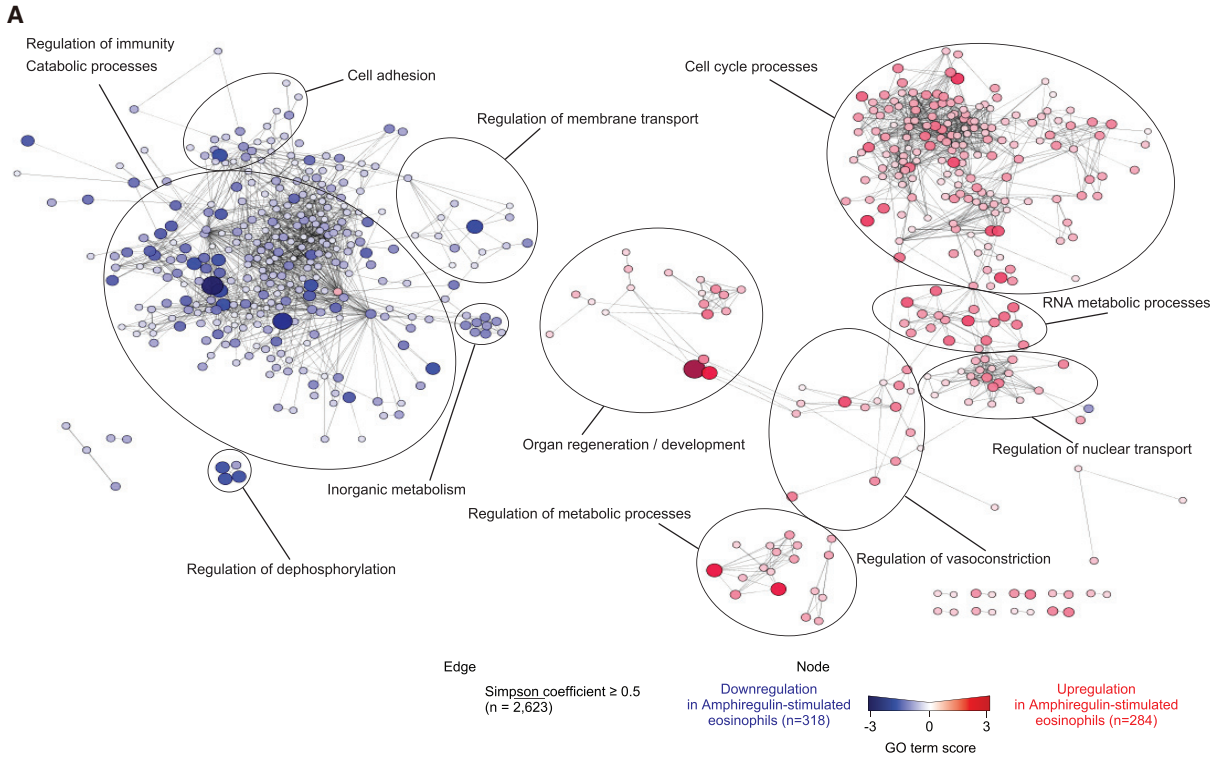
(E) $Areg^{+/+}$ and $Areg^{-/-}$ memory Th2 cells (3×10^6 cells) were transferred i.v. into wild-type mice and subsequently challenged with OVA. Shown is a representative confocal micrograph of lung tissue stained with Sirius red from recipients of $Areg^{+/+}$ and $Areg^{-/-}$ memory Th2 cells (left) from two experiments. Scale bars represent 100 μm. Shown are ratios of areas of randomly selected regions stained with Sirius red surrounding bronchi versus the areas of associated basement membranes (right). More than three mice per group were analyzed.

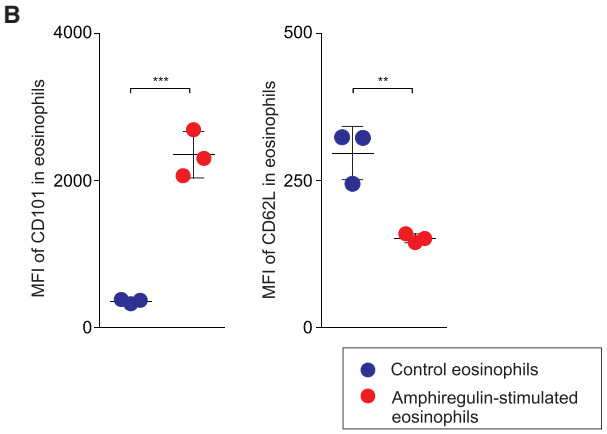
(F and G) Shown is a representative confocal micrograph of lung tissue stained with anti-osteopontin (green) and DAPI (white) from recipients of $Areg^{+/+}$ or $Areg^{-/-}$ memory Th2 cells from two experiments (scale bars represent 50 μm). Three independent experiments were performed with similar results (F). Shown are the absolute number of ostepontin-positive cells in randomly selected lung tissue slices (G). Three mice per group were analyzed.

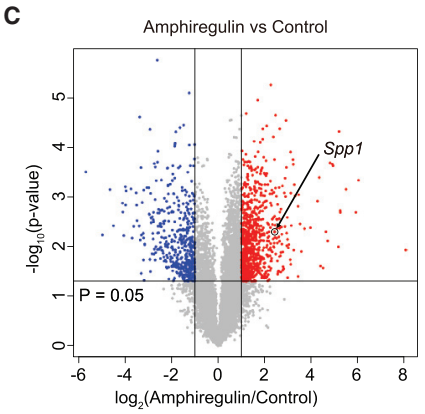
(H) Shown is a representative confocal micrograph of the lung stained with anti-osteopontin (green) and anti-Siglec-F (red) from a mouse challenged with OVA inhalation from four experiments. Scale bars represent 50 μm. Three independent experiments were performed with similar results.

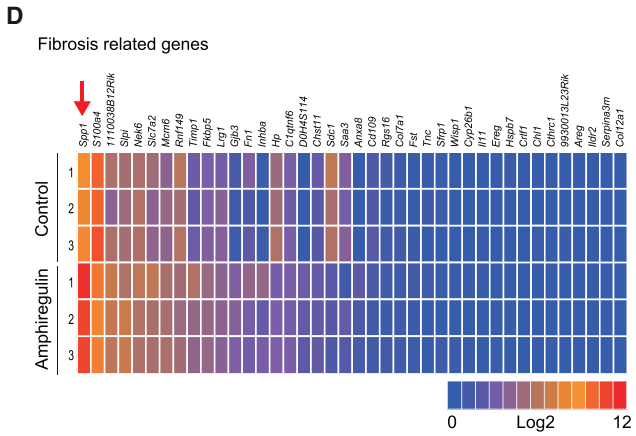
(I) Quantitative RT-PCR analysis of *Spp1* in the indicated cells from the lungs of $Areg^{+/+}$ and $Areg^{-/-}$ mice twice treated with OVA and Alum followed by a series of OVA inhalations (Figure S3A).

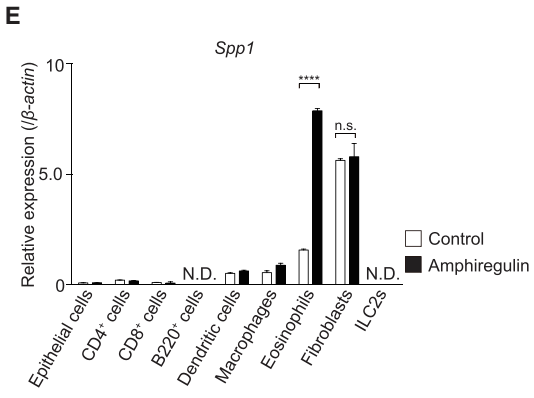
Data are the mean ± SD. $^{**}p < 0.01$, $^{***}p < 0.001$, $^{****}p < 0.0001$; by unpaired t test or one-way analysis of variance (ANOVA). Please see also Figure S3.











(legend on next page)

and regulation of nuclear transport (Figure 4A, Table S1). As compared to control un-stimulated eosinophils, amphiregulin-stimulated eosinophils significantly upregulated genes characteristic of inflammatory eosinophils (Figure S4E; Mesnil et al., 2016). Characteristic of inflammatory eosinophils, amphiregulin-stimulated eosinophils upregulated CD101 and downregulated CD62L (Figure 4B; Mesnil et al., 2016). These results indicate that amphiregulin reprogrammed eosinophil gene expression toward an inflammatory state.

Compared to control stimulation, amphiregulin stimulation led to 846 genes with >2-fold upregulation and 467 genes with <50% downregulation (Figure 4C). As expected, *Spp1* was one of the genes significantly induced by amphiregulin stimulation. Among reported fibrosis-related genes (Wick et al., 2013), *Spp1* was confirmed to be upregulated by amphiregulin in eosinophils (Figure 4D). Quantitative RT-PCR confirmed that amphiregulin stimulation induced the expression of *Spp1* in eosinophils but not in other types of cells including fibroblasts (Figure 4E). These results indicate that inflammatory eosinophils activated by amphiregulin expressed *Spp1*.

Osteopontin Secretion from Eosinophils Is Required for Fibrosis

Mice that genetically lack eosinophils (ΔdblGATA mice) showed ameliorated fibrotic responses by both HDM exposure and OVA-alum immunization followed by OVA inhalation (Figures S5A–S5D). Comparative global gene expression revealed enrichment of lung-tissue repair-related pathways in lungs from wild-type as compared to ΔdblGATA mice (Figures 5A and S5E). *Spp1* was one of the genes upregulated in both amphiregulin-stimulated eosinophils and inflamed lungs from wild-type mice (Figures 5B and S5F). Using a trans-well co-culture system, $Spp1^{+/+}$ but not $Spp1^{-/-}$ eosinophils induced enhanced expression of fibrosis-related molecules from fibroblasts (Figures 5C and S5G–S5I). Consistent with these results, *in vivo* OVA-alum immunization followed by OVA inhalation or repetitive exposure of HDM resulted in ameliorated fibrotic changes in the lungs from $Spp1^{-/-}$ mice (Figures 5D and S5J–S5O).

Next, to determine whether osteopontin produced by eosinophils was physiologically relevant to the induction of lung fibrotic responses *in vivo*, we transferred eosinophils from $Spp1^{+/+}$ mice or $Spp1^{-/-}$ mice together with OVA-specific memory Th2 cells to ΔdblGATA mice and then performed antigen challenge (Figure S5P). Lung collagen deposition was significantly decreased in recipients of $Spp1^{-/-}$ as compared to $Spp1^{+/+}$ eosinophils (Figure 5E). Recipients of $Spp1^{-/-}$ as compared to $Spp1^{+/+}$ eosinophils also exhibited decreased expression of fibrosis-related genes (Figures 5F and 5G). Thus, osteopontin produced by eosinophils was relevant to the induction of lung fibrotic responses.

Inhibition of EGFR Signaling Ameliorates Fibrotic Responses *In Vivo*

Erlotinib, a receptor tyrosine kinase inhibitor acting on the EGFR (Moyer et al., 1997), inhibited amphiregulin-induced *Spp1* upregulation in eosinophils without any obvious effects in the survival of eosinophils (Figures 6A, S6A, and S6B). Erlotinib also had no obvious effect on the survival and cytokine production of $ST2^{hi}$ memory Th2 cells (Figures S6C and S6D). However, Erlotinib treatment *in vivo* resulted in significant decreases in both collagen deposition and expression of fibrosis-related genes in inflamed lungs (Figures 6B and S6E–S6G). Osteopontin-positive eosinophils disappeared from the inflamed lungs of mice treated with Erlotinib (Figures 6C and 6D). Moreover, Erlotinib treatment after the induction of fibrotic changes by repetitive exposure to HDM resulted in ameliorated fibrosis accompanied by disappearance of osteopontin-positive eosinophils (Figures 6E–6G, S6H, and S6I). Thus, the amphiregulin-EGFR-osteopontin axis in eosinophils leads to fibrotic responses *in vivo*.

ECRS Polyps with Fibrotic Changes Exhibit Selective Amphiregulin Production by Memory $CD4^+$ T Cells and Osteopontin Expression by Eosinophils

We sought to determine whether the observed mechanisms were relevant to inflammatory lesions of human chronic allergic diseases. Eosinophilic chronic rhinosinusitis (ECRS) is a chronic upper airway inflammatory disease that often presents with nasal polyps infiltrated with eosinophils (Nakayama et al., 2011). Fibronectin deposition was significantly elevated in the polyps of patient with ECRS as compared to the normal nasal mucosa (Figure 7A). The expression of fibrosis-related genes such as *SPP1*, *TNC*, *COL1A1*, *ACTA2*, and *FN1* was significantly increased in ECRS polyps as compared to normal nasal mucosa tissue (Figure 7B). The expression of *AREG*, *IL33*, *IL1RL1*, and Th2 cytokines was also significantly higher in the ECRS polyps (Figures 7C and S7A). These results prompted us to characterize amphiregulin-producing cell population(s) in local inflammatory sites. Flow cytometry analysis of infiltrating mononuclear cells from ECRS polyps revealed amphiregulin production coming mainly from $CD45RO^+$ memory-type $CD4^+$ T cells, with a minor contribution from innate lymphoid cells (ILCs) (Figures S7B–S7D). Moreover, among polyp-infiltrating cells, ILCs produced significantly less amphiregulin than memory-type $CD4^+$ T cells (Figures 7D and S7E). Among nasal polyp-infiltrating memory-type $CD45RO^+CD4^+$ T cells, IL-5 and amphiregulin production was restricted to $CD161^{hi}CRTH2^{hi}$ cells (Figures 7E and

Figure 4. Amphiegulin Induced Transcriptional Reprogramming of Eosinophils

The global gene expression profiles of mouse bone marrow-derived eosinophils stimulated with or without amphiregulin for 72 hr were assessed by RNA-seq.

(A) Shown is a network visualization of Gene Ontology enrichment analysis. Node colors indicate GO terms that were significantly upregulated (red) or downregulated (blue) in eosinophils stimulated with amphiregulin compared to control eosinophils. Node sizes represent enrichment scores for each GO terms. Node connections were determined using overlap of the elemental gene products in the GO terms (Simpson coefficient $\geq$ 0.5).

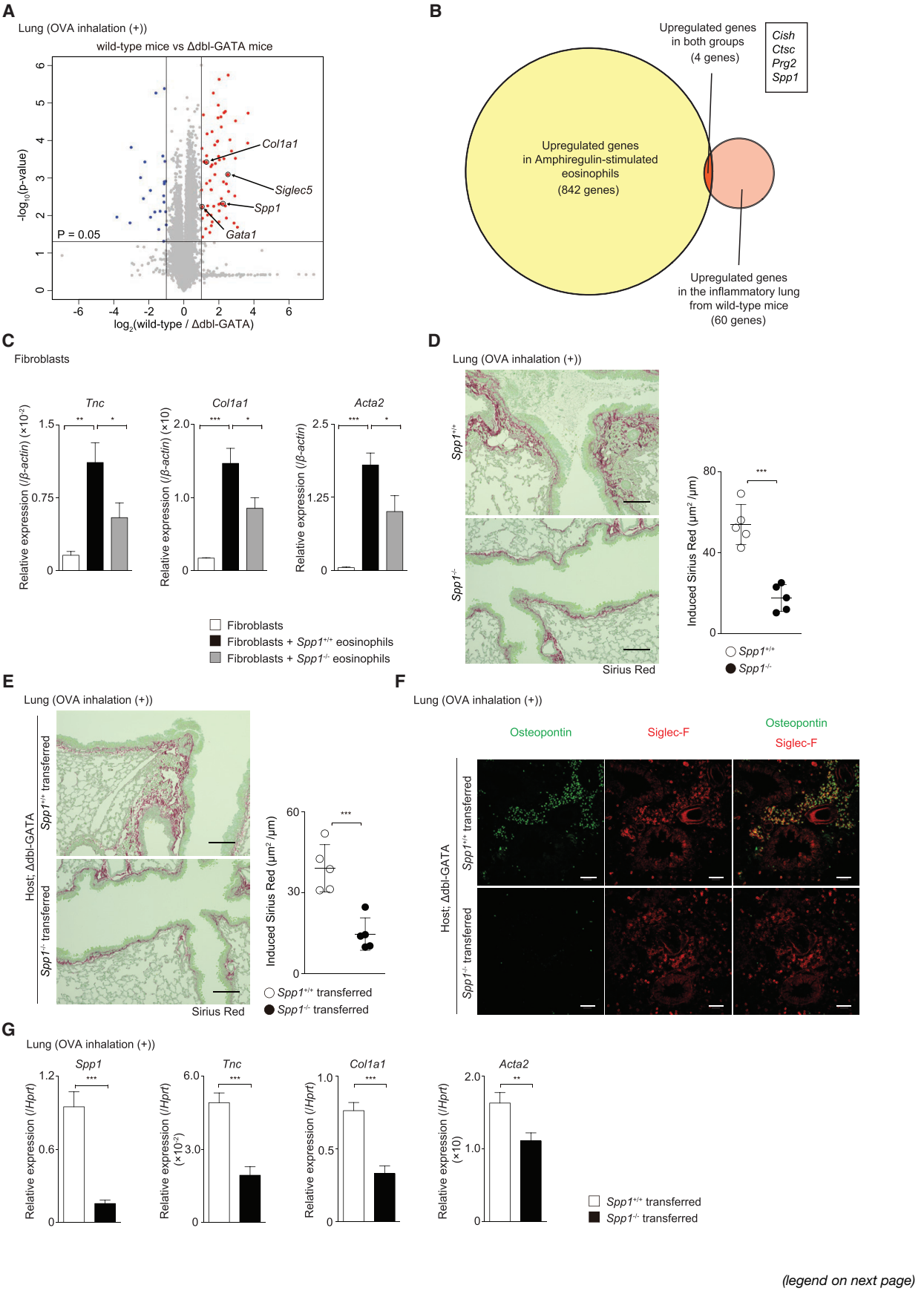
(B) CD101 expression and CD62L expression are shown by geometric mean channel fluorescence.

(C) Volcano plot depicts differential gene expression in eosinophils induced by amphiregulin compared to control. The arrow indicates *Spp1*.

(D) Heatmap of log2 expression values of fibrosis-related genes in eosinophils with or without amphiregulin stimulation.

(E) Quantitative RT-PCR analysis of *Spp1* in the indicated cells from lungs of wild-type mice stimulated with or without amphiregulin for 72 hr.

Data are the mean ± SD. **p < 0.01, ***p < 0.001, ****p < 0.0001; n.s., not significant; by unpaired t test or one-way analysis of variance (ANOVA). Please see also Figure S4.



(legend on next page)

S7F–S7H). However, distinct CD161^{hi}CRTH2^{hi} subpopulations were responsible for amphiregulin and IL-5 production (Figures 7E, S7F, and S7G). Histological analyses of ECRS nasal polyps revealed eosinophil infiltrates associated with dense osteopontin deposits (Figure 7F, lower panel). Eosinophils infiltrating ECRS polyps exhibited significantly elevated expression of *SPP1* as compared to circulating eosinophils in PBMCs obtained from the same patients (Figure 7G). The expression of *SPP1* was induced by amphiregulin in circulating eosinophils, and Erlotinib constrained the induction of *SPP1* (Figures 7H, S7I, and S7J). These results show that amphiregulin-producing memory-type CD4$^+$ T cells co-localize with ostepontin-expressing eosinophils in ECRS polyps where severe fibrotic responses were observed. Thus, we have identified an amphiregulin-producing memory-type CD4$^+$ T cell subpopulation that may direct tissue fibrotic responses via eosinophilic osteopontin in the nasal polyps of ECRS patients.

DISCUSSION

Herein, we have identified that amphiregulin produced by memory-type Th2 cells is a key molecule in the pathogenesis of fibrosis during eosinophilic inflammation. We found that amphiregulin reprogrammed eosinophils to adopt an inflammatory phenotype with enhanced osteopontin production. The genetic deletion of *Il33*, *Il1rl1*, *Areg*, or *Spp1* or the blockade of EGFR signaling *in vivo* attenuated fibrotic responses during eosinophilic inflammation in the lung. The analysis of ECRS polyps revealed severe fibrotic lesion infiltrated with osteopontin-expressing eosinophils and amphiregulin-producing CD161$^+$CRTH2$^+$ memory CD4$^+$ T cells. Amphiregulin-producing memory Th2 cells were distinct from IL-5-producing memory Th2 cells, and the co-operation of both pathogenic Th2 cell subpopulations appear to be critical for the induction of fibrosis in the airways of both mice and humans. Moreover, the blockade of EGFR signaling by Erlotinib resulted in decreased amphiregulin-induced upregulation of *SPP1* expression in eosinophils, indicating that the IL-33-amphiregulin-osteopontin axis could be a therapeutic target for treatment of fibrosis in chronic allergic inflammation.

IL-33 is associated with several fibrotic diseases such as hepatic fibrosis and bleomycin-induced pulmonary fibrosis via activation of type 2 innate lymphoid cells (ILC2s) and macrophages (Li et al., 2014; McHedlidze et al., 2013). The IL-33-ST2 axis plays a protective role in cardiac fibrosis (Sanada et al., 2007). By contrast, we demonstrated that IL-33 drove fibrotic responses in the inflamed lung through the activation of ST2^{hi} memory-type Th2 cells. Thus, IL-33 is a multifunctional cytokine and appears to exert distinct effects in different biological contexts. IL-33 stimulation resulted in selective production of amphiregulin by ST2^{hi} memory-type Th2 cells in models of allergen-induced allergic airway inflammation. Amphiregulin, encoded by *Areg*, belongs to the epidermal growth factor (EGF) family and signals through the EGFR system (Shoyab et al., 1989). Amphiregulin is known to promote tissue-protective epithelial responses in the intestine during helminth infection (Zaiss et al., 2006). Amphiregulin produced by regulatory T (Treg) cells, mast cells, and ILC2s has also been found to be involved in the process of tissue repair of muscle and lungs, thereby contributing to tissue homeostasis (Arpaia et al., 2015; Burzyn et al., 2013; Monticelli et al., 2011; Okumura et al., 2005; Zaiss et al., 2013). Although uncontrolled tissue repair due to chronic inflammation may cause fibrosis (Wick et al., 2013), until the current work the pathogenic role of amphiregulin in the induction of fibrosis had not been not established. In the present study, we have shown that genetic ablation of amphiregulin resulted in ameliorated fibrotic responses, which indicates that amphiregulin contributes to the pathogenesis of inflammation-associated fibrosis. Moreover, we found that ST2^{hi} memory-type Th2 cells were the major producer of amphiregulin in antigen-induced eosinophilic airway inflammation models and thus are key players in lung fibrotic responses. We also found that the majority of amphiregulin-producing ST2^{hi} memory-type Th2 cells did not produce IL-5. These results indicate functional heterogeneity of ST2^{hi} memory Th2 cell populations: IL-5-producing cells to recruit and activate eosinophils and amphiregulin-producing cells to induce fibrotic responses. A two-step interaction between eosinophils and distinct ST2^{hi} memory Th2 cell subpopulations producing either IL-5 or amphiregulin may underlie the establishment of pathological eosinophil-induced fibrotic changes.

Figure 5. Osteopontin Secretion by Eosinophils Is Required for Fibrotic Responses in the Lung

(A) OVA-specific memory Th2 cells (3 × 10^6 cells) were transferred i.v. into wild-type mice and ΔdbI-GATA mice that were subsequently challenged with OVA. Volcano plot depicts differential gene expression in the lungs of wild-type versus ΔdbI-GATA mice. Arrows indicate *Spp1*, *Col1a1*, *Gata1*, and *Siglec5*.

(B) Shown is a Venn diagram of upregulated genes in amphiregulin-stimulated eosinophils (842 genes) and upregulated genes in lungs from wild-type mice with OVA challenges (60 genes). The 4 overlapping genes are shown in a box.

(C) Quantitative RT-PCR analysis of the indicated genes in fibroblasts co-cultured with or without *Spp1*$^{+/+}$ and *Spp1*$^{-/-}$ eosinophils for 24 hr as indicated in Figure S5G. Three independent experiments were performed with similar results.

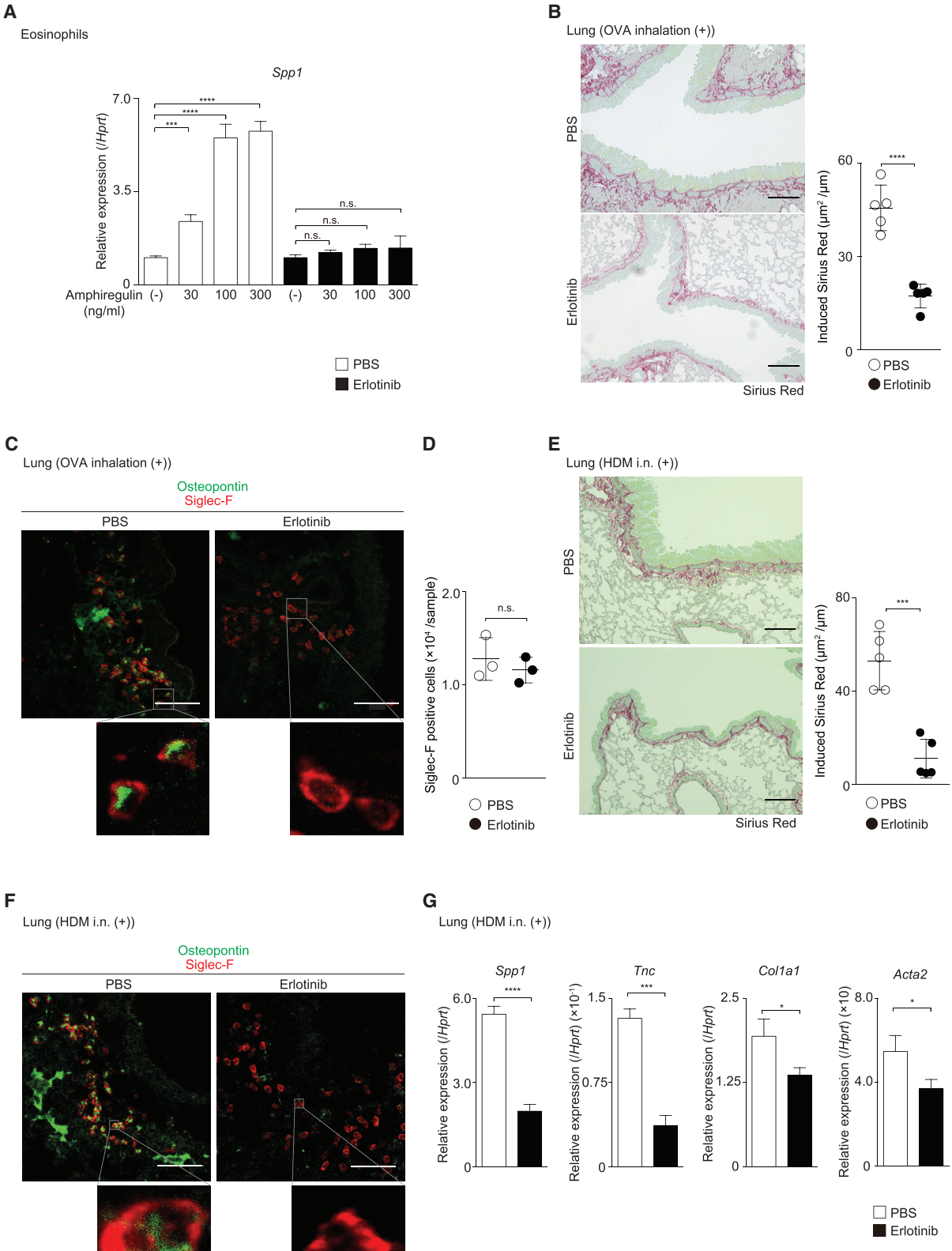
(D) *Spp1*$^{+/+}$ and *Spp1*$^{-/-}$ mice were immunized with OVA and Alum twice followed by a series of OVA inhalations. Shown is a representative confocal micrograph of lung tissue stained with Sirius red from a *Spp1*$^{+/+}$ and a *Spp1*$^{-/-}$ mouse (left) from three experiments. Scale bars represent 100 μm. Shown are ratios of areas of randomly selected regions stained with Sirius red surrounding bronchi versus the areas of associated basement membranes (right). More than three mice per group were analyzed.

(E) Memory Th2 cells (3 × 10^6 cells) were adoptively transferred i.v. into ΔdbI-GATA mice that were subsequently challenged with OVA and then adoptively transferred with *Spp1*$^{+/+}$ and *Spp1*$^{-/-}$ eosinophils (1 × 10^8 cells, i.v.) as indicated in Figure S5P. Shown is a representative confocal micrograph of lung tissue stained with Sirius red from recipients of *Spp1*$^{+/+}$ and *Spp1*$^{-/-}$ eosinophils (left) from two experiments. Scale bars represent 100 μm. Shown are ratios of areas of randomly selected regions stained with Sirius red surrounding bronchi versus the areas of associated basement membranes (right). More than three mice per group were analyzed.

(F) Shown is a representative confocal micrograph of the lungs stained with anti-Osteopontin (green) and Siglec-F (red) from recipients of *Spp1*$^{+/+}$ and *Spp1*$^{-/-}$ eosinophils from two experiments (scale bars represent 50 μm). Three independent experiments were performed with similar results.

(G) Quantitative RT-PCR analysis of the indicated genes in the lungs from recipients of *Spp1*$^{+/+}$ and *Spp1*$^{-/-}$ eosinophils (n = 3 mice per group).

Data are the mean ± SD. **p < 0.01, ***p < 0.001; by unpaired t test or one-way analysis of variance (ANOVA). Please see also Figure S5.



(legend on next page)

In the current study, we also identified eosinophils as critical target cells for amphiregulin in the process of inflammation-associated fibrosis. Amphiregulin is well known to stimulate lung epithelial cells to undergo proliferation and enhanced mucin production (Okumura et al., 2005; Zaiss et al., 2006). Amphiregulin also promotes the proliferation of lung fibroblasts (Al-Muhsen et al., 2011). Amphiregulin from tissue-resident Treg cells contributes to the downregulation of collagens from injured muscle cells (Burzyn et al., 2013). Other groups have reported that amphiregulin from cardiac Ly6C^{lo} macrophages is involved in the adaptive response to pressure overload in the heart (Fujiu et al., 2017). Our genome-wide analyses revealed that amphiregulin stimulation induced transcriptional reprogramming in eosinophils, marked by upregulation of inflammatory genes. One of the genes upregulated by amphiregulin stimulation in eosinophils was *Spp1*, a major component of noncollagenous ECM in fibrotic tissues and a contributor to the pathogenesis of fibrosis (Denhardt et al., 2001; Sabo-Attwood et al., 2011). Refractory asthma is often associated with tissue fibrosis leading to a decrease in lung function. Our findings indicate that eosinophils directly produce noncollagenous ECM and contribute to tissue fibrosis in allergic airway inflammation.

The analysis of ECRS polyps revealed significantly increased deposition of fibronectin and upregulation of various fibrosis-related genes. Previous work has shown that osteopontin is upregulated in nasal polys from patients with chronic rhinosinusitis with nasal polyps (CRSwNP) (Liu et al., 2015). Other work has shown that osteopontin is expressed in eosinophils from patients with atopic dermatitis and that expression of osteopontin is enhanced by GM-CSF and IL-5 (Puxeddu et al., 2010). In this study, we detected the accumulation of both amphiregulin-producing CD161^{hi}CRTH2^{hi} memory-type CD4^{+} T cells and osteopontin-producing eosinophils in ECRS polyps. But very limited numbers of ILC2s were detected in the nasal polyps of patients with ECRS. In particular, amphiregulin production was less than 1.0% in ILC2s as compared to T cells. Though perhaps unexpected given observations from previous publications (Bal et al., 2016; Ho et al., 2015), we provided a direct comparison of amphiregulin production among T cells and ILC2s. Our results show that in ECRS polyps, the major source of amphiregulin is a CD161^{hi}CRTH2^{hi} memory-type CD4^{+} T cell. Cells with this phenotype have been shown to produce large amounts of IL-5 and have been appreciated as ''pathogenic'' in various human allergic diseases, particularly in association with eosinophilic inflammation such as in eosinophilic esophagitis (Mitson-Salazar et al., 2016; Nakayama et al., 2017; Wambre et al., 2017). In the current study, similar to results from mouse systems, we detected both IL-5-producing and amphiregulin-producing subsets among CD161^{hi}CRTH2^{hi} memory-type CD4^{+} T cells infiltrating ECRS polyps. The majority of amphiregulin producers showed limited production of IL-5. Thus, the current study demonstrates functional heterogeneity of pathogenic memory Th2 cells in both mouse and human systems. Treatment with CRTH2 antagonist OC000459 causes reduction of extracellular deposits in patients with eosinophilic esophagitis (Straumann et al., 2013). Thus, the amphiregulin-osteopontin pathway could be a potential therapeutic target for patients with eosinophilic inflammatory disorders including ECRS that are refractory to corticosteroid treatment.

In summary, we have identified the cellular and molecular mechanisms that control the induction of airway fibrotic responses during chronic allergic inflammation. We have elucidated the critical role of the IL-33-amphiregulin-osteopontin axis in the interaction between ST2^{hi} memory-type pathogenic Th2 cells and eosinophils and how this shapes the pathology of fibrotic responses in allergic inflammation, and provides the molecular basis for the development of potential therapeutic strategies for intractable inflammation-associated fibrotic diseases.

STAR★METHODS

Detailed methods are provided in the online version of this paper and include the following:

- KEY RESOURCES TABLE
- CONTACT FOR REAGENT AND RESOURCE SHARING
- EXPERIMENTAL MODEL AND SUBJECT DETAILS
  - Mice
  - Human Samples

Figure 6. Inhibition of EGFR Signaling Ameliorates Fibrotic Responses *In Vivo*

(A) Quantitative RT-PCR analysis of *Spp1* in eosinophils. Eosinophils were cultured with amphiregulin (white) or amphiregulin plus Erlotinib (black) for 72 hr. Three independent experiments were performed and showed similar results.

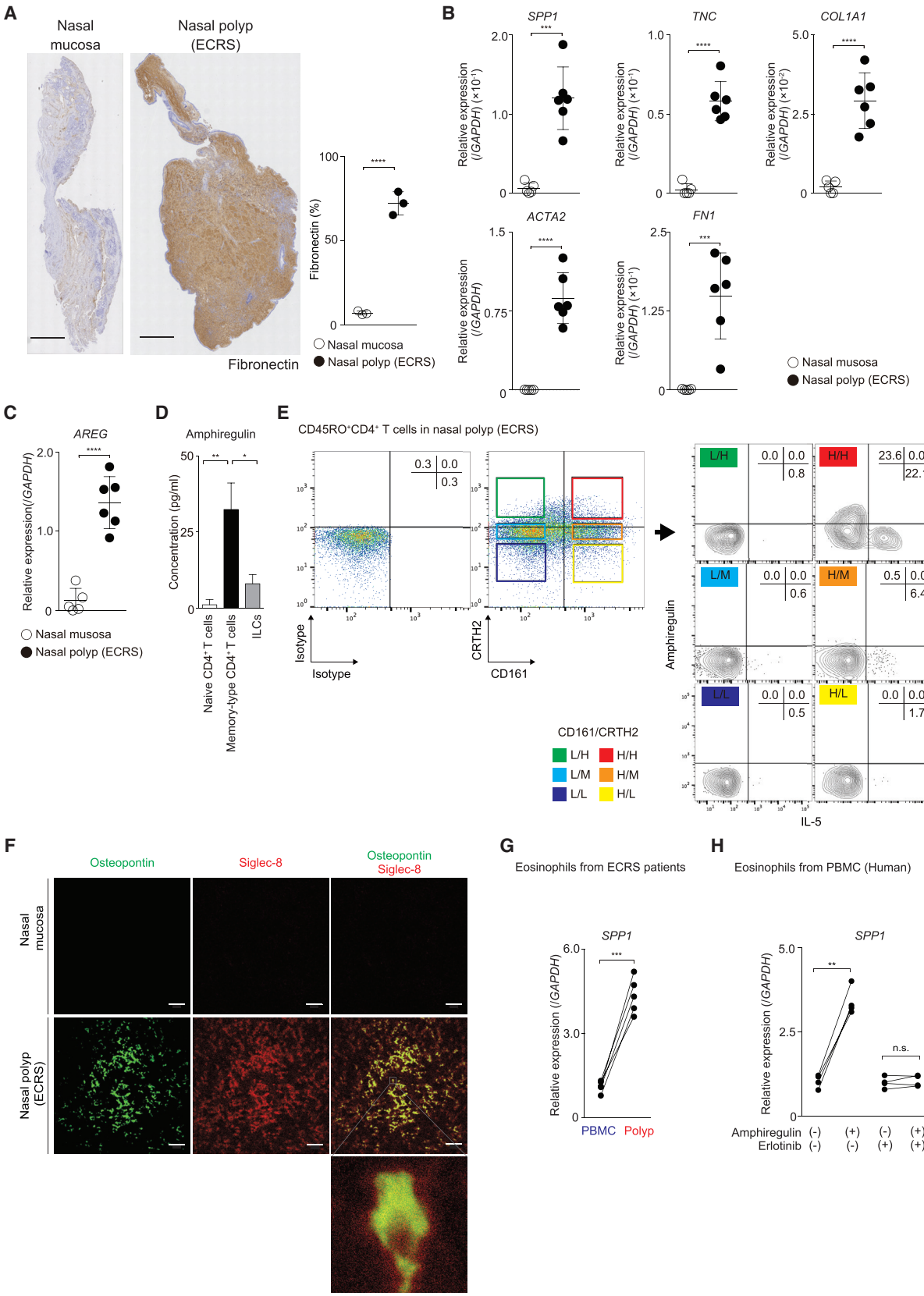
(B) Wild-type mice were OVA challenged with or without simultaneous Erlotinib treatment as indicated in Figure S6E. Shown is a representative confocal micrograph of lung tissue stained with Sirius red from mice treated with PBS (PBS) or Erlotinib (Erlotinib) (left) from three experiments. Scale bars represent 100 μm. Shown are ratios of areas of randomly selected regions stained with Sirius red surrounding bronchi versus the areas of associated basement membranes (right). More than three mice per group were analyzed.

(C and D) Shown is a representative confocal micrograph of the lung stained with anti-osteopontin (green) and anti-Siglec-F (red) from mice with or without simultaneous Erlotinib treatment from three experiments (C). Scale bars represent 50 μm. Three independent experiments were performed with similar results. Shown are the absolute number of Siglec-F-positive cells in randomly selected lung tissue slices. Three mice per group were analyzed (D).

(E) Wild-type mice were HDM challenged with or without subsequent Erlotinib treatment as indicated in Figure S6H. Shown is a representative confocal micrograph of lung tissue stained with Sirius red from mice treated with PBS (PBS) or Erlotinib (Erlotinib) (left) from two experiments. Scale bars represent 100 μm. Shown are ratios of areas of randomly selected regions stained with Sirius red surrounding bronchi versus the areas of associated basement membranes (right). More than three mice per group were analyzed.

(F) Shown is a representative confocal micrograph of the lung stained with anti-osteopontin (green) and anti-Siglec-F (red) from mice with or without subsequent Erlotinib treatment from two experiments. Scale bars represent 50 μm. Three independent experiments were performed with similar results.

(G) Quantitative RT-PCR analysis of the indicated genes in lungs from HDM-exposed mice with or without subsequent Erlotinib treatment (n = 3 mice per group). Data are the mean ± SD. *$p < 0.05$, ***$p < 0.001$, ****$p < 0.0001$; n.s., not significant; by unpaired t test or one-way analysis of variance (ANOVA). Please see also Figure S6.



(legend on next page)

- METHOD DETAILS
  - Histology and immunohistochemistry
  - The Generation and Culture of Effector and Memory Th2 Cells
  - Flow cytometry and sorting
  - Cell Viability Assay
  - ST2 Neutralizing Assay
  - Erlotinib Treatment
  - Quantitative Real-Time PCR
  - RNA Sequencing
  - ELISA for the Measurement of Amphiregulin Expression
  - BAL fluid Collecting
  - Exposure of HDM
  - Immunization and inhalation with OVA
  - Culture of Bone Marrow-Derived Eosinophils
  - *In vitro* treatment of Eosinophils with Amphiregulin
  - Adoptive Transfer of Eosinophils
  - Intratracheal Administration of IL-33
  - Co-culture of Eosinophils and Fibroblasts
  - Cell Isolation From Mouse Lungs
  - Nasal Polyp, Peripheral Blood Mononuclear Cell and Homogenate Preparation
- QUANTIFICATION AND STATISTICAL ANALYSIS
  - Statistical Analysis
  - Analysis and graphic display of RNA-seq data
  - Gene Ontology enrichment analysis
- DATA AND SOFTWARE AVAILABILITY

SUPPLEMENTAL INFORMATION

Supplemental Information includes seven figures and one table and can be found with this article online at https://doi.org/10.1016/j.immuni.2018.04.023.

ACKNOWLEDGMENTS

We are grateful for Drs. Mark Bix, Omid Akbari, and Yuka Kanno for their critical reading and providing valuable suggestions on the manuscript. We thank Toshihiro Ito, Kaoru Sugaya, and Miki Kato for their excellent technical assistance. This work was supported by the following grants: Ministry of Education, Culture, Sports, Science and Technology (MEXT Japan) Grants-in-Aid for Scientific Research (S) 26221305, (C) 17K08876 and 18K07164, and Young Scientists (B) 18K16830; AMED-CREST, AMED (no. JP16gm0410009); AMED-PRIME, AMED (no. JP18gm6110005); Practical Research Project for Allergic Diseases and Immunology (Research on Allergic Diseases and Immunology) from AMED (no. JP18ek0410030, JP18ek0410045); Takeda Science Foundation; and the Naito Foundation.

AUTHOR CONTRIBUTIONS

Y.M., K.H., and T.N. designed experiments. Y.M., K.H., M.K., T.W., T.K., M.O., and K.K. performed experiments. Y.M., K.H., T.I., A.O., D.S., Y.O., and T.N. analyzed and interpreted data. Y.M., K.H., Y.O., and T.N. wrote the paper.

DECLARATION OF INTERESTS

Y.M., K.H., Y.O., and T.N. are inventors of Japanese patent application 2017-176017, which is related to this work, and have assigned the application to Chiba University per the University's invention policy.

Received: July 4, 2017
Revised: March 12, 2018
Accepted: April 19, 2018
Published: June 26, 2018

REFERENCES

Adcock, I.M., Caramori, G., and Chung, K.F. (2008). New targets for drug development in asthma. Lancet *372*, 1073–1087.

Al-Muhsen, S., Johnson, J.R., and Hamid, Q. (2011). Remodeling in asthma. J. Allergy Clin. Immunol. *128*, 451–462, quiz 463–454.

Arpaia, N., Green, J.A., Moltedo, B., Arvey, A., Hemmers, S., Yuan, S., Treuting, P.M., and Rudensky, A.Y. (2015). A distinct function of regulatory T cells in tissue protection. Cell *162*, 1078–1089.

Bal, S.M., Bernink, J.H., Nagasawa, M., Groot, J., Shikhagaie, M.M., Golebski, K., van Drunen, C.M., Lutter, R., Jonkers, R.E., Hombrink, P., et al. (2016). IL-1β, IL-4 and IL-12 control the fate of group 2 innate lymphoid cells in human airway inflammation in the lungs. Nat. Immunol. *17*, 636–645.

Ball, S.L., Mann, D.A., Wilson, J.A., and Fisher, A.J. (2016). The role of the fibroblast in inflammatory upper airway conditions. Am. J. Pathol. *186*, 225–233.

Burzyn, D., Kuswanto, W., Kolodin, D., Shadrach, J.L., Cerletti, M., Jang, Y., Sefik, E., Tan, T.G., Wagers, A.J., Benoist, C., and Mathis, D. (2013). A special population of regulatory T cells potentiates muscle repair. Cell *155*, 1282–1295.

Busse, W.W., and Lemanske, R.F., Jr. (2001). Asthma. N. Engl. J. Med. *344*, 350–362.

Figure 7. Nasal Polyps of ECRS Patients Revealed Massive Deposition of SPP1 Accompanied by Amphiregulin-Producing Memory-type CD4$^+$ T Cells

(A) Representative confocal micrograph of the nasal mucosa from a healthy control subject (left) and a polyp from a patient with ECRS (middle) stained with anti-Fibronectin from three samples in each group (scale bars, 1 mm). The ratios of stained area versus the area of the whole tissue were measured in three samples from both groups (right).

(B) Quantitative RT-PCR analysis of the indicated genes in the nasal mucosa of healthy control subjects (control; n = 5) and in the polyps of patients with ECRS (ECRS; n = 6).

(C) Quantitative RT-PCR analysis of *AREG* in the nasal mucosa from healthy control subjects (control; n = 5) and in the polyps of patients with ECRS (ECRS; n = 6).

(D) Protein expression of amphiregulin from the indicated cells. Three independent experiments were performed with similar results.

(E) Shown is a representative flow cytometry plot of CD161 and CRTH2 surface expression in memory CD4$^+$ T cells from the polyp of a patient with ECRS with isotype controls (left) from 40 independent experiments (n = 40). Shown are representative flow cyometry plots of amphiregulin and IL-5 intracellular-staining for cells in each of the six quadrants of the CD161 and CRTH2 flow cytometry plot (right) from ten independent experiments (n = 10).

(F) Shown are representative confocal micrographs of the nasal mucosa from healthy control subjects (upper) and polyps of patients with ECRS (lower) stained with anti-SPP1 (green) and anti-Siglec-8 (red) from four independent experiments (n = 4) (scale bars represent 50 μm). More than three independent experiments were performed with similar results.

(G) Quantitative RT-PCR analysis of *SPP1* in eosinophils from patients with ECRS. Eosinophils from peripheral blood (PBMC) and polyps were sorted from individual patients (n = 5).

(H) Quantitative RT-PCR analysis of *SPP1* in eosinophils from healthy control subjects. Eosinophils were cultured with medium, amphiregulin, Erlotinib, or amphiregulin plus Erlotinib for 72 hr (n = 4 subjects).

Data are the mean ± SD. **p < 0.01, ***p < 0.001, ****p < 0.0001; n.s., not significant; by unpaired t test or paired t test. Please see also Figure S7.

Denhardt, D.T., Noda, M., O'Regan, A.W., Pavlin, D., and Berman, J.S. (2001). Osteopontin as a means to cope with environmental insults: regulation of inflammation, tissue remodeling, and cell survival. J. Clin. Invest. *107*, 1055–1061.

Doherty, T.A., Soroosh, P., Khorram, N., Fukuyama, S., Rosenthal, P., Cho, J.Y., Norris, P.S., Choi, H., Scheu, S., Pfeffer, K., et al. (2011). The tumor necrosis factor family member LIGHT is a target for asthmatic airway remodeling. Nat. Med. *17*, 596–603.

Durrani, S.R., Viswanathan, R.K., and Busse, W.W. (2011). What effect does asthma treatment have on airway remodeling? Current perspectives. J. Allergy Clin. Immunol. *128*, 439–448, quiz 449–450.

Endo, Y., Iwamura, C., Kuwahara, M., Suzuki, A., Sugaya, K., Tumes, D.J., Tokoyoda, K., Hosokawa, H., Yamashita, M., and Nakayama, T. (2011). Eomesodermin controls interleukin-5 production in memory T helper 2 cells through inhibition of activity of the transcription factor GATA3. Immunity *35*, 733–745.

Endo, Y., Hirahara, K., Iinuma, T., Shinoda, K., Tumes, D.J., Asou, H.K., Matsugae, N., Obata-Ninomiya, K., Yamamoto, H., Motohashi, S., et al. (2015). The interleukin-33-p38 kinase axis confers memory T helper 2 cell pathogenicity in the airway. Immunity *42*, 294–308.

Foster, P.S., Maltby, S., Rosenberg, H.F., Tay, H.L., Hogan, S.P., Collison, A.M., Yang, M., Kaiko, G.E., Hansbro, P.M., Kumar, R.K., and Mattes, J. (2017). Modeling T_H 2 responses and airway inflammation to understand fundamental mechanisms regulating the pathogenesis of asthma. Immunol. Rev. *278*, 20–40.

Fujiu, K., Shibata, M., Nakayama, Y., Ogata, F., Matsumoto, S., Noshita, K., Iwami, S., Nakae, S., Komuro, I., Nagai, R., and Manabe, I. (2017). A heart-brain-kidney network controls adaptation to cardiac stress through tissue macrophage activation. Nat. Med. *23*, 611–622.

Gieseck, R.L., 3rd, Wilson, M.S., and Wynn, T.A. (2018). Type 2 immunity in tissue repair and fibrosis. Nat. Rev. Immunol. *18*, 62–76.

Hamilos, D.L. (2015). Drivers of chronic rhinosinusitis: Inflammation versus infection. J. Allergy Clin. Immunol. *136*, 1454–1459.

Hansbro, P.M., Kim, R.Y., Starkey, M.R., Donovan, C., Dua, K., Mayall, J.R., Liu, G., Hansbro, N.G., Simpson, J.L., Wood, L.G., et al. (2017). Mechanisms and treatments for severe, steroid-resistant allergic airway disease and asthma. Immunol. Rev. *278*, 41–62.

Hirahara, K., Yamashita, M., Iwamura, C., Shinoda, K., Hasegawa, A., Yoshizawa, H., Koseki, H., Gejyo, F., and Nakayama, T. (2008). Repressor of GATA regulates TH2-driven allergic airway inflammation and airway hyperresponsiveness. J. Allergy Clin. Immunol. *122*, 512–520, e511.

Ho, J., Bailey, M., Zaunders, J., Mrad, N., Sacks, R., Sewell, W., and Harvey, R.J. (2015). Group 2 innate lymphoid cells (ILC2s) are increased in chronic rhinosinusitis with nasal polyps or eosinophilia. Clin. Exp. Allergy *45*, 394–403.

Humbles, A.A., Lloyd, C.M., McMillan, S.J., Friend, D.S., Xanthou, G., McKenna, E.E., Ghiran, S., Gerard, N.P., Yu, C., Orkin, S.H., and Gerard, C. (2004). A critical role for eosinophils in allergic airways remodeling. Science *305*, 1776–1779.

Islam, S.A., Chang, D.S., Colvin, R.A., Byrne, M.H., McCully, M.L., Moser, B., Lira, S.A., Charo, I.F., and Luster, A.D. (2011). Mouse CCL8, a CCR8 agonist, promotes atopic dermatitis by recruiting IL-5+ T(H)2 cells. Nat. Immunol. *12*, 167–177.

Kim, H.Y., DeKruyff, R.H., and Umetsu, D.T. (2010). The many paths to asthma: phenotype shaped by innate and adaptive immunity. Nat. Immunol. *11*, 577–584.

Kobayashi, Y., Asako, M., Ooka, H., Kanda, A., Tomoda, K., and Yasuba, H. (2015). Residual exhaled nitric oxide elevation in asthmatics is associated with eosinophilic chronic rhinosinusitis. J. Asthma *52*, 1060–1064.

Lambrecht, B.N., and Hammad, H. (2012). The airway epithelium in asthma. Nat. Med. *18*, 684–692.

Lambrecht, B.N., and Hammad, H. (2015). The immunology of asthma. Nat. Immunol. *16*, 45–56.

Li, D., Guabiraba, R., Besnard, A.G., Komai-Koma, M., Jabir, M.S., Zhang, L., Graham, G.J., Kurowska-Stolarska, M., Liew, F.Y., McSharry, C., and Xu, D. (2014). IL-33 promotes ST2-dependent lung fibrosis by the induction of alternatively activated macrophages and innate lymphoid cells in mice. J. Allergy Clin. Immunol. *134*, 1422–1432, e1411.

Liu, W.L., Zhang, H., Zheng, Y., Wang, H.T., Chen, F.H., Xu, L., Wei, Y., Sun, Y.Q., Shi, J.B., and Li, H.B. (2015). Expression and regulation of osteopontin in chronic rhinosinusitis with nasal polyps. Clin. Exp. Allergy *45*, 414–422.

Martinez, F.D., and Vercelli, D. (2013). Asthma. Lancet *382*, 1360–1372.

McHedlidze, T., Waldner, M., Zopf, S., Walker, J., Rankin, A.L., Schuchmann, M., Voehringer, D., McKenzie, A.N., Neurath, M.F., Pflanz, S., and Wirtz, S. (2013). Interleukin-33-dependent innate lymphoid cells mediate hepatic fibrosis. Immunity *39*, 357–371.

Mesnil, C., Raulier, S., Paulissen, G., Xiao, X., Birrell, M.A., Pirottin, D., Janss, T., Starkl, P., Ramery, E., Henket, M., et al. (2016). Lung-resident eosinophils represent a distinct regulatory eosinophil subset. J. Clin. Invest. *126*, 3279–3295.

Mitson-Salazar, A., Yin, Y., Wansley, D.L., Young, M., Bolan, H., Arceo, S., Ho, N., Koh, C., Milner, J.D., Stone, K.D., et al. (2016). Hematopoietic prostaglandin D synthase defines a proeosinophilic pathogenic effector human T(H)2 cell subpopulation with enhanced function. J. Allergy Clin. Immunol *137*, 907–918, e909.

Monticelli, L.A., Sonnenberg, G.F., Abt, M.C., Alenghat, T., Ziegler, C.G., Doering, T.A., Angelosanto, J.M., Laidlaw, B.J., Yang, C.Y., Sathaliyawala, T., et al. (2011). Innate lymphoid cells promote lung-tissue homeostasis after infection with influenza virus. Nat. Immunol. *12*, 1045–1054.

Moyer, J.D., Barbacci, E.G., Iwata, K.K., Arnold, L., Boman, B., Cunningham, A., DiOrio, C., Doty, J., Morin, M.J., Moyer, M.P., et al. (1997). Induction of apoptosis and cell cycle arrest by CP-358,774, an inhibitor of epidermal growth factor receptor tyrosine kinase. Cancer Res. *57*, 4838–4848.

Nakayama, T., Yoshikawa, M., Asaka, D., Okushi, T., Matsuwaki, Y., Otori, N., Hama, T., and Moriyama, H. (2011). Mucosal eosinophilia and recurrence of nasal polyps - new classification of chronic rhinosinusitis. Rhinology *49*, 392–396.

Nakayama, T., Hirahara, K., Onodera, A., Endo, Y., Hosokawa, H., Shinoda, K., Tumes, D.J., and Okamoto, Y. (2017). Th2 Cells in Health and Disease. Annu. Rev. Immunol. *35*, 53–84.

Oboki, K., Ohno, T., Kajiwara, N., Arae, K., Morita, H., Ishii, A., Nambu, A., Abe, T., Kiyonari, H., Matsumoto, K., et al. (2010). IL-33 is a crucial amplifier of innate rather than acquired immunity. Proc. Natl. Acad. Sci. USA *107*, 18581–18586.

Okumura, S., Sagara, H., Fukuda, T., Saito, H., and Okayama, Y. (2005). FcepsilonRI-mediated amphiregulin production by human mast cells increases mucin gene expression in epithelial cells. J. Allergy Clin. Immunol. *115*, 272–279.

Onodera, A., Tumes, D.J., Watanabe, Y., Hirahara, K., Kaneda, A., Sugiyama, F., Suzuki, Y., and Nakayama, T. (2015). Spatial interplay between Polycomb and Trithorax complexes controls transcriptional activity in T lymphocytes. Mol. Cell. Biol. *35*, 3841–3853.

Pawankar, R., and Nonaka, M. (2007). Inflammatory mechanisms and remodeling in chronic rhinosinusitis and nasal polyps. Curr. Allergy Asthma Rep. *7*, 202–208.

Puxeddu, I., Berkman, N., Ribatti, D., Bader, R., Haitchi, H.M., Davies, D.E., Howarth, P.H., and Levi-Schaffer, F. (2010). Osteopontin is expressed and functional in human eosinophils. Allergy *65*, 168–174.

Rosenberg, H.F., Dyer, K.D., and Foster, P.S. (2013). Eosinophils: changing perspectives in health and disease. Nat. Rev. Immunol. *13*, 9–22.

Rothenberg, M.E., and Hogan, S.P. (2006). The eosinophil. Annu. Rev. Immunol. *24*, 147–174.

Sabo-Attwood, T., Ramos-Nino, M.E., Eugenia-Ariza, M., Macpherson, M.B., Butnor, K.J., Vacek, P.C., McGee, S.P., Clark, J.C., Steele, C., and Mossman, B.T. (2011). Osteopontin modulates inflammation, mucin production, and gene expression signatures after inhalation of asbestos in a murine model of fibrosis. Am. J. Pathol. *178*, 1975–1985.

Sanada, S., Hakuno, D., Higgins, L.J., Schreiter, E.R., McKenzie, A.N., and Lee, R.T. (2007). IL-33 and ST2 comprise a critical biomechanically induced and cardioprotective signaling system. J. Clin. Invest. *117*, 1538–1549.

Seumois, G., Zapardiel-Gonzalo, J., White, B., Singh, D., Schulten, V., Dillon, M., Hinz, D., Broide, D.H., Sette, A., Peters, B., and Vijayanand, P. (2016). Transcriptional profiling of Th2 cells identifies pathogenic features associated with asthma. J. Immunol. *197*, 655–664.

Shinoda, K., Hirahara, K., Iinuma, T., Ichikawa, T., Suzuki, A.S., Sugaya, K., Tumes, D.J., Yamamoto, H., Hara, T., Tani-Ichi, S., et al. (2016). Thy1+IL-7+ lymphatic endothelial cells in iBALT provide a survival niche for memory T-helper cells in allergic airway inflammation. Proc. Natl. Acad. Sci. USA *113*, E2842–E2851.

Shoyab, M., Plowman, G.D., McDonald, V.L., Bradley, J.G., and Todaro, G.J. (1989). Structure and function of human amphiregulin: a member of the epidermal growth factor family. Science *243*, 1074–1076.

Stoll, S., Garner, W., and Elder, J. (1997). Heparin-binding ligands mediate autocrine epidermal growth factor receptor activation In skin organ culture. J. Clin. Invest. *100*, 1271–1281.

Straumann, A., Hoesli, S., Bussmann, Ch., Stuck, M., Perkins, M., Collins, L.P., Payton, M., Pettipher, R., Hunter, M., Steiner, J., and Simon, H.U. (2013). Anti-eosinophil activity and clinical efficacy of the CRTH2 antagonist OC000459 in eosinophilic esophagitis. Allergy *68*, 375–385.

Valladao, A.C., Frevert, C.W., Koch, L.K., Campbell, D.J., and Ziegler, S.F. (2016). STAT6 regulates the development of eosinophilic versus neutrophilic asthma in response to *Alternaria alternata*. J. Immunol. *197*, 4541–4551.

Wambre, E., Bajzik, V., DeLong, J.H., O'Brien, K., Nguyen, Q.A., Speake, C., Gersuk, V.H., DeBerg, H.A., Whalen, E., Ni, C., et al. (2017). A phenotypically and functionally distinct human T_H2 cell subpopulation is associated with allergic disorders. Sci. Transl. Med. *9*, https://doi.org/10.1126/scitranslmed.aam9171.

Wick, G., Grundtman, C., Mayerl, C., Wimpissinger, T.F., Feichtinger, J., Zelger, B., Sgonc, R., and Wolfram, D. (2013). The immunology of fibrosis. Annu. Rev. Immunol. *31*, 107–135.

Yamamoto, H., Okamoto, Y., Horiguchi, S., Kunii, N., Yonekura, S., and Nakayama, T. (2007). Detection of natural killer T cells in the sinus mucosa from asthmatics with chronic sinusitis. Allergy *62*, 1451–1455.

Zaiss, D.M., Yang, L., Shah, P.R., Kobie, J.J., Urban, J.F., and Mosmann, T.R. (2006). Amphiregulin, a TH2 cytokine enhancing resistance to nematodes. Science *314*, 1746.

Zaiss, D.M., van Loosdregt, J., Gorlani, A., Bekker, C.P., Gröne, A., Sibilia, M., van Bergen en Henegouwen, P.M., Roovers, R.C., Coffer, P.J., and Sijts, A.J. (2013). Amphiregulin enhances regulatory T cell-suppressive function via the epidermal growth factor receptor. Immunity *38*, 275–284.

STAR★METHODS

KEY RESOURCES TABLE

REAGENT or RESOURCE	SOURCE	IDENTIFIER
Antibodies		
Mouse Osteopontin/OPN Antibody	R&D systems	Cat#AF808; RRID: AB_2194992
Rat Anti-Mouse Siglec-F	BD Biosciences	Cat#552125; RRID: AB_394340
Anti-Human/Mouse CD11b	TONBO biosciences	Cat#70-0112; RRID: AB_2621483
CD45R (B220) Monoclonal Antibody	eBioscience	Cat#14-0452-81; RRID: AB_467253
Human Osteopontin/OPN Antibody	R&D systems	Cat#MAB1433; RRID: AB_2194981
Human Siglec-8 Antibody	R&D systems	Cat#MAB7975
Fibronectin Antibody	Santa Cruz Biotechnology	Cat#sc-8422; RRID: AB_627598
TCR DO11.10 Monoclonal Antibody	eBioscience	Cat#13-5808-81; RRID: AB_466677
anti–IFN-γ monoclonal antibody	Homemade	N/A
Brilliant Violet 421 anti-mouse IL-33Rα (IL1RL1, ST2) Antibody	BioLegend	Cat#145309; RRID: AB_2565634
Mouse Amphiregulin Antibody	R&D systems	Cat#206220; RRID: AB_2060661
PE anti-mouse/human IL-5 Antibody	BioLegend	Cat#504304; RRID: AB_315328
Brilliant Violet 421 anti-mouse/human IL-5 Antibody	BioLegend	Cat#504311; RRID: AB_2563161
PE/Cy7 anti-mouse IL-4 Antibody	BioLegend	Cat#504118; RRID: AB_10898116
IL-13 Monoclonal Antibody, Alexa Fluor 488	eBioscience	Cat#53-7133-80; RRID: AB_2016639
PE Rat Anti-Mouse Siglec-F	BD Biosciences	Cat#552126; RRID: AB_394341
Mouse CCR3 Alexa Fluor 647-conjugated Antibody	R&D systems	Cat#FAB729R
CD101 Monoclonal Antibody, PE	eBioscience	Cat#12-1011-82; RRID: AB_1210728
APC anti-mouse CD62L Antibody	BioLegend	Cat#104412; RRID: AB_313099
PE/Cy7 anti-human CD4 Antibody	BioLegend	Cat#317414; RRID: AB_571959
Brilliant Violet 421 anti-human CD45RO Antibody	BioLegend	Cat#304224; RRID: AB_2563817
PE anti-human CD161 Antibody	BioLegend	Cat#339904; RRID: AB_1501083
FITC anti-human CD294 (CRTH2) Antibody	BioLegend	Cat#350108; RRID: AB_11204086
Brilliant Violet 510 anti-human Lineage Cocktail	BioLegend	Cat#348807
Brilliant Violet 421 anti-human CD127	BioLegend	Cat#351310; RRID: AB_10960140
Human Amphiregulin Antibody	R&D systems	Cat#MAB262; RRID: AB_2060676
FITC anti-human IFN-γ Antibody	BioLegend	Cat#502506; RRID: AB_315231
Mouse ST2/IL-33 R Antibody	R&D systems	Cat#AF1004; RRID: AB_354527
Biotin Rat Anti-Mouse CD4	BD Biosciences	Cat#553044; RRID: AB_394580
Biotin anti-mouse CD326 (Ep-CAM) Antibody	BioLegend	Cat#118203; RRID: AB_1134174
Biotin Rat Anti-Mouse CD8a	BD Biosciences	Cat#553028; RRID: AB_394566
CD45R (B220) Monoclonal Antibody, Biotin	eBioscience	Cat#13-0452-86; RRID: AB_466451
Biotin Hamster Anti-Mouse CD11c	BD Biosciences	Cat#553800; RRID: AB_395059
Biotin Anti-Human/Mouse CD11b	TONBO biosciences	Cat#30-0112; RRID: AB_2621639
PE Rat Anti-Mouse Siglec-F	BD Biosciences	Cat#552126; RRID: AB_394341
Biotin anti-mouse Lineage Panel	BioLegend	Cat#133307; RRID: AB_11124348
Biotin anti-mouse CD90.2 Antibody	BioLegend	Cat#105304; RRID: AB_313175
Chemicals, Peptides, and Recombinant Proteins		
Recombinant Murine IL-2 Protein	Homemade	N/A
Recombinant Murine IL-4 Protein	PEPROTECH	Cat#214-14

(*Continued on next page*)

Continued

REAGENT or RESOURCE	SOURCE	IDENTIFIER
Recombinant Mouse IL-33 Protein	R&D systems	Cat#3626-ML
Recombinant Mouse IL-17E Protein	R&D systems	Cat#1399-IL
Recombinant Mouse TSLP Protein	R&D systems	Cat#555-TS
DAPI Fluoromount-G	SouthernBiotech	Cat#0100-20
Phorbol 12-myristate 13-acetate	Sigma-Aldrich	Cat#P1585
Ionomycin	Sigma-Aldrich	Cat#I0634
Monensin sodium salt	Sigma-Aldrich	Cat#M5273
Erlotinib HCl	Selleck	Cat#S1023
TRIzol	Invitrogen	Cat#15596026
Mite, House Dust (*Dermatophagoides pteronyssinus*)	Greer Laboratories Inc.	Cat#B84
Albumin from chicken egg white	Sigma-Aldrich	Cat#A5503
Imject Alum Adjuvant	Thermo Fisher Scientific	Cat#77161
Recombinant Mouse SCF Protein	R&D systems	Cat#455-MC
Recombinant Mouse Flt-3 Ligand Protein	R&D systems	Cat#427-FL
Recombinant Mouse IL-5 Protein	R&D systems	Cat#405-ML
Recombinant Mouse IL-33 Protein, CF	R&D systems	Cat#3626-ML/CF
Collagenase from *Clostridium histolyticum*	Sigma-Aldrich	Cat#C5138
Deoxyribonuclease I from bovine pancreas	Sigma-Aldrich	Cat#DN25
Hyaluronidase from sheep testes	Sigma-Aldrich	Cat#H6254
Critical Commercial Assays		
Alexa Fluor 488 Antibody Labeling Kit	Thermo Fisher Scientific	Cat#A20181
Alexa Fluor 555 Antibody Labeling Kit	Thermo Fisher Scientific	Cat#A20187
Alexa Fluor 647 Antibody Labeling Kit	Thermo Fisher Scientific	Cat#A20186
Alexa Fluor 680 Antibody Labeling Kit	Thermo Fisher Scientific	Cat#A20188
Pacific Blue Antibody Labeling Kit	Thermo Fisher Scientific	Cat#A30013
CD4+ T Cell Isolation Kit, mouse	Miltenyi Biotec	Cat#130-104-454
CD62L MicroBeads, mouse	Miltenyi Biotec	Cat#130-049-701
Eosinophil Isolation Kit, human	Miltenyi Biotec	Cat#130-092-010
FITC Annexin V Apoptosis Detection Kit I	BD Biosciences	Cat#556547
TruSeq RNA Sample Prep Kit v2	Illumina	Cat#RS-122-2001
Mouse Amphiregulin DuoSet ELISA kit	R&D systems	Cat#DY989
Human Amphiregulin DuoSet ELISA kit	R&D systems	Cat#DY262
Diff-Quik stain Kit	sysmex	Cat#16920
6.5mm Transwell with 0.4μm Pore Polycarbonate Membrane Insert, Sterile	Corning	Cat#3413
Deposited Data		
Raw and analyzed data	This paper	GEO: GSE114921
Software and Algorithms		
Photoshop	Adobe Systems Inc.	https://www.adobe.com/products/photoshop.html
Illustrator	Adobe Systems Inc.	https://www.adobe.com/products/illustrator.html
Bowtie 2	SOURCEFORGE	https://sourceforge.net/projects/bowtie-bio/files/bowtie2/2.0.0-beta7/
TopHat	Center for Computational Biology at Johns Hopkins University	https://ccb.jhu.edu/software/tophat/index.shtml
Cufflinks	Cole Trapnell	http://cole-trapnell-lab.github.io/cufflinks/
Prism	GraphPad	https://www.graphpad.com/scientific-software/prism/

(*Continued on next page*)

Continued

REAGENT or RESOURCE	SOURCE	IDENTIFIER
R	R Foundation	https://www.r-project.org/
Julia	NumFocus	https://julialang.org
Cytoscape	National Resource for Network Biology	http://www.cytoscape.org/
FlowJo	Tree Star, Inc.	https://www.flowjo.com/
Image J	NIH	https://imagej.nih.gov/ij/
Other		
BIOREVO	KEYENCE	https://www.keyence.com/ss/products/microscope/bz-x700/
autoMACS Pro Separator	Miltenyi Biotec	https://www.miltenyibiotec.com/JP-en/products/macs-cell-separation/instruments/automacs-pro-separator.html
BD FACSAria II Cell Sorter	BD Biosciences	N/A
BD FACSVerse 6 color Flow Cytometer	BD Biosciences	http://www.bdbiosciences.com/us/instruments/research/cell-analyzers/bd-facsverse/bd-facsverse-system/bd-facsverse-6-color-flow-cytometer/p/651154
Illumina HiSeq 1500 System	Illumina	N/A
Supersonic Nebulizer NE-U07	Omron	N/A

CONTACT FOR REAGENT AND RESOURCE SHARING

Further information and requests for resources and reagents should be directed to and will be fulfilled by the Lead Contact, Toshinori Nakayama (tnakayama@faculty.chiba-u.jp).

EXPERIMENTAL MODEL AND SUBJECT DETAILS

Mice

The animals used in this study were backcrossed to C57BL/6 or BALB/c mice more than ten times. *Areg*$^{-/-}$ mice were kindly provided by Dr. David C. Lee (University of Geogia, GA, USA). Anti-OVA-specific TCR-αβ (DO11.10) transgenic(Tg) mice were provided by Dr. D. Loh (Washington University School of Medicine, St. Louis). For antigen specific activation of CD4^{+} T cells mice expressing the OT-II-TCRαβ specific for residues 323-339 of OVA were also used. *Il33*$^{-/-}$ mice were generated as previously described (Oboki et al., 2010). *Il1rl1*$^{-/-}$ mice were kindly provided by Dr. Andrew N.J. McKenzie (Medical Research Council, Cambridge). *Spp1*$^{-/-}$ mice were kindly provided by Dr. David T. Denhardt (Rutgers University, Greensboro). All mice were used at 6-8 weeks old and were maintained under specific-pathogen-free conditions. Δdbl-GATA mice were purchased from The Jackson laboratory (Bar Harbor, ME, USA). Ly5.1 mice were purchased from Sankyo Laboratory (Tokyo, Japan). BALB/c, BALB/c nu/nu, and C57BL/6 mice were purchased from CLEA Japan (Tokyo, Japan). All of animals used in this study were female. The littermates of the same sex were randomly assigned to experimental groups. The research proposals were reviewed by the ethics committee for animals at Chiba University (registration number: 29-98, 29-99).

Human Samples

All participants with ECRS fulfilled the diagnostic criteria for ECRS prescribed by the Ministry of Health, Labor and Welfare, Japan. All participants as healthy controls did not have ECRS, asthma, other allergic diseases and any diseases that could affect their immune systems. The participants for this study were both male and female aged 20 to 68. The research proposals were reviewed by the ethics committee at Chiba University (registration number: 677). Informed consent was obtained from all participants.

METHOD DETAILS

Histology and immunohistochemistry

Pathological changes were evaluated by Haematoxylin & Eosin (H&E), Giemsa staining, Sirius-Red staining and immunofluororescent staining as previously described (Hirahara et al., 2008; Shinoda et al., 2016). Anti-Osteopontin (AF808, R&D Systems), anti-Siglec-F (E50-2440, BD Biosciences), anti-CD11b (M1/70, TONBO biosciences), anti-B220 (RA3-6B2, eBioscience) and DAPI Fluoromount-G® (SouthernBiotech) were used for immunofluorescent staining for mouse samples. Anti-Osteopontin (190312, R&D Systems) and anti-Siglec-8 (837535, R&D Systems) were used for immunofluorescent staining for human samples. Anti-Fibronectin

(EP5, Santa Cruz Biotechnology) was used for immunohistochemistry staining for human samples. The area of peribronchial Sirius Red staining in a paraffin-embedded lung was outlined and quantified using a light microscope (BIOREVO; KEYENCE Corp., Osaka, Japan) attached to an image-analysis system (Photoshop; Adobe Systems Inc., San Jose, California, USA). Results are expressed as the area of Sirius Red staining per micrometer length of basement membrane of bronchioles with 100 μm internal diameter. At least five bronchioles were counted in each slide. Basement membrane thickening was assessed as basement membrane per micrometer length of bronchus epithelium as previously reported (Valladao et al., 2016). At least five bronchioles were counted in each slide. Histological scores were determined based on the presence of the following: perivascular eosinophils (0–2), alveolar eosinophils (0–2), perivascular mononuclear cells (0–2), alveolar mononuclear cells (0–2), epithelial desquamation (normal = 0; elongation/distortion = 1; elongation, infolding, and narrowing = 2; loss of cells with broken airways = 3).

The Generation and Culture of Effector and Memory Th2 Cells

Splenic $CD62L^{+}CD44^{-}KJ1^{+}CD4^{+}$ T cells from DO11.10 OVA-specific TCR Tg mice were stimulated with an OVA peptide (Loh15, 1 μM) plus antigen-presenting cells (irradiated splenocytes) under Th2-cell-culture conditions (25 U/ml IL-2, 10 U/ml IL-4, and anti-IFN-γ monoclonal antibody) for 6 days *in vitro*. The effector Th2 cells (3×10^{7}) were transferred intravenously into BALB/c *nu/nu* or BALB/c recipient mice. Five weeks after cell transfer, $KJ1^{+}CD4^{+}$ T cells in the spleen were purified by autoMACS Sorter (Miltenyi Biotec, Bergisch Gladbach, Germany) and cell sorting (BD Aria II) and used as memory Th2 cells. Unless otherwise specifically noted, cells were stimulated with IL-33 at a concentration of 10 ng/ml for 72 hours. In some experiments, cells were stimulated with IL-25 (10 ng/ml) or TSLP (10 ng/ml).

Flow cytometry and sorting

Mouse memory Th2 cells were stained with anti-IL1rL1(ST2) (DIH9, BioLegend), and two subpopulations ($ST2^{low}$, $ST2^{high}$) were purified by FACS. Memory Th2 cells were stimulated with immobilized anti-TCRβ for 4 hours. Anti-Amphiregulin (206220, R&D Systems) was conjugated by ourselves using an Antibody Labeling Kit (Thermo Fisher Scientific) and used for intracellular staining of mouse samples. Anti-IL-5 (TRFK5, BioLegend), Anti-IL-4 (11B11, BioLegend) and Anti-IL-13 (eBio13A, eBioscience) were used for intracellular staining of mouse samples.

Anti-Siglec-F (E50-2440, BD Biosciences), Anti-CCR3 (83101, R&D Systems), Anti-CD101 (Moushi101, eBioscience) and Anti-CD62L (MEL-14, BioLegend) were used for cell surface staining of mouse samples.

T cells from PBMC and dissociated cells from the ECRS polyps were stained with anti-CD4 (OKT4, BioLegend), anti-CD45RO (UCHL1, BioLegend), anti-CD161 (HP-3G10, BioLegend), anti-CRTH2 (BM16, BioLegend), anti-Lineage Cocktails (BioLegend) and anti-CD127 (A019D5, BioLegend). Anti-Amphiregulin (31221, R&D Systems) was conjugated by ourselves using an Antibody Labeling Kit (Thermo Fisher Scientific) and used for intracellular staining for human samples. Anti-IL-5 (TRFK5, BioLegend) and anti-IFNγ (4S.B3, BioLegend) were used for intracellular staining of human samples.

Cell Viability Assay

Experiments were performed by using a FITC Annexin V Apoptosis Detection Kit I (BD Biosciences). Cells were washed, re-suspended in 100 μL 1X Binding Buffer, treated with 5 μL of FITC Annexin V and 5 μL PI, incubated for 15 min at RT in the dark, supplemented with 400 μL of 1X Binding Buffer and finally analyzed by flow cytometry.

ST2 Neutralizing Assay

Cells were incubated in the presence or absence of either anti-ST2 antibody (R&D Systems) or an isotype control antibody at a concentration of 1 μg/ml for 24 hours. After washing, cells were stimulated with IL-33 at a concentration of 10 ng/ml for 3 days.

Erlotinib Treatment

Erlotinib (Selleck, Houston, TX, USA) was dissolved in DMSO as described in the product manual. For *in vitro* experiments, Erlotinib was used to treat cells at a concentration of 100 nM and an equal amount of DMSO was used as a control. For *in vivo* experiments, Erlotinib was diluted with PBS and administered intraperitoneally at 12.5 mg/kg/day and an equal amount of DMSO diluted with PBS was administered intraperitoneally as a control.

Quantitative Real-Time PCR

Total RNA isolation, cDNA synthesis, and Quantitative real-time PCR was described previously (Endo et al., 2015). Primers and Roche Universal probes were purchased from Sigma and Roche, respectively. Primers and TaqMan probes were purchased from Applied Biosystems. Gene expression was normalized with the *Hprt* and *β-actin* mRNA signals and *GAPDH* (Human) mRNA signals.

RNA Sequencing

RNA-seq was carried out as previously described (Onodera et al., 2015). Total cellular RNA was extracted with TRIzol reagent (Invitrogen). For cDNA library construction, we used TruSeq RNA Sample Prep Kit v2 (Illumina) according to the manufacturer's protocol. Sequencing library fragments was performed on the HiSeq 1500 System. For data analysis, read sequences (50 bp) were

aligned to the mm10 mouse reference genome (University of California, Santa Cruz (UCSC) December 2011) using Bowtie 2 (version 2.0.0) and TopHat (version 1.3.2). Fragments per kilobase of exon per million mapped reads (FPKM) for each gene were calculated using Cufflinks (version 2.0.2).

ELISA for the Measurement of Amphiregulin Expression

Cells were stimulated with immobilized anti-TCR (10 μg/ml) in 48-well flat bottom plates (1.0×10^5 cells/well) for 24 hours at 37°C. The production of Amphiregulin was evaluated with a Mouse Amphiregulin DuoSet® ELISA kit (R&D systems) for mouse samples and with a Human Amphiregulin DuoSet® ELISA kit (R&D systems) for human samples according to the manufacturer's protocol.

BAL fluid Collecting

The trachea was exposed and lavaged with 1 mL PBS using a 20-gauge catheter. The collected cells in BAL fluid were sprayed on a glass slide, fixed, and stained with May-Giemsa staining using Diff-Quik stain. Cells on the slide glass were counted using a microscope.

Exposure of HDM

Dermatophagoides pteronyssinus extracts (Greer Laboratories Inc.) were administered to mice intranasaly: 200 μg on day 0, 100 μg on days 7 and 14, and then 50 μg of HDM was given twice per week for 4 weeks as reported previously (Doherty et al., 2011).

Immunization and inhalation with OVA

Mice were immunized i.p. with 250 μg of OVA (chicken egg albumin from Sigma-Aldrich) in 4 mg of aluminum hydroxide gel (Alum) on days 1 and 8. Mice were treated with aerosolized 1% OVA in saline for 30 min using a supersonic nebulizer (model NE-U07; Omron) on days 30, 33, 35, 37, 40 and 42. On day 43, various assays were performed.

For adoptive transfer experiments, OVA specific memory Th2 cells (3×10^6 cells) were transferred into mice, and then challenged with aerosolized 1% OVA on days 1, 3, 8 and 10. On day 11, various assays were performed.

Culture of Bone Marrow-Derived Eosinophils

Isolated bone marrow cells from BALB/c were stimulated with 100 ng/ml SCF (R & D Systems) plus 100 ng/ml FLT3 ligand (R & D Systems) for 4 days *in vitro*. After 4 days of culture, expanded cells were stimulated with 10 ng/ml IL-5 (R & D Systems) for 10 days.

In vitro treatment of Eosinophils with Amphiregulin

Eosinophils (1×10^6) from BALB/c bone marrow were stimulated with graded doses of Amphiregulin (0, 30, 100 and 300 ng/ml) in the presence or absence of Erlotinib (100 nM) for 72 hours. Unless otherwise specifically noted, eosinophils were cultured with Amphiregulin at a concentration of 100 ng/ml for 72 hours.

Adoptive Transfer of Eosinophils

OVA specific memory Th2 cells were transferred to mice on day 0. On days 1, 3, 8 and 10 bone marrow-derived eosinophils from *Spp1*$^{+/+}$ or *Spp1*$^{-/-}$ (1×10^8 in 200 μL saline) were injected intravenously into ΔdbI-GATA mice and finally exposed to aerosolized 1% OVA.

Intratracheal Administration of IL-33

On day 0, *Il33*$^{-/-}$ mice received recombinant mouse IL-33 (5cμg dissolved in 50cμl sterile saline; R&D Systems, Minneapolis, MN, USA) or control saline intratrachealy followed by adoptive transfer of OVA specific memory Th2 cells (3×10^6 cells). On days 1, 3, 8 and 10 mice were challenged with aerosolized 1% OVA.

Co-culture of Eosinophils and Fibroblasts

Experiments were performed with Transwell plates (0.4-mm pores; Corning, NY, USA). Fibroblasts in DMEM (with 10% FCS and Penicillin/Streptomycin) were cultured to confluence in 24-well tissue culture plates. Transwell inserts containing eosinophils (5×10^5) in RPMI complete media were co-cultured with the confluent fibroblasts at 37°C for 24 hours before fibroblasts were collected using Trypsin-EDTA.

Cell Isolation From Mouse Lungs

Epithelial cells, CD4$^+$ cells, CD8$^+$ cells, B220$^+$ cells, dendritic cells, macrophages, eosinophils and ILC2s were purified by autoMACS (Miltenyi Biotec, Bergisch Gladbach, Germany) from the lungs of mice. The following antibodies were used to identify each cell population; anti-EpCAM (G8.8, BioLegend), anti-CD4 (RM4-5, BD Biosciences), anti-CD8 (53-6.7, BD Biosciences), anti-B220 (RA3-6B2, eBioscience), anti-CD11c (HL3, BD Biosciences), anti-CD11b (M1/70, TONBO biosciences), anti-Siglec-F (E50-2440, BD Biosciences), anti-Lineage Cocktails (BioLegend) and anti-CD90.2 (30-H12, BioLegend). For the collection of fibroblasts, dissociated cells from lungs were seeded on 10 cm culture dish in DMEM including 10% FCS and Penicillin/Streptomycin and cultured at 37°C for 24 hours. After aspiration of supernatants, adherent fibroblasts were collected using Trypsin-EDTA.

Nasal Polyp, Peripheral Blood Mononuclear Cell and Homogenate Preparation

Nasal polyp mononuclear cells (NPMCs) were obtained as previously described (Yamamoto et al., 2007). In brief, freshly obtained nasal polyps were immediately minced and incubated in RPMI 1640 medium containing 1 mg/ml collagenase, 0.5 mg/ml hyaluronidase, and 0.2 mg/ml DNase I (Sigma-Aldrich). After incubation, NPMCs were purified by Ficoll-Hypaque technique. A volume of 1 mL of PBS was added for every 100 mg of tissue and was supplemented with aprotinin and leupeptin (Roche). Peripheral blood mononuclear cells (PBMCs) were obtained similarly. Human eosinophils were purified by autoMACS from PBMC and from nasal polyps using the Eosinophil Isolation Kit (Miltenyi Biotec, Bergisch Gladbach, Germany). FACS cell sorting (BD Aria II) was used to purify naive $CD4^+$ T cells ($CD4^+CD45RO^-$), memory-type $CD4^+$ T cells ($CD4^+CD45RO^+$) and ILCs ($Lineage^-CD127^+$).

QUANTIFICATION AND STATISTICAL ANALYSIS

Statistical Analysis

Data were analyzed with GraphPad Prism software (version 6). Comparisons of two groups were calculated with unpaired t test. Comparison of more than three groups were calculated with one-way analysis of variance (ANOVA) with Tukey's test. Differences with *p*-values below 0.05 were considered significant.

Analysis and graphic display of RNA-seq data

10,899 genes in which maximum FPKM value of each gene was equal to or greater than 1.0 were used for further analysis. Principal component analysis (PCA, rgl package) was perform by R (https://www.r-project.org/). A volcano plot was constructed by R (https://www.r-project.org/). Julia (https://julialang.org/, PyPlot and seaborn package) was used for constructing heatmaps.

Gene Ontology enrichment analysis

Gene Ontology enrichment analysis was performed with 10,899 genes by R and GSA package and c5.all.v5.2.symbols.gmt as GO term database (http://software.broadinstitute.org/gsea/msigdb) with FDR < 0.10 and p value < 0.01 as the cutoff value. A network of enriched GO terms was generated by Julia. Connection of the nodes was determined with cutoff level of Simpson coefficient $\geq$ 0.5. The network graph was visualized using Cytoscape (http://www.cytoscape.org/) and the Force Directed Layout with Simpson coefficient as a weight for the length of the spring.

DATA AND SOFTWARE AVAILABILITY

Raw and analyzed data reported in this paper are available under accession number GEO: GSE114921.

Immunity, Volume *49*

Supplemental Information

Amphiregulin-Producing Pathogenic Memory T Helper 2 Cells Instruct Eosinophils to Secrete Osteopontin and Facilitate Airway Fibrosis

Yuki Morimoto, Kiyoshi Hirahara, Masahiro Kiuchi, Tomoko Wada, Tomomi Ichikawa, Toshio Kanno, Mikiko Okano, Kota Kokubo, Atsushi Onodera, Daiju Sakurai, Yoshitaka Okamoto, and Toshinori Nakayama

Supplementary Information

Amphiregulin-producing pathogenic memory T helper-2 cells instruct eosinophils to secrete Osteopontin and facilitate airway fibrosis

Yuki Morimoto, Kiyoshi Hirahara, Masahiro Kiuchi, Tomoko Wada, Tomomi Ichikawa, Toshio Kanno, Mikiko Okano, Kota Kokubo, Atsushi Onodera, Daijyu Sakurai, Yoshitaka Okamoto, and Toshinori Nakayama

Figures and Figure Legends S1-S7

Figure S1

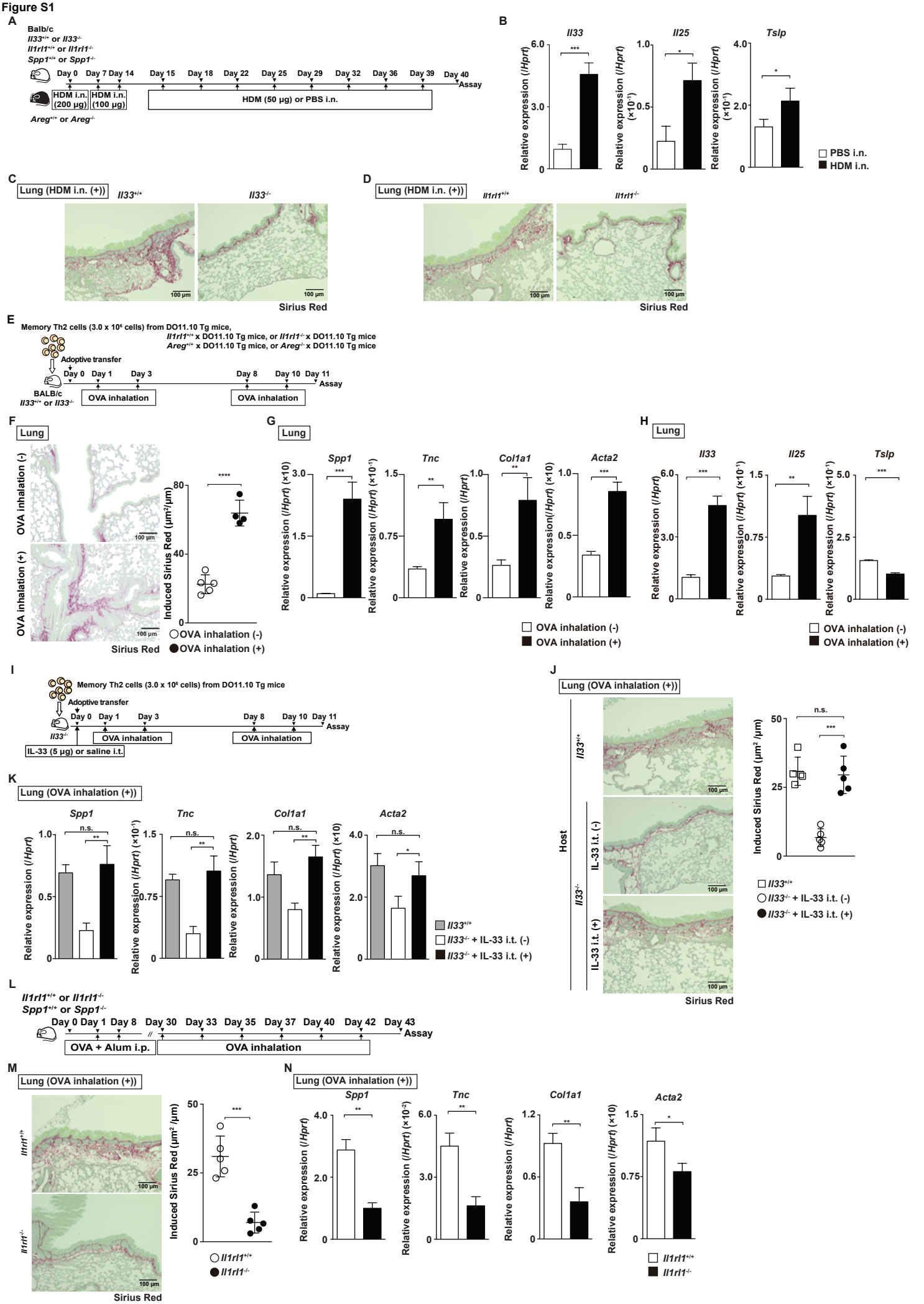

A
Balb/c
Il33+/+ or Il33-/-
Il1rl1+/+ or Il1rl1-/-
Spp1+/+ or Spp1-/-
Day 0 Day 7 Day 14 Day 15 Day 18 Day 22 Day 25 Day 29 Day 32 Day 36 Day 39 Day 40 Assay
HDM i.n. (200 μg)
HDM i.n. (100 μg)
HDM (50 μg) or PBS i.n.
Areg+/+ or Areg-/-
B
Il33
Il25
Tslp
Relative expression (/Hprt)
PBS i.n.
HDM i.n.
C
Lung (HDM i.n. (+))
Il33+/+
Il33-/-
100 μm
Sirius Red
D
Lung (HDM i.n. (+))
Il1rl1+/+
Il1rl1-/-
100 μm
Sirius Red
E
Memory Th2 cells (3.0 x 10^6 cells) from DO11.10 Tg mice,
Il1rl1+/+ x DO11.10 Tg mice, or Il1rl1-/- x DO11.10 Tg mice
Areg+/+ x DO11.10 Tg mice, or Areg-/- x DO11.10 Tg mice
Adoptive transfer
Day 0 Day 1 Day 3 Day 8 Day 10 Day 11 Assay
BALB/c
Il33+/+ or Il33-/-
OVA inhalation
OVA inhalation
F
Lung
OVA inhalation (-)
OVA inhalation (+)
100 μm
Induced Sirius Red (μm²/μm)
OVA inhalation (-)
OVA inhalation (+)
Sirius Red
G
Lung
Spp1
Tnc
Col1a1
Acta2
Relative expression (/Hprt)
OVA inhalation (-)
OVA inhalation (+)
H
Lung
Il33
Il25
Tslp
Relative expression (/Hprt)
OVA inhalation (-)
OVA inhalation (+)
I
Memory Th2 cells (3.0 x 10^6 cells) from DO11.10 Tg mice
Adoptive transfer
Day 0 Day 1 Day 3 Day 8 Day 10 Day 11 Assay
Il33-/-
OVA inhalation
OVA inhalation
IL-33 (5 μg) or saline i.t.
J
Lung (OVA inhalation (+))
Host
Il33+/+
Il33-/-
IL-33 i.t. (-)
IL-33 i.t. (+)
100 μm
Sirius Red
Induced Sirius Red (μm² /μm)
n.s.
Il33+/+
Il33-/- + IL-33 i.t. (-)
Il33-/- + IL-33 i.t. (+)
K
Lung (OVA inhalation (+))
Spp1
Tnc
Col1a1
Acta2
Relative expression (/Hprt)
n.s.
Il33+/+
Il33-/- + IL-33 i.t. (-)
Il33-/- + IL-33 i.t. (+)
L
Il1rl1+/+ or Il1rl1-/-
Spp1+/+ or Spp1-/-
Day 0 Day 1 Day 8 Day 30 Day 33 Day 35 Day 37 Day 40 Day 42 Day 43 Assay
OVA + Alum i.p.
OVA inhalation
M
Lung (OVA inhalation (+))
Il1rl1+/+
Il1rl1-/-
100 μm
Induced Sirius Red (μm² /μm)
Il1rl1+/+
Il1rl1-/-
Sirius Red
N
Lung (OVA inhalation (+))
Spp1
Tnc
Col1a1
Acta2
Relative expression (/Hprt)
Il1rl1+/+
Il1rl1-/-

Figure S1. Related to Figure 1. Antigen dependent airway inflammation causes lung fibrotic responses via the IL-33-ST2 axis.

(**A**) Experimental protocol for an airway inflammation mouse model using repetitive intranasal exposure to HDM. (**B**) Quantitative RT-PCR analysis of the indicated genes in lungs of mice with or without HDM exposure (n = 3 mice per group). Three independent experiments were performed with similar results. (**C**) Representative histology of lungs of *Il33*$^{+/+}$ and *Il33*$^{-/-}$ mice with HDM exposure as indicated in Figure **S1A**, fixed and stained with Sirius Red. Scale bars, 100 μm. More than 3 mice per group were analyzed. (**D**) Representative histology of lungs of *Il1rl1*$^{+/+}$ and *Il1rl1*$^{-/-}$ mice with HDM exposure as indicated in Figure S1**A**, fixed and stained with Sirius Red. Scale bars, 100 μm. More than 3 mice per group were analyzed. (**E**) Experimental protocol for Th2 cell-dependent allergic inflammation mouse model employing adoptive transfer of memory Th2 cells. (**F**) Representative histology of lungs of mice with or without OVA inhalation, fixed and stained with Sirius Red (left). Scale bars, 100 μm. Shown are ratios of areas of randomly selected regions stained with Sirius Red surrounding bronchi versus the areas of associated basement membranes (right). More than 3 mice per group were analyzed. (**G**) Quantitative RT-PCR analysis of the indicated genes in lung of mice with or without OVA inhalation (n = 3 mice per group). Three independent experiments were performed with similar results. (**H**) Quantitative RT-PCR analysis of the indicated genes in lungs of mice with or without OVA inhalation (n = 3 mice per group). Three independent experiments were performed with similar results. (**I**) Experimental protocol for an allergic inflammation mouse model employing adoptive transfer of memory Th2 cells followed by intratracheal (i.t.) administration of recombinant IL-33. (**J**) Representative histology of lungs of *Il33*$^{+/+}$ and *Il33*$^{-/-}$ mice with or without administration of IL-33 or saline followed by OVA inhalation, fixed and stained with Sirius Red (left). Scale bars, 100 μm. Shown are ratios of areas of randomly selected regions stained with Sirius Red surrounding bronchi versus areas of associated basement membranes (right). More than 3 mice per group were analyzed. (**K**) Quantitative RT-PCR analysis of the indicated genes in lungs of *Il33*$^{+/+}$ and *Il33*$^{-/-}$ mice with or without administration of IL-33 or saline followed by OVA inhalation (n = 3 mice per group). Three independent experiments were performed with similar results. Data are the mean ± SD. **P* < 0.05, ***P* < 0.01, ****P* < 0.001; n.s., not significant; by unpaired t test or one-way analysis of variance (ANOVA). (**L**) Experimental protocol for an allergic airway inflammation mouse model using intraperitoneal (i.p.) immunization with OVA and aluminum hydroxide gel (Alum) followed by OVA inhalation. (**M**) Representative histology of lungs of *Il1rl1*$^{+/+}$ and *Il1rl1*$^{-/-}$ mice challenged with OVA as indicated in Figure **S1L**, fixed and stained with Sirius Red (left). Scale bars, 100 μm. Shown are ratios of areas of randomly selected regions stained with Sirius Red surrounding bronchi versus areas of associated basement membranes (right). More than 3 mice per group were analyzed. (**N**) Quantitative RT-PCR analysis of the indicated genes in *Il1rl1*$^{+/+}$ and *Il1rl1*$^{-/-}$ mice challenged with OVA as indicated in Figure **S1L** (n = 3 mice per group). Three independent experiments were performed with similar results. Data are the mean ± SD. **P* < 0.05, ***P* < 0.01, ****P* < 0.001; n.s., not significant; by unpaired t test or one-way analysis of variance (ANOVA).

Figure S2

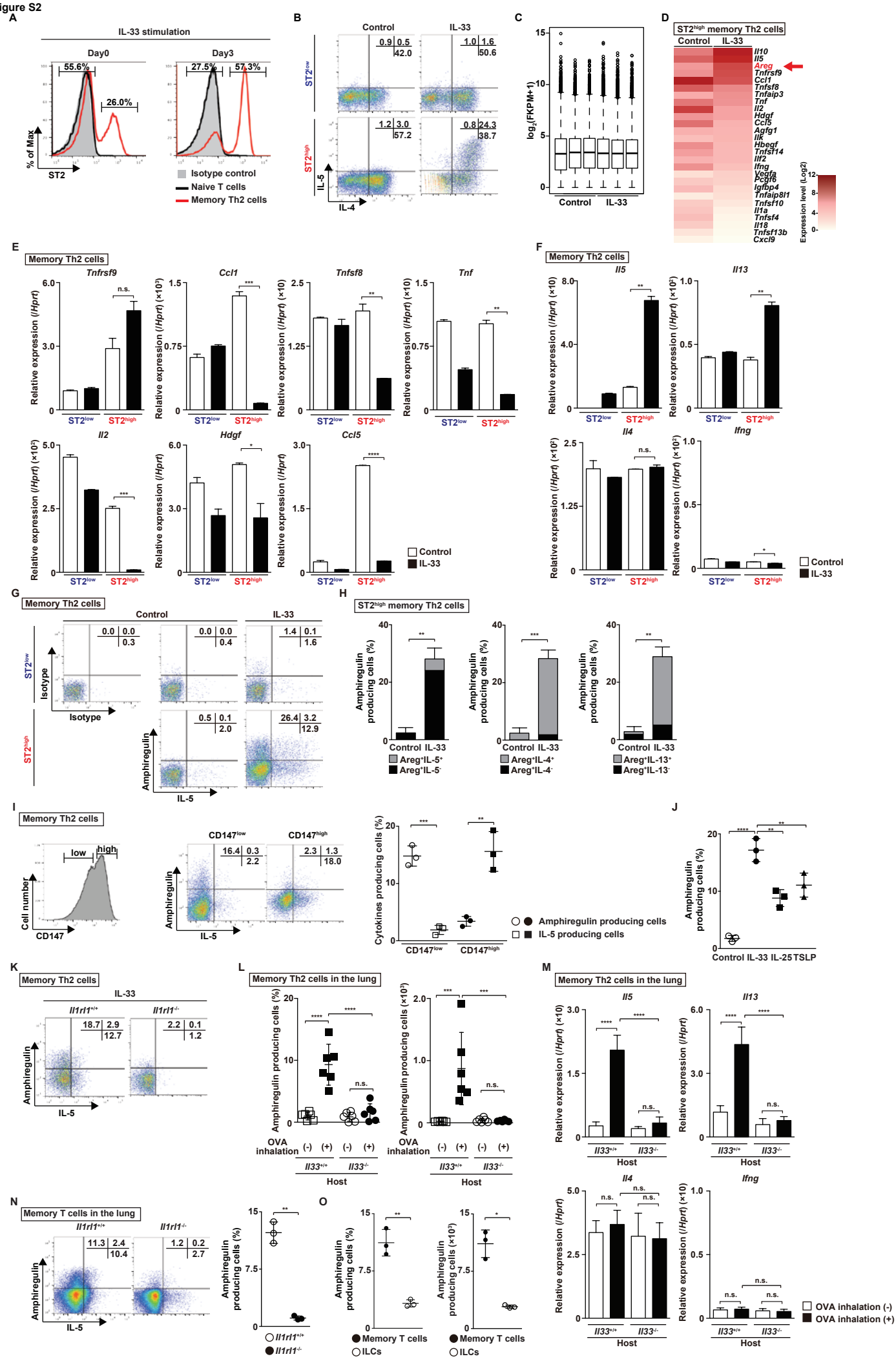

A
IL-33 stimulation
Day0
Day3
55.6%
26.0%
27.5%
57.3%
% of Max
ST2
Isotype control
Naive T cells
Memory Th2 cells
B
Control
IL-33
ST2low
ST2high
IL-5
IL-4
C
log2(FKPM+1)
Control
IL-33
D
ST2high memory Th2 cells
Control
IL-33
Il10
Il5
Areg
Tnfrsf9
Ccl1
Tnfsf8
Tnfaip3
Tnf
Il2
Hdgf
Ccl5
Agfg1
Ilk
Hbegf
Tnfsf14
Il1f2
Ifng
Vegfa
Pc3f6
Igfbp4
Tnfaip8l1
Tnfsf10
Il1a
Tnfsf4
Il18
Tnfsf13b
Cxcl9
Expression level (Log2)
E
Memory Th2 cells
Tnfrsf9
Ccl1
Tnfsf8
Tnf
Il2
Hdgf
Ccl5
Relative expression (/Hprt)
n.s.
ST2low
ST2high
Control
IL-33
F
Memory Th2 cells
Il5
Il13
Il4
Ifng
G
Memory Th2 cells
Control
IL-33
Isotype
Amphiregulin
IL-5
H
ST2high memory Th2 cells
Amphiregulin producing cells (%)
Areg+IL-5+
Areg+IL-5-
Areg+IL-4+
Areg+IL-4-
Areg+IL-13+
Areg+IL-13-
I
Memory Th2 cells
low
high
Cell number
CD147
CD147low
CD147high
Cytokines producing cells (%)
Amphiregulin producing cells
IL-5 producing cells
J
Amphiregulin producing cells (%)
Control
IL-33
IL-25
TSLP
K
Memory Th2 cells
IL-33
Il1rl1+/+
Il1rl1-/-
L
Memory Th2 cells in the lung
Amphiregulin producing cells (%)
Amphiregulin producing cells (×10³)
OVA inhalation
Il33+/+
Il33-/-
Host
M
Memory Th2 cells in the lung
Il5
Il13
Il4
Ifng
N
Memory T cells in the lung
O
Memory T cells
ILCs
OVA inhalation (-)
OVA inhalation (+)

Figure S2. Related to Figure 2. IL-33 stimulation induces production of Amphiregulin and type 2 cytokines in ST2^{hi} memory Th2 cells both *in vitro* and *in vivo*.

(**A**) Shown are cell surface-staining profiles of ST2 in naïve and memory Th2 cells before (left panel) and after (right) IL-33 stimulation. (**B**) Shown are intracellular-staining profiles of IL-4 and IL-5 in naïve and memory Th2 cells with or without IL-33 stimulation. (**C**) Shown are box plots of RNA-Seq data from ST2^{hi} memory Th2 cells stimulated with or without IL-33. (**D**) ST2^{hi} memory Th2 cells were cultured with or without IL-33 for 72 hours. Shown is a heatmap depicting humoral factor genes with statistically significant changes between IL-33 treated or untreated samples. (**E**, **F**) Shown are plots of quantitative RT-PCR analyses of the indicated genes in ST2^{low} or ST2^{hi} memory Th2 cells. Four independent experiments were performed with similar results. (**G**) Shown are FACS plots of intracellular Amphiregulin and IL-5 with isotype controls. (**H**) Shown is percentage of Amphiregulin-producing ST2^{hi} memory Th2 cells among ST2^{hi} memory Th2 cells with or without IL33 stimulation. Amphiregulin only-producing ST2^{hi} memory Th2 cells (Areg^{+}IL-5^{-}, Areg^{+}IL-4^{-} and Areg^{+}IL-13^{-}) are shown in black, and ST2^{hi} memory Th2 cells producing Amphiregulin with the indicated cytokines (Areg^{+}IL-5^{+}, Areg^{+}IL-4^{+} and Areg^{+}IL-13^{+}) are shown in gray. Data are the mean ± SD. **P* < 0.05, ***P* < 0.01, ****P* < 0.001, *****P* < 0.0001; n.s., not significant; by unpaired t test or one-way analysis of variance (ANOVA). (**I**) Shown is a cell surface-staining profile of CD147 in memory Th2 cells (left panel). Shown are FACS plots of intracellular Amphiregulin and IL-5 expression in CD147^{low} memory Th2 cells and CD147^{high} memory Th2 cells (middle panel). Shown are the percentages of Amphiregulin producing cells (circle) and IL-5 producing cells (square) in CD147^{low} memory Th2 cells (white) or CD147^{high} memory Th2 cells (black) (right panel). Data are the mean ± SD. ***P* < 0.01, ****P* < 0.001; by unpaired t test. (**J**) Shown are the percentage of Amphiregulin-producing memory Th2 cells among memory Th2 cells stimulated with the indicated cytokines for 72 hours. (**K**) Shown are FACS plots of intracellular Amphiregulin and IL-5 in *Il1rl1*$^{+/+}$ and *Il1rl1*$^{-/-}$ memory Th2 cells stimulated with IL-33 for 72 hours. (**L**) Shown are the ratios of Amphiregulin producing memory Th2 cells in whole memory Th2 cells (left) and absolute numbers of them (right) in the lungs from *Il33*$^{+/+}$ and *Il33*$^{-/-}$ recipients with or without OVA challenges. (**M**) Shown are quantitative RT-PCR analyses of the indicated genes in lung memory Th2 cells from *Il33*$^{+/+}$ and *Il33*$^{-/-}$ recipients (n = 6). (**N**) Shown are FACS plots of intracellular Amphiregulin and IL-5 in lung memory T cells from *Il1rl1*$^{+/+}$ and *Il1rl1*$^{-/-}$ mice treated with OVA and Alum twice followed by a series of OVA inhalations (left). Shown is the percentage of Amphiregulin-producing memory T cells among memory T cells from the lungs of *Il1rl1*$^{+/+}$ and *Il1rl1*$^{-/-}$ mice (right). (**O**) Shown is the percentage of Amphiregulin-producing cells among memory T cells or ILCs (left), and the absolute numbers of Amphiregulin-producing memory T cells and ILCs (right) in the lungs of mice challenged with OVA as indicated in Figure **S1L**. Data are the mean ± SD. **P* < 0.05, ***P* < 0.01, ****P* < 0.001, *****P* < 0.0001; n.s., not significant; by unpaired t test or one-way analysis of variance (ANOVA).

Figure S3

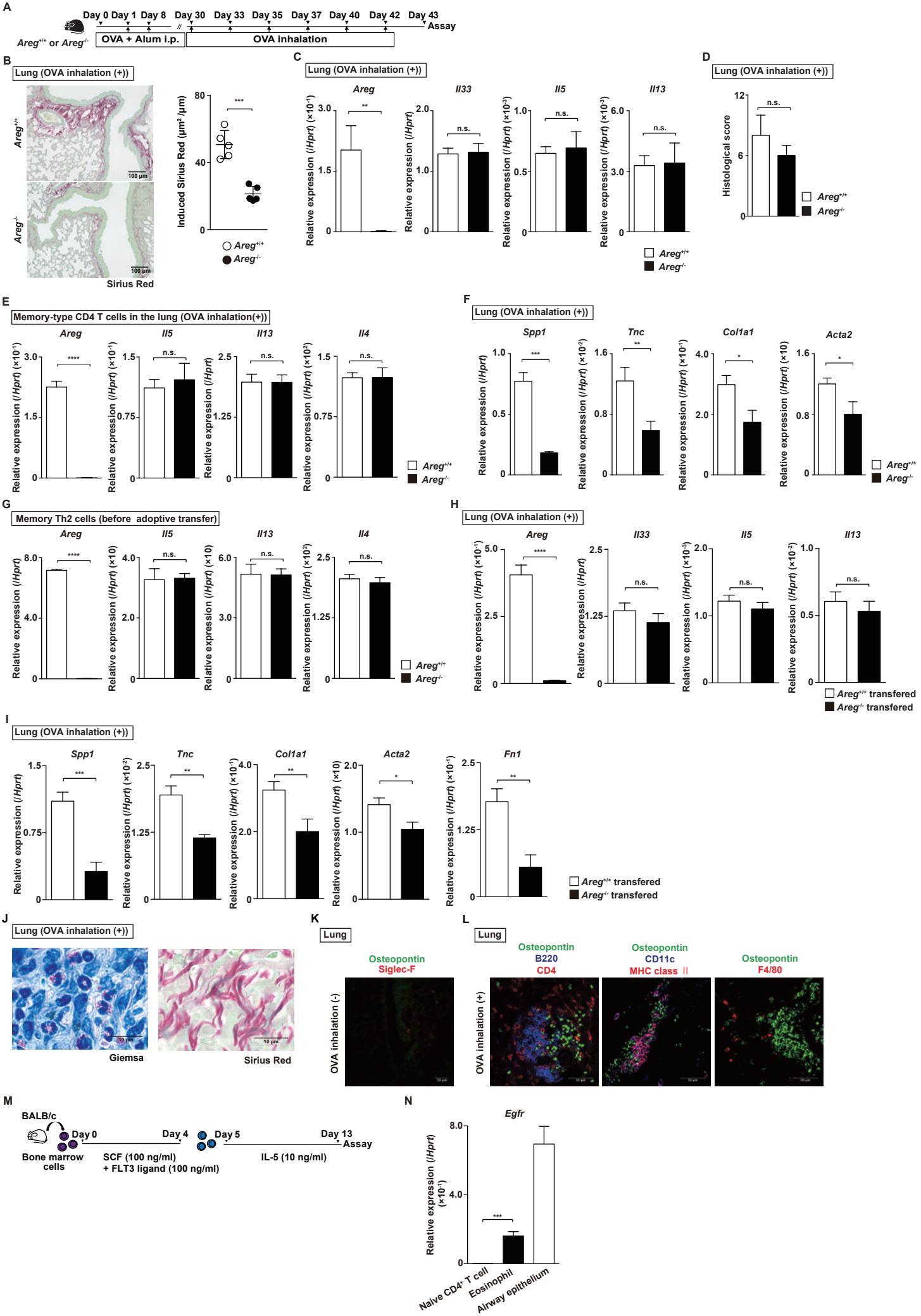

A
Day 0 Day 1 Day 8 Day 30 Day 33 Day 35 Day 37 Day 40 Day 42 Day 43
Assay
Areg+/+ or Areg-/-
OVA + Alum i.p.
OVA inhalation
B
Lung (OVA inhalation (+))
Areg+/+
Areg-/-
100 μm
Induced Sirius Red (μm2 /μm)
***
Areg+/+
Areg-/-
Sirius Red
C
Lung (OVA inhalation (+))
Areg
Il33
Il5
Il13
Relative expression (/Hprt)
**
n.s.
Areg+/+
Areg-/-
D
Lung (OVA inhalation (+))
Histological score
n.s.
Areg+/+
Areg-/-
E
Memory-type CD4 T cells in the lung (OVA inhalation(+))
Areg
Il5
Il13
Il4
Relative expression (/Hprt)
****
n.s.
Areg+/+
Areg-/-
F
Lung (OVA inhalation (+))
Spp1
Tnc
Col1a1
Acta2
Relative expression (/Hprt)
***
**
*
Areg+/+
Areg-/-
G
Memory Th2 cells (before adoptive transfer)
Areg
Il5
Il13
Il4
Relative expression (/Hprt)
****
n.s.
Areg+/+
Areg-/-
H
Lung (OVA inhalation (+))
Areg
Il33
Il5
Il13
Relative expression (/Hprt)
****
n.s.
Areg+/+ transfered
Areg-/- transfered
I
Lung (OVA inhalation (+))
Spp1
Tnc
Col1a1
Acta2
Fn1
Relative expression (/Hprt)
***
**
*
Areg+/+ transfered
Areg-/- transfered
J
Lung (OVA inhalation (+))
10 μm
Giemsa
Sirius Red
K
Lung
Osteopontin
Siglec-F
OVA inhalation (-)
L
Lung
Osteopontin
B220
CD4
Osteopontin
CD11c
MHC class II
Osteopontin
F4/80
OVA inhalation (+)
M
BALB/c
Day 0
Day 4
Day 5
Day 13
Assay
Bone marrow cells
SCF (100 ng/ml) + FLT3 ligand (100 ng/ml)
IL-5 (10 ng/ml)
N
Egfr
Relative expression (/Hprt) (×10-1)
***
Naive CD4+ T cell
Eosinophil
Airway epithelium

Figure S3. Related to Figure 3. OVA challenge induces fibrotic changes by Amphiregulin produced from memory Th2 cells and production of Osteopontin from eosinophils in the asthmatic lung.

(**A**) Experimental protocol for an allergic airway inflammation mouse model using intraperitoneal (i.p.) OVA and aluminum hydroxide gel (Alum) treatment. (**B**) *Areg*$^{+/+}$ and *Areg*$^{-/-}$ mice were challenged with OVA as indicated in Figure **S3A**. Shown is a representative confocal micrograph of lung tissue stained with Sirius Red from an *Areg*$^{+/+}$ and an *Areg*$^{-/-}$ mouse (left). Scale bars represent 100 μm. Shown are ratios of areas of randomly selected regions stained with Sirius Red surrounding bronchi versus the areas of associated basement membranes (right). More than 3 mice per group were analyzed. (**C**) Shown are quantitative RT-PCR analyses of the indicated genes in the lungs of *Areg*$^{+/+}$ and *Areg*$^{-/-}$ mice challenged with OVA inhalation (n = 3 mice per group). Three independent experiments were performed with similar results. (**D**) Shown are the histological scores of H & E-stained lung sections from *Areg*$^{+/+}$ and *Areg*$^{-/-}$ mice. Histological scores were calculated according to the criteria indicated in STAR Methods (n = 3). (**E**) Shown are quantitative RT-PCR analyses of the indicated genes in lung memory Th2 cells from *Areg*$^{+/+}$ or *Areg*$^{-/-}$ mice (n = 3). (**F**) Quantitative RT-PCR analysis of the indicated genes in the lungs of *Areg*$^{+/+}$ and *Areg*$^{-/-}$ mice with OVA inhalation (n = 3 mice per group). (**G**) Shown are quantitative RT-PCR analyses of the indicated genes in memory Th2 cells from *Areg*$^{+/+}$ or *Areg*$^{-/-}$ mice (n = 3) prior to adoptive transfer. (**H**) Shown are quantitative RT-PCR analyses of the indicated genes in lungs from recipients of *Areg*$^{+/+}$ or *Areg*$^{-/-}$ memory Th2 cells (n = 3 mice per group). (**I**) Shown are quantitative RT-PCR analyses of the indicated genes in lungs from recipients of *Areg*$^{+/+}$ or *Areg*$^{-/-}$ memory Th2 cells (n = 3 mice per group). Data are the mean ± SD. $*P < 0.05$, $**P < 0.01$, $***P < 0.001$, $****P < 0.0001$; n.s., not significant; by unpaired t test or one-way analysis of variance (ANOVA). (**J**) Shown is a representative histological analysis of lungs from mice fixed and stained with Giemsa (left) and Sirius Red (right). Scale bars represent 10 μm. Three independent experiments were performed with similar results. (**K**) Shown are representative confocal micrographs of lungs stained with anti-Osteopontin (green) and anti-Siglec-F (red) from mice without OVA inhalation. Scale bars represent 50 μm. (**L**) Shown are representative confocal micrographs of mouse lungs stained with anti-CD4 (red), anti- Osteopontin (green), and anti-B220 (blue) (left), anti-MHC class II (red), anti-Osteopontin (green), and anti-CD11c (blue) (middle), anti- Osteopontin (green), and anti-F4/80 (red). Scale bars represent 50 μm. Three independent experiments were performed with similar results. (**M**) Experimental protocol for differentiation of mouse bone marrow derived eosinophils. (**N**) Shown is a quantitative RT-PCR analysis of *Egfr* in the indicated cell types. Bone marrow-derived eosinophils were cultured with or without Amphiregulin for 72 hours. Data are the mean ± SD. $***P < 0.001$; by one-way analysis of variance (ANOVA).

Figure S4

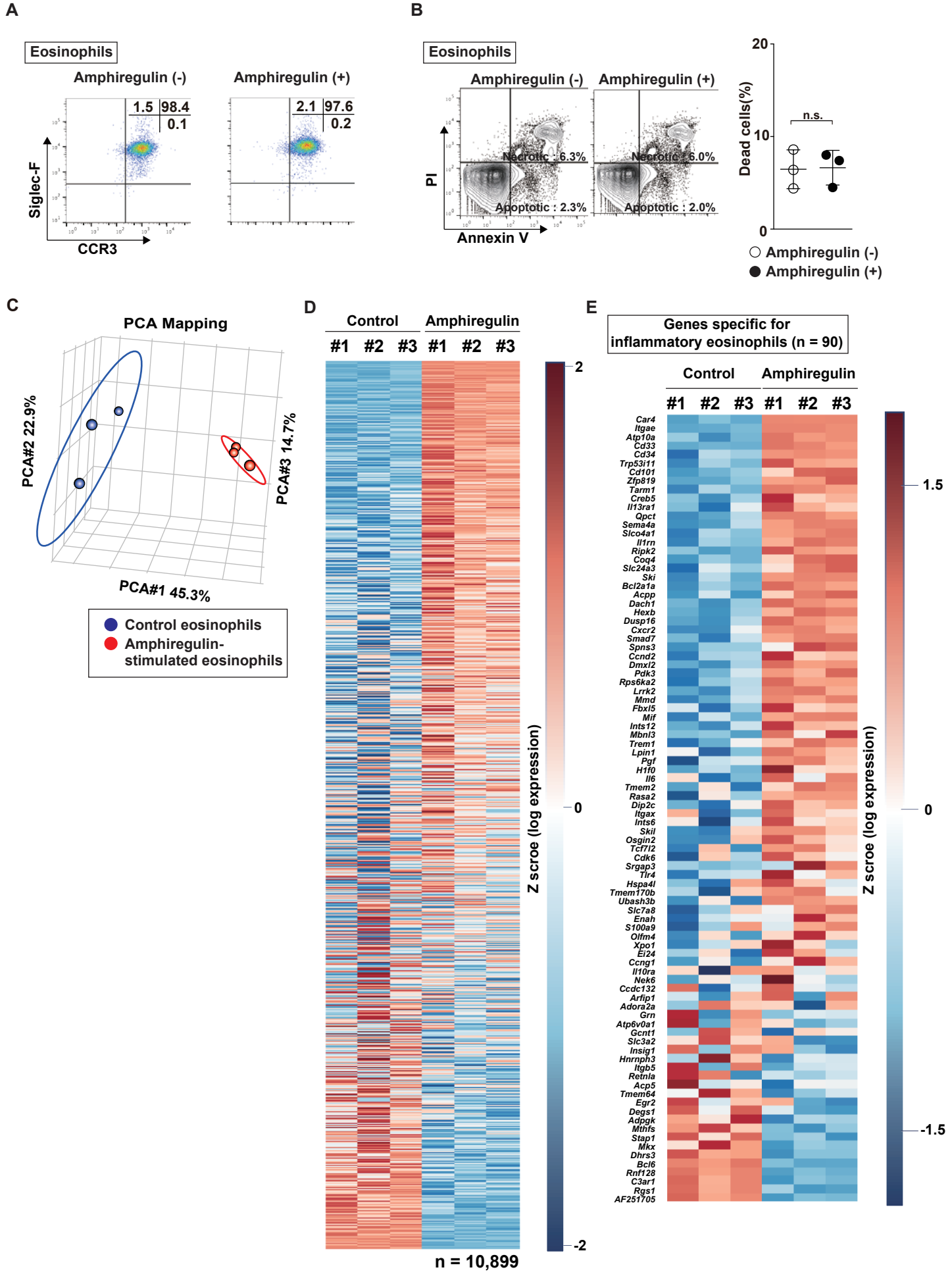

A
Eosinophils
Amphiregulin (-)
Amphiregulin (+)
1.5
98.4
0.1
2.1
97.6
0.2
Siglec-F
CCR3
B
Eosinophils
Amphiregulin (-)
Amphiregulin (+)
Necrotic : 6.3%
Necrotic : 6.0%
Apoptotic : 2.3%
Apoptotic : 2.0%
PI
Annexin V
Dead cells(%)
20
10
0
n.s.
Amphiregulin (-)
Amphiregulin (+)
C
PCA Mapping
PCA#2 22.9%
PCA#3 14.7%
PCA#1 45.3%
Control eosinophils
Amphiregulin-stimulated eosinophils
D
Control
Amphiregulin
#1 #2 #3 #1 #2 #3
2
0
-2
Z scroe (log expression)
n = 10,899
E
Genes specific for inflammatory eosinophils (n = 90)
Control
Amphiregulin
#1 #2 #3 #1 #2 #3
Car4
Itgae
Atp10a
Cd33
Cd34
Trp53i11
Cd101
Zfp819
Tarm1
Creb5
Il13ra1
Qpct
Sema4a
Slco4a1
Il1rn
Ripk2
Coq4
Slc24a3
Ski
Bcl2a1a
Acpp
Dach1
Hexb
Dusp16
Cxcr2
Smad7
Spns3
Ccnd2
Dmxl2
Pdk3
Rps6ka2
Lrrk2
Mmd
Fbxl5
Mif
Ints12
Mbnl3
Trem1
Lpin1
Pgf
H1f0
Il6
Tmem2
Rasa2
Dip2c
Itgax
Ints6
Skil
Osgin2
Tcf7l2
Cdk6
Srgap3
Tlr4
Hspa4l
Tmem170b
Ubash3b
Slc7a8
Enah
S100a9
Olfm4
Xpo1
Ei24
Ccng1
Il10ra
Nek6
Ccdc132
Arfip1
Adora2a
Grn
Atp6v0a1
Gcnt1
Slc3a2
Insig1
Hnrnph3
Itgb5
Retnla
Acp5
Tmem64
Egr2
Degs1
Adpgk
Mthfs
Stap1
Mkx
Dhrs3
Bcl6
Rnf128
C3ar1
Rgs1
AF251705
1.5
0
-1.5
Z scroe (log expression)

Figure S4. Related to Figure 4. Amphiregulin stimulation induces Osteopontin production via EGFR signaling both *in vitro* and *in vivo*.

(**A**) Shown are FACS plots of CCR3 and Siglec-F expression in eosinophils with or without Amphiregulin stimulation for 72 hours. (**B**) Shown are FACS plots of PI and Annexin V expression in eosinophils with or without Amphiregulin stimulation for 72 hours as indicated in STAR Methods (left). Shown are the percentage of dead cells among total cells (right). (**C**) Shown is a PCA plot of RNA-Seq data from eosinophils stimulated with or without Amphiregulin. (**D**) Shown is a heatmap of the expression of 10,899 genes in eosinophils stimulated with Amphiregulin and in control unstimulated eosinophils (n = 3 per group). (**E**) Shown is a heat map of Log10 expression values of signature genes for inflammatory eosinophils (n = 90) [as defined in a previous report *(Mesnil et al, J Clin Invest, 2016;PMID:27548519)*], in eosinophils stimulated with or without Amphiregulin. Data are the mean ± SD. n.s., not significant; by unpaired t test.

Figure S5

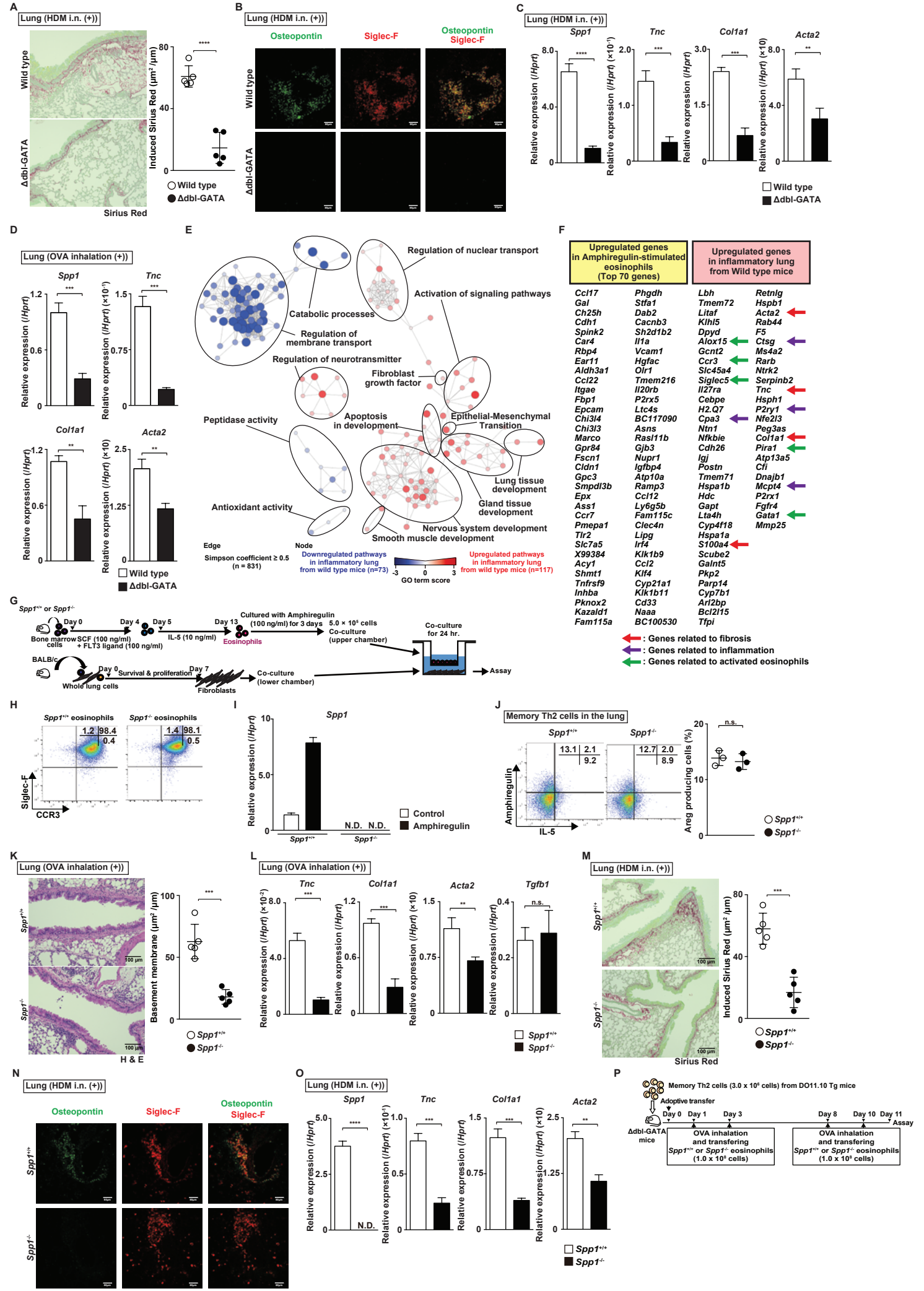

A
Lung (HDM i.n. (+))
Wild type
ΔdblGATA
Sirius Red
Induced Sirius Red (μm² /μm)
Wild type
ΔdblGATA
B
Lung (HDM i.n. (+))
Osteopontin
Siglec-F
Osteopontin Siglec-F
Wild type
ΔdblGATA
C
Lung (HDM i.n. (+))
Spp1
Tnc
Col1a1
Acta2
Relative expression (/Hprt)
Wild type
ΔdblGATA
D
Lung (OVA inhalation (+))
Spp1
Tnc
Col1a1
Acta2
Relative expression (/Hprt)
Wild type
ΔdblGATA
E
Regulation of nuclear transport
Activation of signaling pathways
Catabolic processes
Regulation of membrane transport
Regulation of neurotransmitter
Fibroblast growth factor
Peptidase activity
Apoptosis in development
Epithelial-Mesenchymal Transition
Lung tissue development
Gland tissue development
Antioxidant activity
Nervous system development
Smooth muscle development
Edge
Node
Simpson coefficient ≥ 0.5 (n = 831)
Downregulated pathways in inflammatory lung from wild type mice (n=73)
GO term score
Upregulated pathways in inflammatory lung from wild type mice (n=117)
F
Upregulated genes in Amphiregulin-stimulated eosinophils (Top 70 genes)
Upregulated genes in inflammatory lung from Wild type mice
Ccl17 Gal Ch25h Cdh1 Spink2 Car4 Rbp4 Ear11 Aldh3a1 Ccl22 Itgae Fbp1 Epcam Chi3l4 Chi3l3 Marco Gpr84 Fscn1 Cldn1 Gpc3 Smpdl3b Epx Ass1 Ccr7 Pmepa1 Tlr2 Slc7a5 X99384 Acy1 Shmt1 Tnfrsf9 Inhba Pknox2 Kazald1 Fam115a
Phgdh Stfa1 Dab2 Cacnb3 Sh2d1b2 Il1a Vcam1 Hgfac Olr1 Tmem216 Il20rb P2rx5 Ltc4s BC117090 Asns Rasl11b Gjb3 Nupr1 Igfbp4 Atp10a Ramp3 Ccl12 Ly6g5b Fam115c Clec4n Lipg Irf4 Klk1b9 Ccl2 Klf4 Cyp21a1 Klk1b11 Cd33 Naaa BC100530
Lbh Tmem72 Litaf Klhl5 Dpyd Alox15 Gcnt2 Ccr3 Slc45a4 Siglec5 Il27ra Cebpe H2.Q7 Cpa3 Ntn1 Nfkbie Cdh26 Igj Postn Tmem71 Hspa1b Hdc Gapt Lta4h Cyp4f18 Hspa1a S100a4 Scube2 Galnt5 Pkp2 Parp14 Cyp7b1 Arl2bp Bcl2l15 Tfpi
Retnlg Hspb1 Acta2 Rab44 F5 Ctsg Ms4a2 Rarb Ntrk2 Serpinb2 Tnc Hsph1 P2ry1 Nfe2l3 Peg3as Col1a1 Pira1 Atp13a5 Cfi Dnajb1 Mcpt4 P2rx1 Fgfr4 Gata1 Mmp25
: Genes related to fibrosis
: Genes related to inflammation
: Genes related to activated eosinophils
G
Spp1+/+ or Spp1-/-
Bone marrow cells
Day 0
SCF (100 ng/ml) + FLT3 ligand (100 ng/ml)
Day 4
Day 5
IL-5 (10 ng/ml)
Day 13
Eosinophils
Cultured with Amphiregulin (100 ng/ml) for 3 days
5.0 × 10⁵ cells Co-culture (upper chamber)
Co-culture for 24 hr.
Assay
BALB/c
Whole lung cells
Day 0
Survival & proliferation
Day 7
Fibroblasts
Co-culture (lower chamber)
H
Spp1+/+ eosinophils
Spp1-/- eosinophils
Siglec-F
CCR3
I
Spp1
Relative expression (/Hprt)
N.D.
Control
Amphiregulin
J
Memory Th2 cells in the lung
Spp1+/+
Spp1-/-
Amphiregulin
IL-5
Areg producing cells (%)
n.s.
K
Lung (OVA inhalation (+))
Spp1+/+
Spp1-/-
H & E
Basement membrane (μm² /μm)
L
Lung (OVA inhalation (+))
Tnc
Col1a1
Acta2
Tgfb1
Relative expression (/Hprt)
n.s.
M
Lung (HDM i.n. (+))
Spp1+/+
Spp1-/-
Sirius Red
Induced Sirius Red (μm² /μm)
N
Lung (HDM i.n. (+))
Osteopontin
Siglec-F
Osteopontin Siglec-F
Spp1+/+
Spp1-/-
O
Lung (HDM i.n. (+))
Spp1
Tnc
Col1a1
Acta2
Relative expression (/Hprt)
N.D.
P
Memory Th2 cells (3.0 x 10⁶ cells) from DO11.10 Tg mice
Adoptive transfer
ΔdblGATA mice
Day 0
Day 1
Day 3
Day 8
Day 10
Day 11
Assay
OVA inhalation and transfering Spp1+/+ or Spp1-/- eosinophils (1.0 x 10⁵ cells)
OVA inhalation and transfering Spp1+/+ or Spp1-/- eosinophils (1.0 x 10⁵ cells)

Figure S5. Related to Figure 5. Amphiregulin stimulation induces Osteopontin production via EGFR signaling both *in vitro* and *in vivo*.

(**A**) Wild type mice and Δdbl-GATA mice were exposed to HDM as indicated in Figure **S1A**. Shown is a representative confocal micrograph of lung tissue stained with Sirius Red from a wild type mouse and a Δdbl-GATA mouse (left). Scale bars represent 100 μm. Shown are ratios of areas of randomly selected regions stained with Sirius Red surrounding bronchi versus areas of associated basement membranes (right). More than 3 mice per group were analyzed. (**B**) Shown is a representative confocal micrograph of lungs stained with anti-Osteopontin (green) and Siglec-F (red) from wild type and Δdbl-GATA mice with HDM exposure (Scale bars represent 50 μm). Three independent experiments were performed with similar results. (**C**) Quantitative RT-PCR analysis of the indicated genes in the lungs from wild type mice and Δdbl-GATA mice with HDM exposure (n = 3 mice per group). (**D**) OVA specific memory Th2 cells (3 x 10^6 cells) were transferred i.v. into wild type and Δdbl-GATA mice that were subsequently challenged with OVA. Quantitative RT-PCR analysis of the indicated genes in the lungs of wild type and Δdbl-GATA mice challenged with OVA. (n = 3 mice per group). (**E**) Shown is a network visualization of Gene Ontology enrichment analysis. Node colors indicate GO terms that were significantly upregulated (red) or downregulated (blue) in the lungs of wild type mice challenged with OVA compared to Δdbl-GATA mice challenged with OVA. Node sizes are proportional to enrichment scores for each GO terms. Node connections were determined using overlap of the elemental gene products in the GO terms (Simpson coefficient ≥ 0.5). (**F**) Shown is a list of the top 70 upregulated genes in Amphiregulin-stimulated eosinophils and all upregulated genes in inflamed lungs from wild-type mice. Red arrows indicate genes related to fibrosis, purple arrows indicate genes related to inflammation and green arrows indicate genes related to activated eosinophils. (**G**) Experimental protocol for co-culture of eosinophils and fibroblasts as indicated in STAR Methods. (**H**) Shown are FACS plots of CCR3 and Siglec-F expression on *Spp1*$^{+/+}$ and *Spp1*$^{-/-}$ eosinophils. (**I**) Quantitative RT-PCR analysis of *Spp1* in *Spp1*$^{+/+}$ and *Spp1*$^{-/-}$ eosinophils treated with or without Amphiregulin for 72 hours (n = 3 samples per group). (**J**) *Spp1*$^{+/+}$ and *Spp1*$^{-/-}$ mice were challenged with OVA as indicated in Figure **S1L**. Shown are FACS plots of intracellular Amphiregulin and IL-5 in lung memory CD4$^+$ T cells from *Spp1*$^{+/+}$ and *Spp1*$^{-/-}$ mice (left). Shown is the percentage of Amphiregulin producing memory T cells among total memory T cells of lungs from *Spp1*$^{+/+}$ and *Spp1*$^{-/-}$ mice (right). (**K**) Shown is a representative confocal micrograph of H & E stained lung tissue from a *Spp1*$^{+/+}$ mouse and a *Spp1*$^{-/-}$ mouse (left). Scale bars represent 100 μm. Shown are ratios of areas of basement membranes surrounding bronchi versus length of bronchus epithelium (right). More than 3 mice per group were analyzed. (**L**) Quantitative RT-PCR analysis of the indicated genes in the lungs of *Spp1*$^{+/+}$ and *Spp1*$^{-/-}$ mice challenged with OVA. (n = 3 mice per group). Data are the mean ± SD. $^{**}P < 0.01$, $^{***}P < 0.001$, $^{****}P < 0.0001$; n.s., not significant; by unpaired t test. (**M**) *Spp1*$^{+/+}$ and *Spp1*$^{-/-}$ mice were exposed to HDM as indicated in Figure **S1A**. Shown is a representative confocal micrograph of lung tissue stained with Sirius Red from a *Spp1*$^{+/+}$ and a *Spp1*$^{-/-}$ mouse (left). Scale bars represent 100 μm. Shown are ratios of areas of randomly

selected regions stained with Sirius Red surrounding bronchi versus the areas of associated basement membranes (right). More than 3 mice per group were analyzed. (**N**) Shown is a representative confocal micrograph of the lungs stained with anti-Osteopontin (green) and Siglec-F (red) from *Spp1*$^{+/+}$ and *Spp1*$^{-/-}$ mice with HDM exposure (Scale bars represent 50 μm). Three independent experiments were performed with similar results. (**O**) Quantitative RT-PCR analysis of the indicated genes in the lungs from *Spp1*$^{+/+}$ and *Spp1*$^{-/-}$ mice with HDM exposure (n = 3 mice per group). (**P**) Experimental protocol for a Th2 cell-dependent allergic inflammation mouse model employing adoptive transfer of memory Th2 cells followed by the transfer of eosinophils from *Spp1*$^{+/+}$ or *Spp1*$^{-/-}$ mice as indicated in STAR Methods. Data are the mean ± SD. $^{**}P < 0.01$, $^{***}P < 0.001$; by unpaired t test.

Figure S6

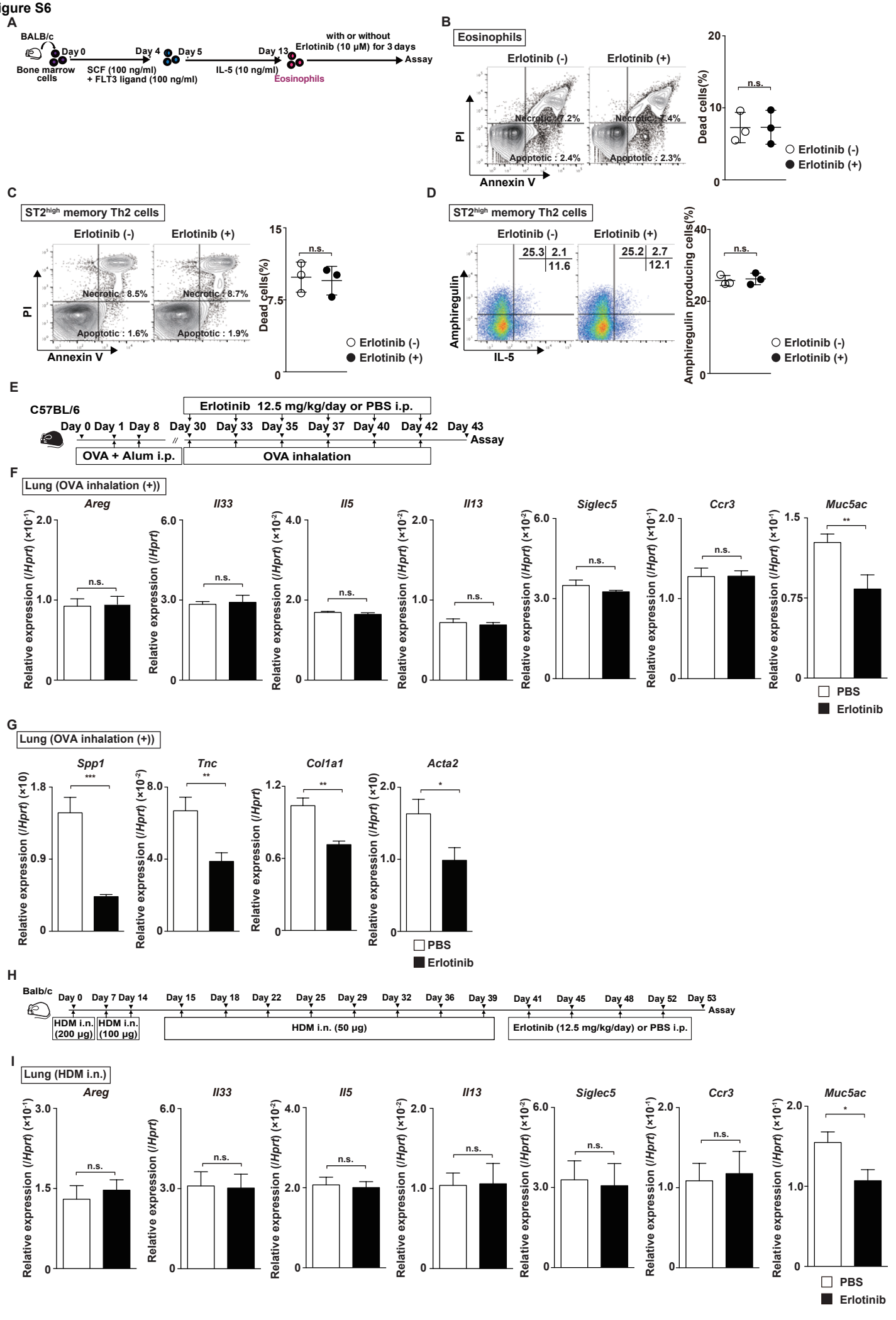

A
BALB/c
Day 0
Bone marrow cells
Day 4
SCF (100 ng/ml) + FLT3 ligand (100 ng/ml)
Day 5
Day 13
IL-5 (10 ng/ml)
Eosinophils
with or without Erlotinib (10 μM) for 3 days
Assay
B
Eosinophils
Erlotinib (-)
Erlotinib (+)
Necrotic : 7.2%
Necrotic : 7.4%
Apoptotic : 2.4%
Apoptotic : 2.3%
PI
Annexin V
Dead cells(%)
n.s.
Erlotinib (-)
Erlotinib (+)
C
ST2high memory Th2 cells
Erlotinib (-)
Erlotinib (+)
Necrotic : 8.5%
Necrotic : 8.7%
Apoptotic : 1.6%
Apoptotic : 1.9%
PI
Annexin V
Dead cells(%)
n.s.
Erlotinib (-)
Erlotinib (+)
D
ST2high memory Th2 cells
Erlotinib (-)
Erlotinib (+)
25.3
2.1
11.6
25.2
2.7
12.1
Amphiregulin
IL-5
Amphiregulin producing cells(%)
n.s.
Erlotinib (-)
Erlotinib (+)
E
C57BL/6
Erlotinib 12.5 mg/kg/day or PBS i.p.
Day 0 Day 1 Day 8 Day 30 Day 33 Day 35 Day 37 Day 40 Day 42 Day 43
Assay
OVA + Alum i.p.
OVA inhalation
F
Lung (OVA inhalation (+))
Areg
Il33
Il5
Il13
Siglec5
Ccr3
Muc5ac
Relative expression (/Hprt)
n.s.
**
PBS
Erlotinib
G
Lung (OVA inhalation (+))
Spp1
Tnc
Col1a1
Acta2
Relative expression (/Hprt)
***
**
*
PBS
Erlotinib
H
Balb/c
Day 0 Day 7 Day 14 Day 15 Day 18 Day 22 Day 25 Day 29 Day 32 Day 36 Day 39 Day 41 Day 45 Day 48 Day 52 Day 53
Assay
HDM i.n. (200 μg)
HDM i.n. (100 μg)
HDM i.n. (50 μg)
Erlotinib (12.5 mg/kg/day) or PBS i.p.
I
Lung (HDM i.n.)
Areg
Il33
Il5
Il13
Siglec5
Ccr3
Muc5ac
Relative expression (/Hprt)
n.s.
*
PBS
Erlotinib

Figure S6. Related to Figure 6. Inhibition of EGFR signaling ameliorates fibrotic responses *in vivo*. (**A**) Experimental protocol for the induction of bone marrow-derived eosinophils. The detailed protocol is in STAR Methods. (**B**) Shown are FACS plots of PI and Annexin V expression in eosinophils cultured with or without Erlotinib for 72 hours (left). Shown are the percentage of dead cells among total cells (right). (**C**) Shown are FACS plots of PI and Annexin V expression in $ST2^{hi}$ memory Th2 cells cultured with or without Erlotinib for 72 hours (left). Shown is percentage of dead cells among total cells (right). (**D**) Shown are FACS plots of intracellular Amphiregulin and IL-5 in $ST2^{hi}$ memory Th2 cells cultured with or without Erlotinib for 72 hours (left). Shown is the percentage of Amphiregulin-producing $ST2^{hi}$ memory Th2 cells among total $ST2^{hi}$ memory Th2 cells. (**E**) Experimental protocol for simultaneous Erlotinib treatment in an allergic airway inflammation mouse model using intraperitoneal (i.p.) OVA and aluminum hydroxide gel (Alum). C57BL/6 mice were sensitized by OVA and Alum i.p on days 1 and 8. Subsequently, mice were challenged with OVA inhalation and simultaneously treated with Erlotinib (12.5 mg/kg) or PBS i.p. on days 30, 33, 35, 37, 40 and 42. (**F**, **G**) Shown are quantitative RT-PCR analyses of the indicated genes in the lungs of OVA challenged mice simultaneously treated with PBS or Erlotinib (n = 3 mice per group). (**H**) Experimental protocol for subsequent Erlotinib treatment in an allergic inflammation mouse model with HDM exposure. BALB/c mice were exposed with HDM as indicated in STAR Methods. Subsequently, these mice were treated with Erlotinib (12.5 mg/kg) or PBS i.p. on days 41, 45, 48 and 52. (**I**) Shown are quantitative RT-PCR analyses of the indicated genes in the lungs of OVA challenged mice subsequently treated with PBS or Erlotinib (n = 3 mice per group). Data are the mean ± SD. $*P < 0.05$, $**P < 0.01$, $***P < 0.001$; n.s., not significant; by unpaired t test.

Figure S7

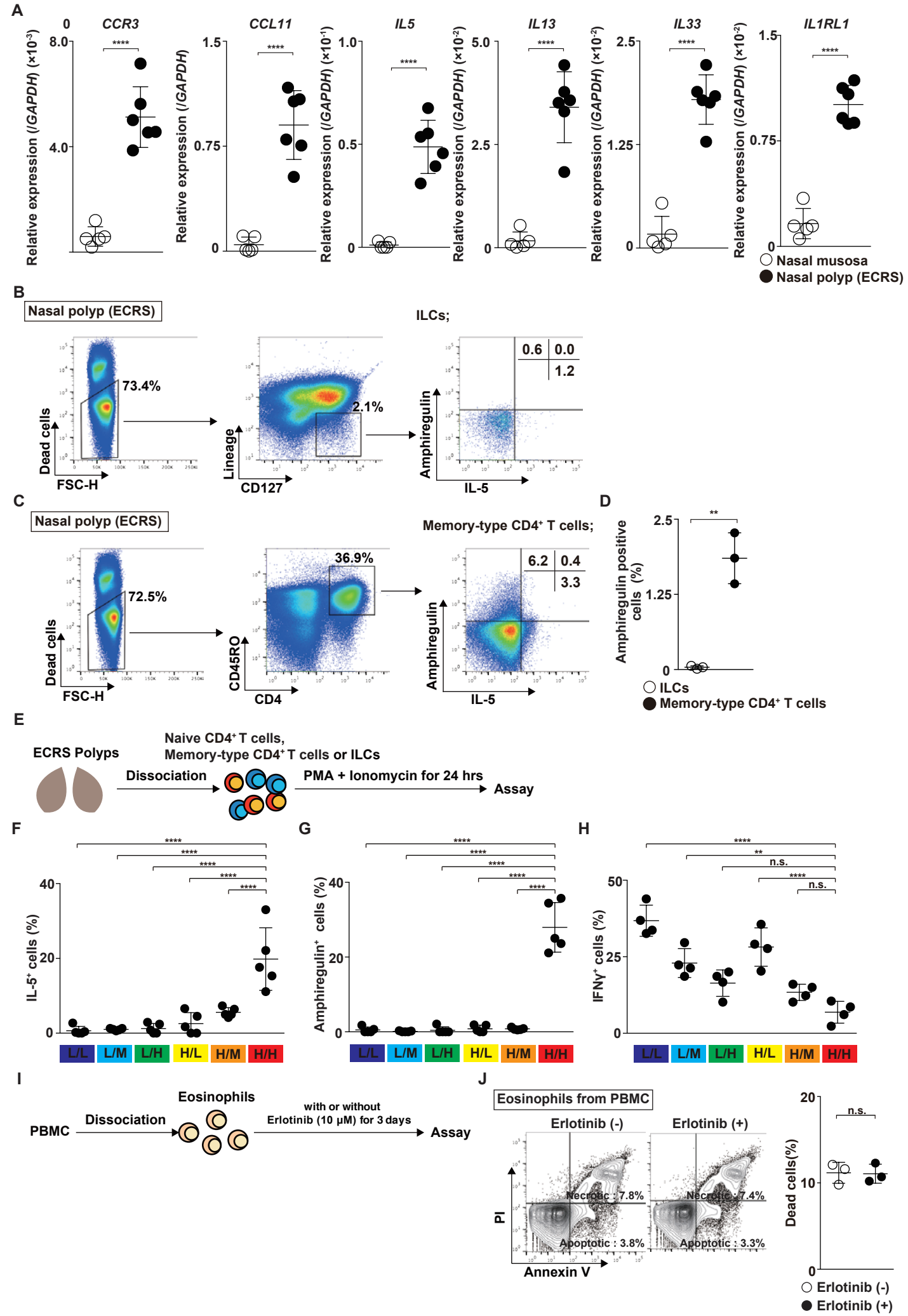

A
CCR3
CCL11
IL5
IL13
IL33
IL1RL1
Relative expression (/GAPDH)
Nasal musosa
Nasal polyp (ECRS)
B
Nasal polyp (ECRS)
ILCs;
73.4%
2.1%
0.6
0.0
1.2
Dead cells
FSC-H
Lineage
CD127
Amphiregulin
IL-5
C
Nasal polyp (ECRS)
Memory-type CD4⁺ T cells;
72.5%
36.9%
6.2
0.4
3.3
CD45RO
CD4
D
Amphiregulin positive cells (%)
ILCs
Memory-type CD4⁺ T cells
E
ECRS Polyps
Naive CD4⁺ T cells,
Memory-type CD4⁺ T cells or ILCs
Dissociation
PMA + Ionomycin for 24 hrs
Assay
F
IL-5⁺ cells (%)
G
Amphiregulin⁺ cells (%)
H
IFNγ⁺ cells (%)
n.s.
L/L
L/M
L/H
H/L
H/M
H/H
I
PBMC
Dissociation
Eosinophils
with or without
Erlotinib (10 μM) for 3 days
Assay
J
Eosinophils from PBMC
Erlotinib (-)
Erlotinib (+)
Necrotic : 7.8%
Necrotic : 7.4%
Apoptotic : 3.8%
Apoptotic : 3.3%
PI
Annexin V
Dead cells(%)

Figure S7. Related to Figure 7. Large numbers of Amphiregulin-producing memory-type CD4$^+$ T cells in the nasal polyps of ECRS patients.

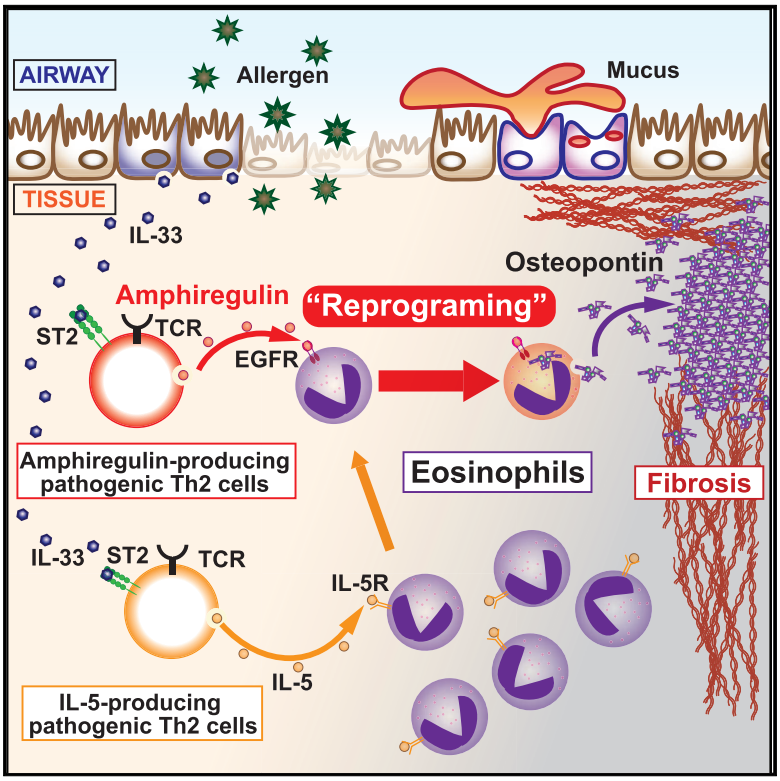
(**A**) Shown are quantitative RT-PCR analyses of the indicated genes in the nasal mucosa of healthy control subjects (Control; n = 5) and in the polyps of patients with ECRS (ECRS; n = 6). (**B**) Shown are representative FACS plots of intracellular Amphiregulin and IL-5 expression by lineage$^-$ CD127$^+$ cells from a polyp of a patient with ECRS. (**C**) Shown are representative FACS plots of intracellular Amphiregulin and IL-5 in CD4$^+$ CD45RO$^+$ cells from a polyp of a patient with ECRS. (**D**) Shown is a comparison of the absolute numbers of ILCs and memory-type CD4$^+$ T cells that produce Amphiregulin. Three independent donors were analyzed. (**E**) Experimental protocol for the collection of the indicated cells from ECRS polyps followed by stimulation with PMA and Ionomycin for 24 hours. (**F**, **G**, **H**) Shown is pooled data from five (Amphiregulin and IL-5) or four (IFNγ) separate experiments depicting IL-5-producing cells (**F**) , Amphiregulin-producing cells (**G**) and IFNγ-producing cells (**H**) gated into 6 subpopulations by the expression of CD161 and CRTH2, as described in Figure 7E. (**I**) Experimental protocol for the collection of eosinophils from PBMC followed by stimulation with or without Erlotinib. (**J**) Shown are FACS plots of PI and Annexin V expression on eosinophils from PBMC cultured with or without Erlotinib for 72 hours as indicated in STAR Methods (left). Shown is the percentage of dead cells among total cells (right). Data are the mean ± SD. $^{**}P < 0.01$, $^{****}P < 0.0001$; n.s., not significant; by unpaired t test or one-way analysis of variance (ANOVA).

Article

Immunity

Amphiregulin-Producing Pathogenic Memory T Helper 2 Cells Instruct Eosinophils to Secrete Osteopontin and Facilitate Airway Fibrosis

Graphical Abstract



Highlights

- Pathogenic memory Th2 cells induce amphiregulin (Areg) via IL-33
- Areg reprograms the transcriptome of eosinophils toward an inflammatory state
- Areg-reprogramed eosinophils produce osteopontin to trigger airway fibrosis
- Areg^{+} Th2 cells and osteopontin^{+} eosinophils co-localize in fibrotic ECRS polyps

Authors

Yuki Morimoto, Kiyoshi Hirahara, Masahiro Kiuchi, ..., Daiju Sakurai, Yoshitaka Okamoto, Toshinori Nakayama

Correspondence

tnakayama@faculty.chiba-u.jp

In Brief

Asthma is a chronic allergic inflammatory disease with airway remodeling including fibrotic changes. Morimoto and colleagues find that the IL-33-ST2-amphiregulin-EGRF-osteopontin axis directs fibrotic responses in chronic allergic inflammation with the involvement of airway epithelial cells, pathogenic memory Th2 cells, and inflammatory eosinophils in both mouse and human.

Morimoto et al., 2018, Immunity *49*, 1–17
July 17, 2018 © 2018 Elsevier Inc.
https://doi.org/10.1016/j.immuni.2018.04.023

CellPress

Please cite this article in press as: Morimoto et al., Amphiregulin-Producing Pathogenic Memory T Helper 2 Cells Instruct Eosinophils to Secrete Osteopontin and Facilitate Airway Fibrosis, Immunity (2018), https://doi.org/10.1016/j.immuni.2018.04.023

CellPress

Amphiregulin-Producing Pathogenic Memory T Helper 2 Cells Instruct Eosinophils to Secrete Osteopontin and Facilitate Airway Fibrosis

Yuki Morimoto,[1,2,6] Kiyoshi Hirahara,[1,3,6] Masahiro Kiuchi,[1] Tomoko Wada,[1] Tomomi Ichikawa,[1] Toshio Kanno,[1] Mikiko Okano,[1] Kota Kokubo,[1] Atsushi Onodera,[1,4] Daiju Sakurai,[2] Yoshitaka Okamoto,[2] and Toshinori Nakayama[1,5,7,*]
[1]Department of Immunology, Graduate School of Medicine, Chiba University, 1-8-1 Inohana, Chuo-ku, Chiba 260-8670, Japan
[2]Department of Otorhinolaryngology, Head and Neck Surgery, Graduate School of Medicine, Chiba University, 1-8-1 Inohana, Chuo-ku, Chiba 260-8670, Japan
[3]AMED-PRIME, AMED, 1-8-1 Inohana, Chuo-ku, Chiba 260-8670, Japan
[4]Institute for Global Prominent Research, Chiba University, 1-8-1 Inohana, Chuo-ku, Chiba 260-8670, Japan
[5]AMED-CREST, AMED, 1-8-1 Inohana, Chuo-ku, Chiba 260-8670, Japan
[6]These authors contributed equally
[7]Lead Contact
*Correspondence: tnakayama@faculty.chiba-u.jp
https://doi.org/10.1016/j.immuni.2018.04.023

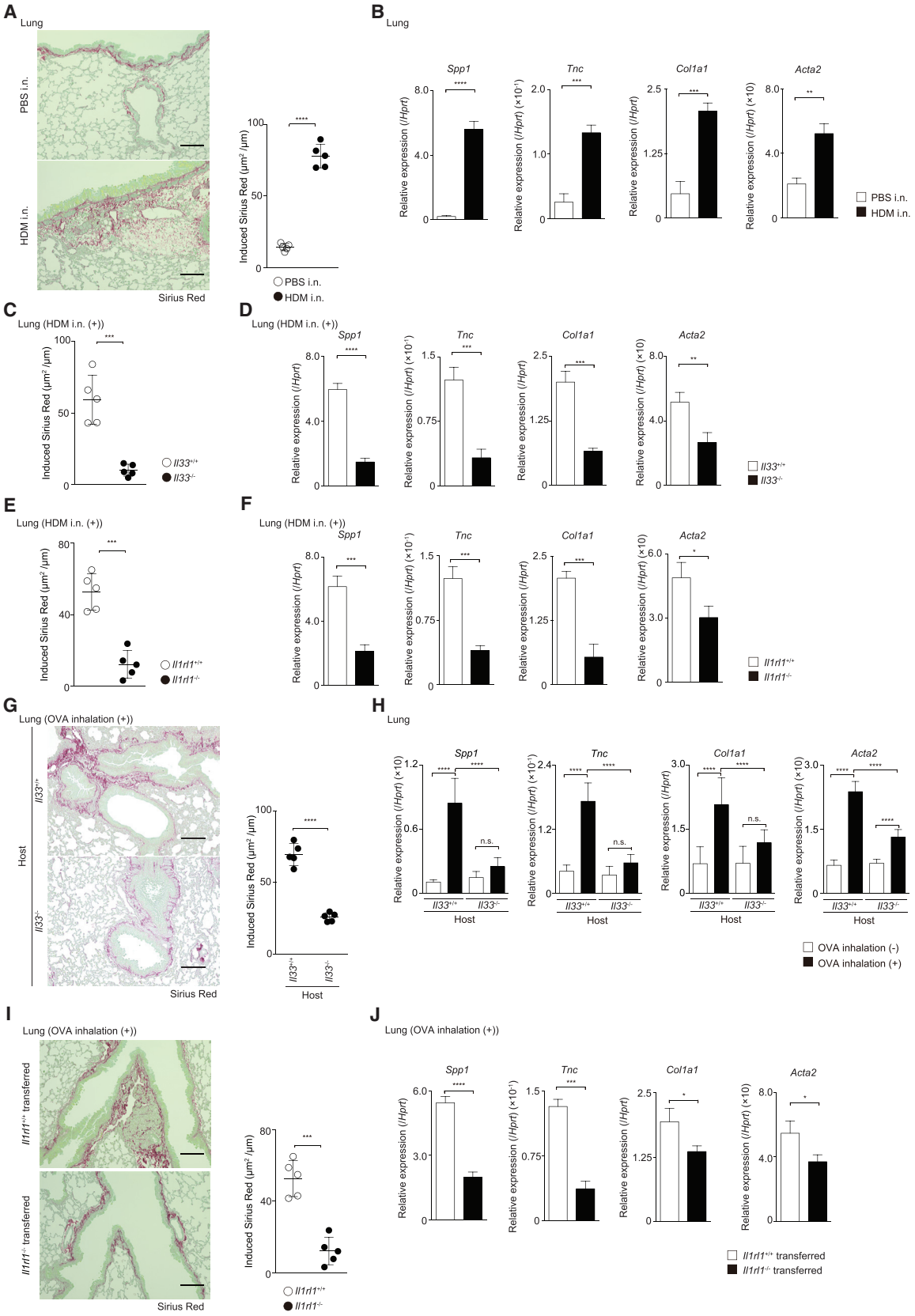
SUMMARY

Memory T cells provide long-lasting protective immunity, and distinct subpopulations of memory T cells drive chronic inflammatory diseases such as asthma. Asthma is a chronic allergic inflammatory disease with airway remodeling including fibrotic changes. The immunological mechanisms that induce airway fibrotic changes remain unknown. We found that interleukin-33 (IL-33) enhanced amphiregulin production by the IL-33 receptor, ST2^{hi} memory T helper 2 (Th2) cells. Amphiregulin-epidermal growth factor receptor (EGFR)-mediated signaling directly reprogramed eosinophils to an inflammatory state with enhanced production of osteopontin, a key profibrotic immunomodulatory protein. IL-5-producing memory Th2 cells and amphiregulin-producing memory Th2 cells appeared to cooperate to establish lung fibrosis. The analysis of polyps from patients with eosinophilic chronic rhinosinusitis revealed fibrosis with accumulation of amphiregulin-producing CRTH2^{hi}CD161^{hi}CD45RO^{+}CD4^{+} Th2 cells and osteopontin-producing eosinophils. Thus, the IL-33-amphiregulin-osteopontin axis directs fibrotic responses in eosinophilic airway inflammation and is a potential target for the treatment of fibrosis induced by chronic allergic disorders.

INTRODUCTION

Asthma is characterized by chronic airway inflammation, mucus hyperproduction, airway hyper-responsiveness (AHR), and variable airway obstruction (Busse and Lemanske, 2001; Kim et al., 2010). Airway remodeling, structural alterations of the airway wall such as subepithelial thickening, vascular changes, and fibrosis are central to the irreversible pathology of asthma (Al-Muhsen et al., 2011; Foster et al., 2017; Lambrecht and Hammad, 2012). Airway remodeling causes AHR, persistent airflow limitation, and a decrease in lung function. Corticosteroids are a key medicine used for the treatment of asthma. Clinical studies regarding the therapeutic effects of corticosteroids on airway remodeling have led to controversial results (Adcock et al., 2008; Durrani et al., 2011; Hansbro et al., 2017). About 5%–10% of asthmatics are refractory to corticosteroid treatment and often need to be hospitalized, and the degree of airway remodeling in asthmatics correlates with disease severity (Lambrecht and Hammad, 2015; Martinez and Vercelli, 2013).

Fibrosis consists of excessive deposition of collagenous and noncollagenous extracellular matrix (ECM) components in lung parenchyma as a consequence of proliferation and activation of fibroblasts, myofibroblasts, and immune cells (Wick et al., 2013). Fibrosis develops as a result of long-lasting inflammation such as occurs in asthma. Both innate and adaptive immunity are involved in the pathogenesis of fibrotic responses during allergic inflammation (Wick et al., 2013). T helper 2 (Th2) cells are a central population in the pathogenesis of allergic airway inflammation and fibrosis (Gieseck et al., 2018; Nakayama et al., 2017; Wick et al., 2013). Interleukin-5 (IL-5) is a key cytokine for the development, recruitment to inflammatory sites, and activation of eosinophils (Rosenberg et al., 2013). Local inflammation causes recruitment of eosinophils with inflammatory features (Mesnil et al., 2016). Eosinophil-induced inflammatory mediators such as reactive oxygen species (ROS), cytokines, and lipid mediators damage airway epithelial cells and nerves and induce asthmatic inflammation together with AHR (Rosenberg et al., 2013; Rothenberg and Hogan, 2006). Eosinophils are also involved in the pathogenesis of airway remodeling characterized by collagen fibril deposition (Humbles et al., 2004), but the molecular mechanisms through which eosinophils induce the fibrotic changes remain uncertain. Recently, pathogenic memory Th2 cells producing high amounts of IL-5 have been shown to direct eosinophilic inflammation (Nakayama et al., 2017). They show high expression of the ST2 receptor,



(legend on next page)

are selectively induced by IL-33 (the ligand of the ST2 receptor), and play critical role in the pathogenesis of chronic eosinophilic inflammation both in human and mouse systems (Endo et al., 2011, 2015; Nakayama et al., 2017). Similar pathogenic Th2 cells producing high amounts of IL-5 have been reported in the skin of patients with atopic dermatitis (Islam et al., 2011) and in the peripheral blood of patients with eosinophilic gastrointestinal disease and asthma (Mitson-Salazar et al., 2016; Seumois et al., 2016; Wambre et al., 2017). However, the pathogenic Th2 cell subpopulation shaping the pathology of fibrosis remains unclear.

Chronic rhinosinusitis (CRS) is a multifactorial disease associated with chronic inflammation and characteristic cytokine and airway remodeling patterns (Ball et al., 2016). Based on diagnostic histological changes, CRS with polyps is classified as either eosinophilic CRS (ECRS) or non-eosinophilic CRS (NECRS) (Hamilos, 2015). Patients with ECRS often present with asthma and their polyps exhibit eosinophilic infiltration, suggesting that aberrant type 2 immune responses are involved in the pathogenesis of ECRS (Hamilos, 2015). The pathogenesis of asthma and ECRS appear to be closely related (Kobayashi et al., 2015). Histological analysis of ECRS shows basement membrane thickening that is the result of a severe fibrotic response typified by accumulation of fibronectin and type I, III, and V collagens (Ball et al., 2016; Pawankar and Nonaka, 2007). A high proportion of patients with ECRS are refractory to current conventional pharmacologic therapy such as corticosteroid treatment and suffer frequent disease recurrence. The precise cellular and molecular mechanisms that cause the type of persistent sino-nasal type 2 inflammation that leads to fibrosis remain unclear.

Herein, we investigated the cellular and molecular mechanisms that control the pathogenesis of airway fibrosis during chronic allergic inflammation. We found that an epithelial cytokine IL-33 drives lung fibrotic responses during antigen-induced Th2 cell-dependent allergic airway inflammation. IL-33 induced amphiregulin production by $ST2^{hi}$ memory-type pathogenic Th2 cells. Amphiregulin reprogrammed the transcriptome of eosinophils toward an inflammatory state that included enhanced production of osteopontin. Amphiregulin-producing $ST2^{hi}$ memory Th2 cells and IL-5-producing $ST2^{hi}$ memory Th2 cells appeared to be distinct subpopulations, and cooperate to establish airway fibrosis during eosinophilic inflammation. Analysis of nasal polyps of ECRS patients revealed increased infiltration of amphiregulin-producing $CD161^{+}CRTH2^{+}$ memory-type $CD4^{+}$ T cells and osteopontin-producing eosinophils accompanied by dense fibrotic responses. Pharmacological blockade of epidermal growth factor receptor (EGFR) signaling resulted in attenuated expression of *Spp1*, which encodes osteopontin in mouse and human eosinophils. Thus, the IL-33-amphiregulin-osteopontin axis directs fibrotic responses in chronic allergic inflammation in both mouse and human systems, and these molecules may be potential therapeutic targets for intractable chronic eosinophilic inflammatory disorders.

RESULTS

Lung Fibrotic Responses Are Induced by Antigen-Induced Type 2 Inflammation via the IL-33-ST2 Axis

Repetitive exposure of house dust mite (HDM) to mice induced a significant increase in collagen deposition around the respiratory tract as detected by Sirius red staining accompanied by increased expression of *Il33*, *Il25*, and *Tslp* in inflamed lungs (Figures S1A, S1B, and 1A; Doherty et al., 2011). In addition, the expression of molecules relevant to fibrotic responses such as *Spp1* (which encodes osteopontin), *Tenascin C* (*Tnc*), *Collagen type 1 alpha 1* (*Col1a1*), and *Actin alpha 2 smooth muscle aorta* (*Acta2*) was significantly enhanced in the lungs of mice with HDM exposure (Figure 1B). Genetic deletion of *Il33* or *Il1rl1*, which encodes ST2 (a component of the IL-33 receptor), resulted in significantly reduced expression of fibrosis-related genes in the lungs together with decreased collagen deposition (Figures 1C–1F, S1C, and S1D). Mice that had received

Figure 1. IL-33 Signaling Induces Lung Fibrotic Changes

(A) Representative histology of lungs of mice with HDM or PBS exposure (Figure S1A), fixed and stained with Sirius red (left) from three experiments. Scale bars, 100 μm. Shown are ratios of areas of randomly selected regions stained with Sirius red surrounding bronchi versus the areas of associated basement membranes (right). More than three mice per group were analyzed.

(B, D, and F) Quantitative RT-PCR analysis of the indicated genes in the lungs of wild-type mice with or without HDM exposure (n = 3 mice per group) (B), the lungs of $Il33^{+/+}$ and $Il33^{-/-}$ mice with HDM exposure (n = 3 mice per group) (D), and the lungs of $Il1rl1^{+/+}$ and $Il1rl1^{-/-}$ mice with HDM exposure (n = 3 mice per group) (F). Three independent experiments were performed with similar results.

(C and E) Shown are ratios of areas of randomly selected regions stained with Sirius red surrounding bronchi versus the areas of associated basement membranes in the lungs of $Il33^{+/+}$ and $Il33^{-/-}$ mice with HDM exposure (C) or the lungs of $Il1rl1^{+/+}$ and $Il1rl1^{-/-}$ mice with HDM exposure (E). More than three mice per group were analyzed.

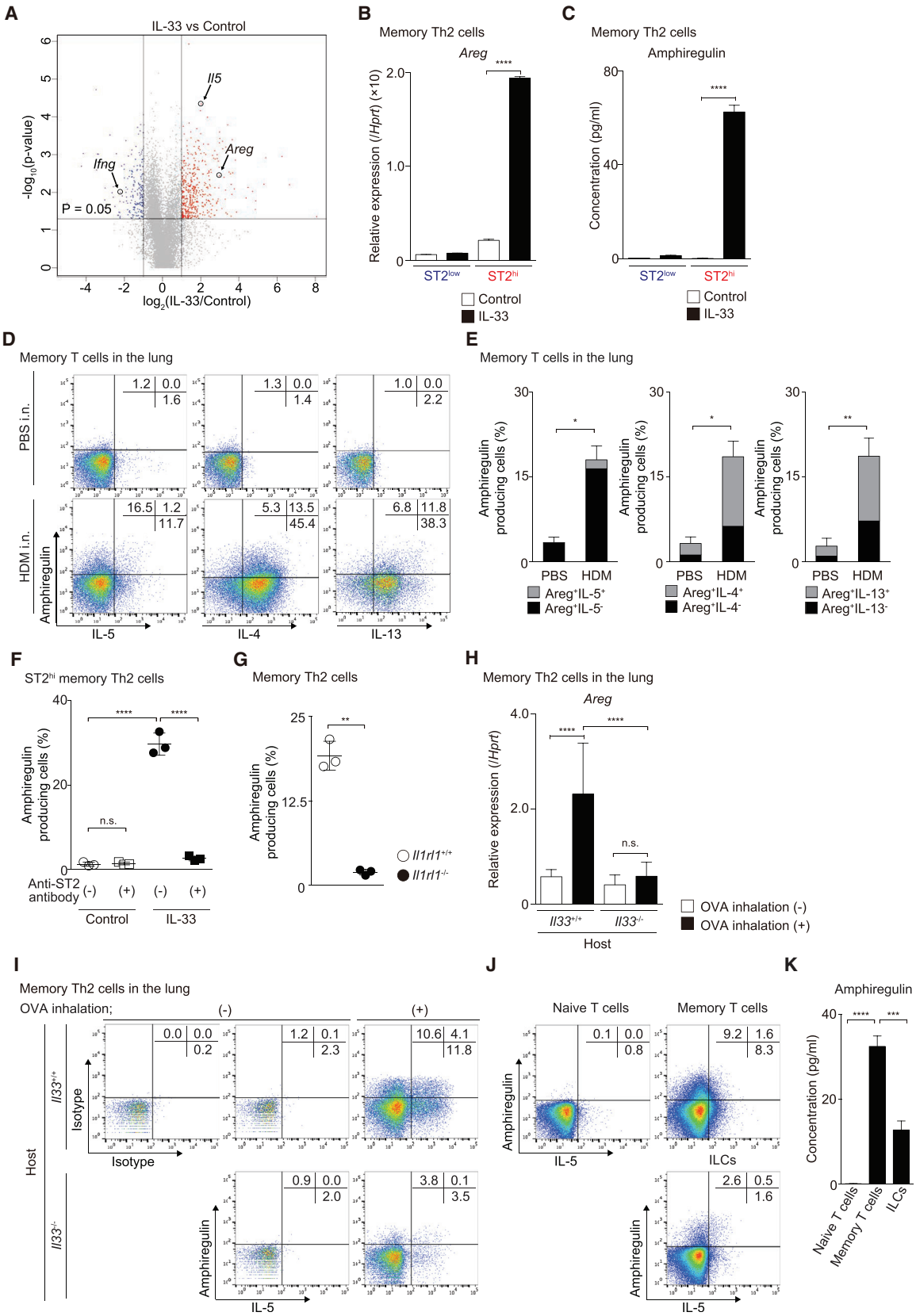
(G) OVA-specific memory Th2 cells (3×10^6 cells) were transferred i.v. into $Il33^{+/+}$ and $Il33^{-/-}$ mice that were subsequently challenged with OVA as indicated in Figure S1E. Shown is a representative confocal micrograph of lung tissue stained with Sirius red from an $Il33^{+/+}$ and an $Il33^{-/-}$ mouse (left) from four experiments. Scale bars represent 100 μm. Shown are ratios of areas of randomly selected regions stained with Sirius red surrounding bronchi versus the areas of associated basement membranes (right). More than three mice per group were analyzed.

(H) Quantitative RT-PCR analysis of gene expression in the lungs of $Il33^{+/+}$ (upper) and $Il33^{-/-}$ (lower) mice challenged with or without OVA inhalation (n = 6 mice per group).

(I) $Il1rl1^{+/+}$ and $Il1rl1^{-/-}$ OVA-specific memory Th2 cells (3×10^6 cells) were transferred i.v. into BALB/c mice that were subsequently challenged with OVA as indicated in Figure S1E. Shown is a representative confocal micrograph of lung tissue stained with Sirius red from an $Il1rl1^{+/+}$ and an $Il1rl1^{-/-}$ memory Th2 cell-transferred mouse (left) from three experiments. Scale bars represent 100 μm. Shown are ratios of areas of randomly selected regions stained with Sirius red surrounding bronchi versus the areas of associated basement membranes (right). More than three mice per group were analyzed.

(J) Quantitative RT-PCR analysis of the indicated genes in the lungs from $Il1rl1^{+/+}$ and $Il1rl1^{-/-}$ memory Th2 cell-transferred mice challenged with OVA inhalation (n = 3 mice per group).

Data are the mean ± SD. *p < 0.05, **p < 0.01, ***p < 0.001, ****p < 0.0001; n.s., not significant; by unpaired t test or one-way analysis of variance (ANOVA). Please see also Figure S1.



(legend on next page)

OVA-specific memory Th2 cells followed by multiple antigen challenges also exhibited a significant increase in fibrotic changes together with increased expression of *Il33* and *Il25* but not *Tslp* in the lungs (Figures S1E–S1H). *Il33*$^{-/-}$ mice that had received OVA-specific memory Th2 cells exhibited significantly decreased collagen deposition in the lungs (Figure 1G). The fibrosis-related genes *Spp1*, *Tnc*, *Col1a1*, and *Acta2* were less induced by OVA inhalation in the lungs of *Il33*$^{-/-}$ mice as compared to those of *Il33*$^{+/+}$ mice (Figure 1H). The ameliorated fibrotic changes in *Il33*$^{-/-}$ mice were reversed by intratracheal administration of IL-33 (Figures S1I–S1K). Mice that had received *Il1rl1*$^{-/-}$ memory Th2 cells also showed significant decrease in fibrotic changes (Figures 1I and 1J). We next immunized *Il1rl1*$^{+/+}$ or *Il1rl1*$^{-/-}$ mice with OVA and Alum twice followed by a series of OVA inhalations (Figure S1L). Collagen deposition together with the expression of fibrosis-related genes in the lungs were significantly decreased in *Il1rl1*$^{-/-}$ mice (Figures S1M and S1N). Thus, the IL-33-ST2 axis plays a critical role in the induction of lung fibrotic responses in our *in vivo* experimental settings.

IL-33 Induces Amphiregulin Production by ST2^{hi} Memory Th2 Cells Both *In Vitro* and *In Vivo*

To explore the molecules expressed in ST2^{hi} memory Th2 cells that are critical for the induction of lung fibrotic responses, we assessed changes in global gene expression in ST2^{hi} OVA-specific memory Th2 cells following 3 days of *in vitro* IL-33 stimulation (Figures S2A–S2C). 745 genes exhibited a >2-fold change between control and IL-33-stimulated ST2^{hi} memory Th2 cells (Figure 2A). One of the genes exhibiting elevated expression in IL-33-stimulated cells was *Areg*, encoding amphiregulin, a key molecule for tissue repair (Figures 2A and S2D; Stoll et al., 1997). Quantitative RT-PCR confirmed selective induction of *Areg* in IL-33-stimulated ST2^{hi} memory Th2 cells (Figures 2B and S2E). Consistent with this, IL-33 stimulation induced amphiregulin protein production by ST2^{hi} memory Th2 cells (Figure 2C). IL-33-stimulated ST2^{hi} memory Th2 cells also exhibited enhanced expression of *Il5* and *Il13* (Figure S2F) but not *Il4* or *Ifng*. IL-33-induced amphiregulin expression correlated with the chromatin status such as increased H3-K4 trimethylation and reduced H3-K27 trimethylation at the *Areg* locus (data not shown). Flow cytometric analysis revealed that the majority of amphiregulin-positive cells did not produce IL-5 (Figures S2G and S2H). In contrast, the majority of amphiregulin-producing cells also produced IL-4 and IL-13 (Figure S2H). To characterize the amphiregulin-producing memory Th2 cells and the IL-5-producing memory Th2 cells, we performed flow cytometric analyses with various antibodies. The expression of CD147, a member of the immunoglobulin superfamily, was significantly lower on amphiregulin-producing memory Th2 cells as compared to IL-5-producing memory Th2 cells (Figure S2I). Amphiregulin-producing memory CD4$^+$ T cells induced by HDM exposure *in vivo* did not overlap with IL-5-producing memory CD4$^+$ T cells (Figures 2D and 2E). IL-33 did not induce amphiregulin production in other types of cells such as naive CD4$^+$ T cells, effector Th2 cells, peripheral regulatory T cells, and activated CD8$^+$ T cells (data not shown).

IL-25 or thymic stromal lymphopoietin (TSLP) stimulation also induced amphiregulin-producing memory Th2 cells, although induction was not as efficient as with IL-33 stimulation (Figure S2J). Blockade of the IL-33-ST2 axis by treatment with anti-ST2 antibody or genetic deletion of *Il1rl1* diminished amphiregulin-producing memory Th2 cells *in vitro* (Figures 2F, 2G, and S2K). Memory Th2 cells under IL-33-sufficient conditions exhibited significantly increased production of amphiregulin after OVA inhalation *in vivo*, while memory Th2 cells in IL-33-deficient conditions failed to produce significant amounts of amphiregulin (Figures 2H, 2I, and S2L). The expression of *Il5* and *Il13* but not *Il4* or *Ifng* was induced in memory Th2 cells in wild-type but not *Il33*$^{-/-}$ mice (Figure S2M). Furthermore, memory CD4$^+$ T cells in the lungs of *Il1rl1*$^{-/-}$ mice treated with OVA and Alum twice followed by a series of OVA inhalations (Figure S1L) showed significant reduction of amphiregulin-producing memory CD4$^+$ T cells (Figure S2N). ILCs from inflamed lungs also

Figure 2. IL-33 Induces Amphiregulin Production from ST2^{hi} Memory Th2 Cells Both *In Vitro* and *In Vivo*

(A) OVA-specific ST2^{hi} memory Th2 cells were cultured with or without IL-33 for 72 hr. RNA-seq data were computed as FPKM (fragments per kilobase of transcript per million mapped reads). Arrows indicate *Areg*, *Il5*, and *Ifng* expression. Volcano plot depicts differential gene expression induced by IL-33 compared to control.

(B) Quantitative RT-PCR analysis of *Areg* in ST2^{lo} or ST2^{hi} memory Th2 cells. Four independent experiments were performed with similar results.

(C) Protein expression of amphiregulin from ST2^{lo} or ST2^{hi} memory Th2 cells. Three independent experiments were performed with similar results.

(D) Shown are intracellular-staining profiles of amphiregulin together with IL-5 (left), IL-4 (middle), and IL-13 (right) in memory CD4$^+$ T cells from the lungs of mice with HDM exposure.

(E) Shown are the percentages of amphiregulin-producing memory CD4$^+$ T cells in the lungs of mice with HDM exposure. Amphiregulin single producers (Areg$^+$IL-5$^-$, Areg$^+$IL-4$^-$, and Areg$^+$IL-13$^-$) are shown in black, and amphiregulin and indicated cytokines double producers (Areg$^+$IL-5$^+$, Areg$^+$IL-4$^+$, and Areg$^+$IL-13$^+$) are shown in gray.

(F) Shown are the percentages of amphiregulin-producing ST2^{hi} memory Th2 cells with (square) or without (circle) neutralizing anti-ST2 antibody followed by IL-33 stimulation (black) or control stimulation (white).

(G) Shown are the percentages of amphiregulin-producing memory Th2 cells derived from *Il1rl1*$^{+/+}$ and *Il1rl1*$^{-/-}$ mice with IL-33 stimulation.

(H) Quantitative RT-PCR analysis of *Areg* in the lung memory Th2 cells from *Il33*$^{+/+}$ and *Il33*$^{-/-}$ recipients challenged with or without OVA (n = 6 mice per group).

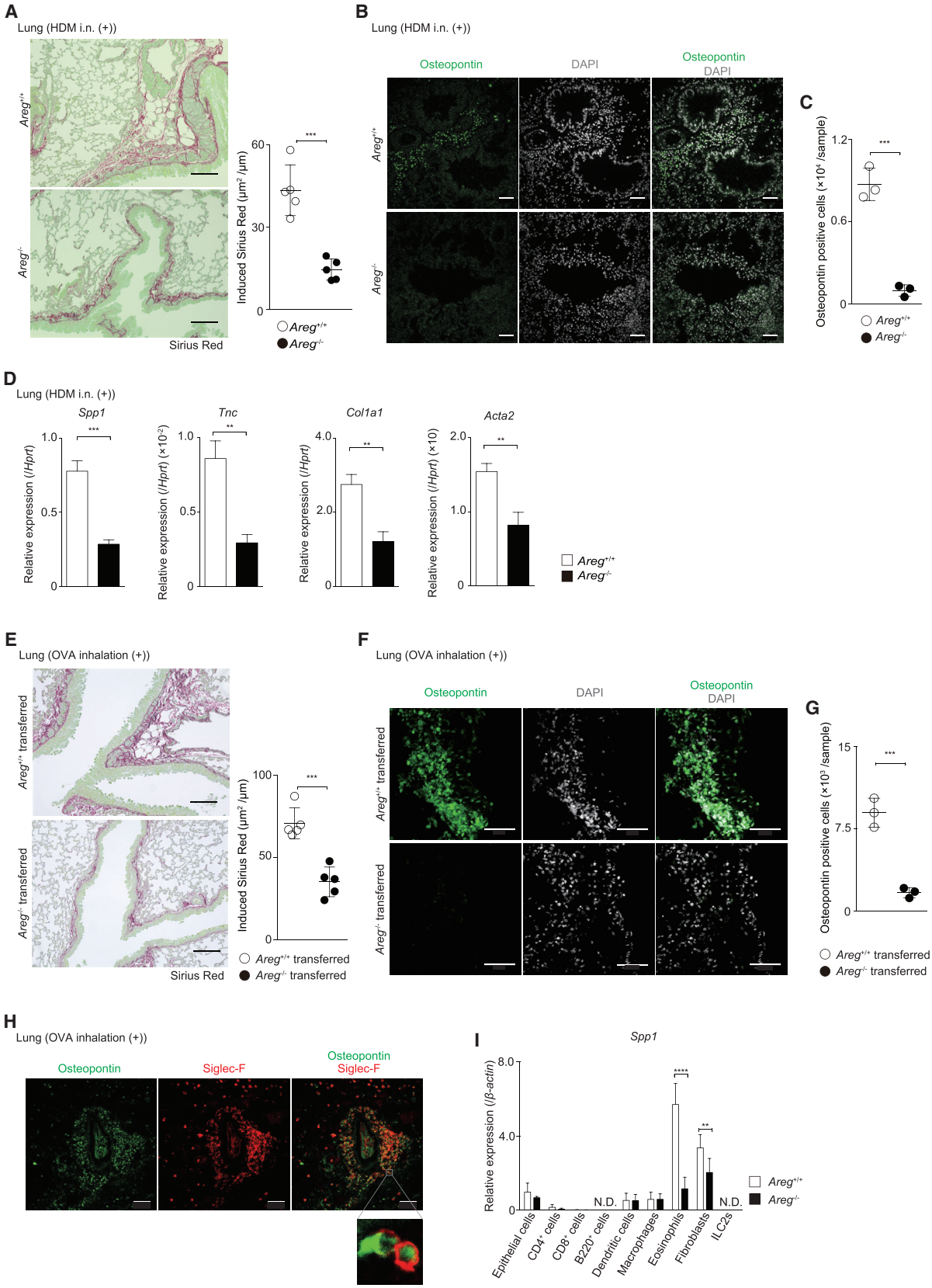
(I) Shown are intracellular-staining profiles of amphiregulin and IL-5 with isotype controls in the lung memory Th2 cells from *Il33*$^{+/+}$ and *Il33*$^{-/-}$ recipients. Six independent experiments were performed with similar results.

(J) Shown are intracellular-staining profiles of amphiregulin and IL-5 in memory CD4$^+$ T cells and ILCs from the lungs of mice with OVA and Alum twice followed by a series of OVA inhalations (Figure S1L).

(K) Protein expression of amphiregulin from naive CD4$^+$ T cells, memory CD4$^+$ T cells, and ILCs. Three independent experiments were performed with similar results.

Data are the mean ± SD. *$p < 0.05$, **$p < 0.01$, ***$p < 0.001$, ****$p < 0.0001$; n.s., not significant; by unpaired t test or one-way analysis of variance (ANOVA). Please see also Figure S2.

Please cite this article in press as: Morimoto et al., Amphiregulin-Producing Pathogenic Memory T Helper 2 Cells Instruct Eosinophils to Secrete Osteopontin and Facilitate Airway Fibrosis, Immunity (2018), https://doi.org/10.1016/j.immuni.2018.04.023



(legend on next page)

produced amphiregulin, but more than 70% reduction compared to that produced by memory $CD4^+$ T cells (Figures 2J, 2K, and S2O). These results indicate that both *in vitro* and *in vivo* IL-33 stimulation is essential for the induction of amphiregulin production by memory Th2 cells.

Amphiregulin Produced by Memory Th2 Cells Induces Lung Fibrotic Responses during Type 2 Inflammation *In Vivo*

Next, we wanted to identify the role of amphiregulin in lung fibrotic responses during allergic inflammation. Deletion of *Areg* resulted in the amelioration of HDM-induced fibrotic changes in the lung (Figures 3A–3D). Collagen deposition in the lung was also significantly decreased in $Areg^{-/-}$ mice treated with OVA and Alum twice followed by a series of OVA inhalations (Figures S3A and S3B). However, expression of *Il33*, *Il5*, and *Il13*, inflammatory cell infiltration in the lung parenchyma, were comparable between $Areg^{+/+}$ and $Areg^{-/-}$ mice (Figures S3C and S3D). $Areg^{+/+}$ and $Areg^{-/-}$ lung memory-type ($CD44^+CD62L^{lo}$) $CD4^+$ T cells also exhibited similar expression of *Il5* and *Il13* (Figure S3E). Molecules relevant to fibrosis exhibited decreased expression in the lungs of $Areg^{-/-}$ mice (Figure S3F). These results indicate that amphiregulin is critical for induction of the lung fibrotic response during allergic airway inflammation. In addition, amphiregulin appeared to be a major downstream target of IL-33 in the induction of lung fibrotic responses.

Next, to determine whether amphiregulin produced by memory Th2 cells was physiologically relevant to the induction of lung fibrotic responses *in vivo*, we transferred OVA-specific memory Th2 cells from $Areg^{+/+}$ mice or $Areg^{-/-}$ mice to wild-type mice and then performed antigen challenge (Figure S1E). Transferred $Areg^{+/+}$ and $Areg^{-/-}$ memory Th2 cells exhibited similar production of IL-5 and IL-13 (Figure S3G). However, lung collagen deposition was diminished in recipients of $Areg^{-/-}$ as compared to $Areg^{+/+}$ memory Th2 cells (Figure 3E). Recipients of $Areg^{-/-}$ as compared to $Areg^{+/+}$ memory Th2 cells also exhibited decreased lung osteopontin deposition accompanied by decreased expression of fibrosis-related genes (Figures 3F, 3G, S3H, and S3I). These results indicated that amphiregulin produced by memory Th2 cells was relevant to the induction of lung fibrotic responses. Thus, Th2 cells play a crucial role in lung fibrotic responses induced by the IL-33-amphiregulin axis during allergen-induced allergic airway inflammation.

Amphiregulin Stimulates Eosinophils to Produce Osteopontin via EGF Receptor Signaling

We next explored the major cellular source of osteopontin in our experimental settings. Histological analysis of inflamed lungs in mice that received OVA-specific memory Th2 cells followed by antigen challenge (Figure S1E) revealed that collagen was deposited adjacent to infiltrating eosinophils (Figure S3J). The majority of osteopontin-stained cells in the asthmatic lung were co-localized with Siglec-F^+ cells (Figure 3H). $B220^+$ cells, $CD4^+$ cells, MHC class II^+ cells, $CD11c^+$ cells, and $F4/80^+$ cells also found in asthmatic lungs were not co-localized with osteopontin-stained cells (Figures S3K and S3L). Amphiregulin belongs to the epidermal growth factor (EGF)-like protein family, which interacts with EGFR to transmit signals into target cells (Shoyab et al., 1989). Compared to airway epithelial cells, bone marrow-derived eosinophils exhibited moderate expression of *Egfr* (Figures S3M and S3N). Deletion of *Areg* resulted in reduced *Spp1* expression from eosinophils of inflamed lungs *in vivo* (Figure 3I). Thus, amphiregulin-stimulated eosinophils are the main cellular source of osteopontin in lungs undergoing allergic inflammatory fibrotic responses.

Amphiregulin Induced Transcriptional Reprogramming of Eosinophils via EGF Receptor Signaling

To determine the consequence of amphiregulin stimulation in eosinophils, we examined the global gene expression profile of eosinophils after stimulation with amphiregulin for 3 days. Amphiregulin stimulation had no obvious effect on expressions of CCR3 and Siglec-F nor on the survival of eosinophils (Figures S4A and S4B). Principle component analysis revealed that amphiregulin dramatically altered the eosinophil transcriptome (Figure S4C). Substantial numbers of genes were upregulated in eosinophils after amphiregulin stimulation (Figure S4D). Gene Ontology enrichment analysis of 10,899 genes indicated that amphiregulin stimulation upregulated genes related to cell activation, cell cycle processes, RNA metabolic processes,

Figure 3. Amphiregulin by Memory Th2 Cells Induces Fibrotic Changes Accompanied by Osteopontin-Positive Eosinophils

(A) Shown is a representative confocal micrograph of lung tissue stained with Sirius red from an $Areg^{+/+}$ and an $Areg^{-/-}$ mouse with HDM exposure (left) from three experiments. Scale bars represent 100 μm. Shown are ratios of areas of randomly selected regions stained with Sirius red surrounding bronchi versus the areas of associated basement membranes (right). More than three mice per group were analyzed.

(B and C) Shown is a representative confocal micrograph of lung tissue stained with anti-osteopontin (green) and DAPI (white) from an $Areg^{+/+}$ and an $Areg^{-/-}$ mouse from three experiments (scale bars represent 50 μm) (B). Shown is the absolute number of ostepontin-positive cells in randomly selected lung tissue slices (C). Three mice per group were analyzed.

(D) Quantitative RT-PCR analysis of the indicated genes in the lungs of $Areg^{+/+}$ and $Areg^{-/-}$ mice with HDM exposure (n = 3 mice per group).

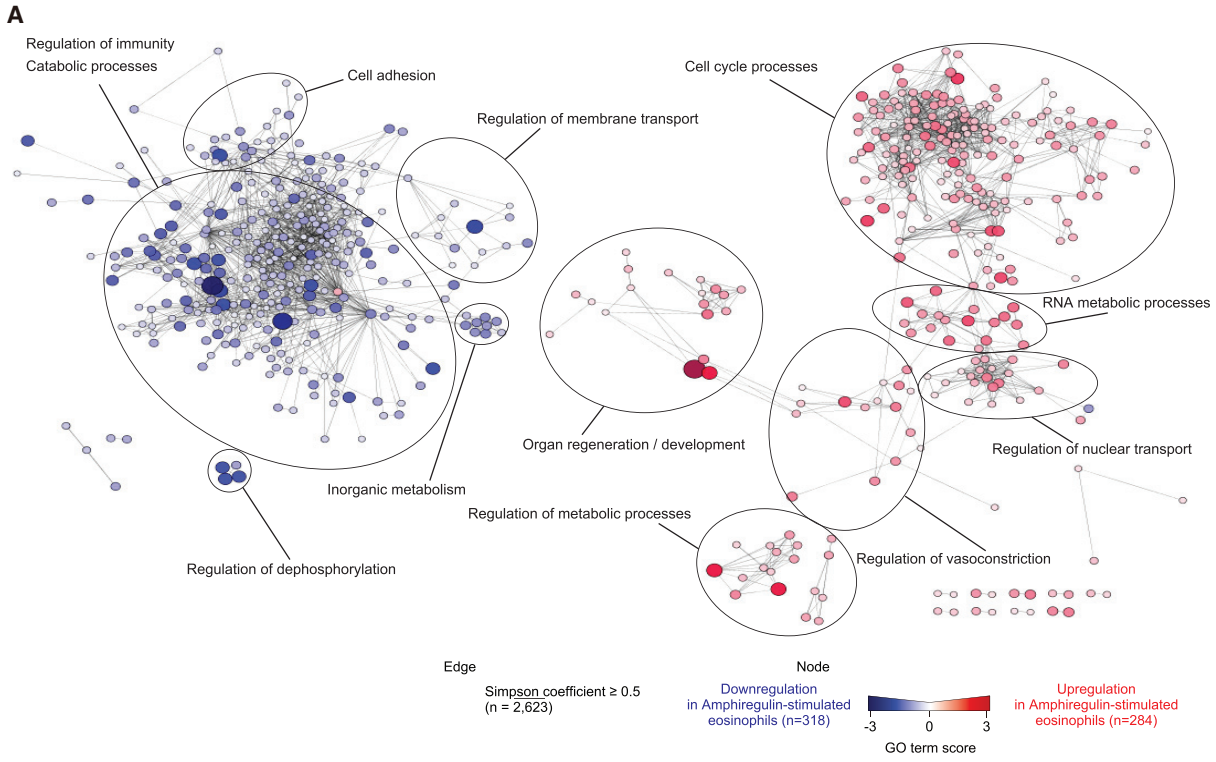
(E) $Areg^{+/+}$ and $Areg^{-/-}$ memory Th2 cells (3×10^6 cells) were transferred i.v. into wild-type mice and subsequently challenged with OVA. Shown is a representative confocal micrograph of lung tissue stained with Sirius red from recipients of $Areg^{+/+}$ and $Areg^{-/-}$ memory Th2 cells (left) from two experiments. Scale bars represent 100 μm. Shown are ratios of areas of randomly selected regions stained with Sirius red surrounding bronchi versus the areas of associated basement membranes (right). More than three mice per group were analyzed.

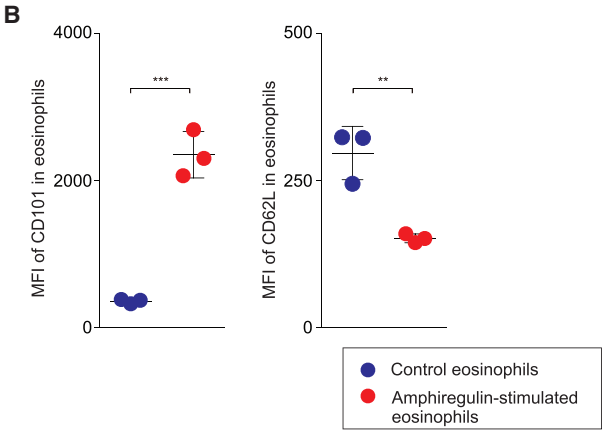
(F and G) Shown is a representative confocal micrograph of lung tissue stained with anti-osteopontin (green) and DAPI (white) from recipients of $Areg^{+/+}$ or $Areg^{-/-}$ memory Th2 cells from two experiments (scale bars represent 50 μm). Three independent experiments were performed with similar results (F). Shown are the absolute number of ostepontin-positive cells in randomly selected lung tissue slices (G). Three mice per group were analyzed.

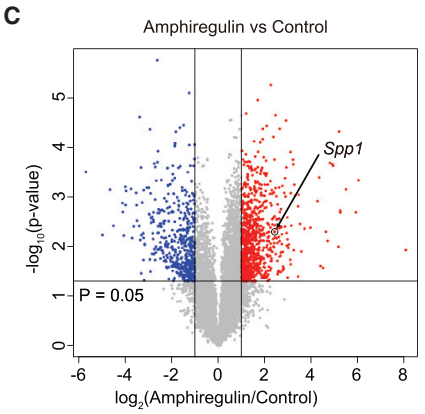
(H) Shown is a representative confocal micrograph of the lung stained with anti-osteopontin (green) and anti-Siglec-F (red) from a mouse challenged with OVA inhalation from four experiments. Scale bars represent 50 μm. Three independent experiments were performed with similar results.

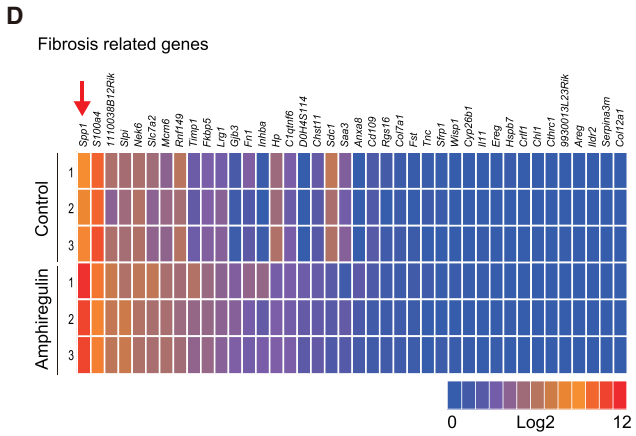
(I) Quantitative RT-PCR analysis of *Spp1* in the indicated cells from the lungs of $Areg^{+/+}$ and $Areg^{-/-}$ mice twice treated with OVA and Alum followed by a series of OVA inhalations (Figure S3A).

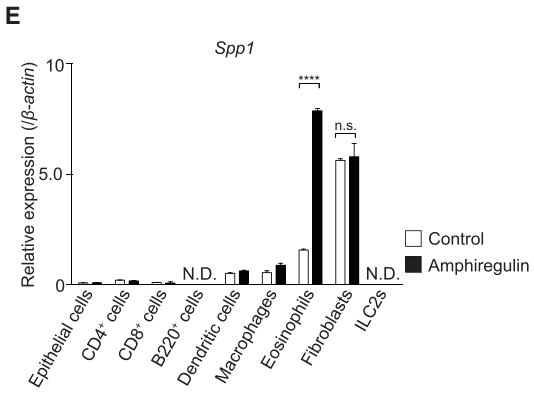
Data are the mean ± SD. $^{**}p < 0.01$, $^{***}p < 0.001$, $^{****}p < 0.0001$; by unpaired t test or one-way analysis of variance (ANOVA). Please see also Figure S3.











(legend on next page)

and regulation of nuclear transport (Figure 4A, Table S1). As compared to control un-stimulated eosinophils, amphiregulin-stimulated eosinophils significantly upregulated genes characteristic of inflammatory eosinophils (Figure S4E; Mesnil et al., 2016). Characteristic of inflammatory eosinophils, amphiregulin-stimulated eosinophils upregulated CD101 and downregulated CD62L (Figure 4B; Mesnil et al., 2016). These results indicate that amphiregulin reprogrammed eosinophil gene expression toward an inflammatory state.

Compared to control stimulation, amphiregulin stimulation led to 846 genes with >2-fold upregulation and 467 genes with <50% downregulation (Figure 4C). As expected, *Spp1* was one of the genes significantly induced by amphiregulin stimulation. Among reported fibrosis-related genes (Wick et al., 2013), *Spp1* was confirmed to be upregulated by amphiregulin in eosinophils (Figure 4D). Quantitative RT-PCR confirmed that amphiregulin stimulation induced the expression of *Spp1* in eosinophils but not in other types of cells including fibroblasts (Figure 4E). These results indicate that inflammatory eosinophils activated by amphiregulin expressed *Spp1*.

Osteopontin Secretion from Eosinophils Is Required for Fibrosis

Mice that genetically lack eosinophils (ΔdblGATA mice) showed ameliorated fibrotic responses by both HDM exposure and OVA-alum immunization followed by OVA inhalation (Figures S5A–S5D). Comparative global gene expression revealed enrichment of lung-tissue repair-related pathways in lungs from wild-type as compared to ΔdblGATA mice (Figures 5A and S5E). *Spp1* was one of the genes upregulated in both amphiregulin-stimulated eosinophils and inflamed lungs from wild-type mice (Figures 5B and S5F). Using a trans-well co-culture system, $Spp1^{+/+}$ but not $Spp1^{-/-}$ eosinophils induced enhanced expression of fibrosis-related molecules from fibroblasts (Figures 5C and S5G–S5I). Consistent with these results, *in vivo* OVA-alum immunization followed by OVA inhalation or repetitive exposure of HDM resulted in ameliorated fibrotic changes in the lungs from $Spp1^{-/-}$ mice (Figures 5D and S5J–S5O).

Next, to determine whether osteopontin produced by eosinophils was physiologically relevant to the induction of lung fibrotic responses *in vivo*, we transferred eosinophils from $Spp1^{+/+}$ mice or $Spp1^{-/-}$ mice together with OVA-specific memory Th2 cells to ΔdblGATA mice and then performed antigen challenge (Figure S5P). Lung collagen deposition was significantly decreased in recipients of $Spp1^{-/-}$ as compared to $Spp1^{+/+}$ eosinophils (Figure 5E). Recipients of $Spp1^{-/-}$ as compared to $Spp1^{+/+}$ eosinophils also exhibited decreased expression of fibrosis-related genes (Figures 5F and 5G). Thus, osteopontin produced by eosinophils was relevant to the induction of lung fibrotic responses.

Inhibition of EGFR Signaling Ameliorates Fibrotic Responses *In Vivo*

Erlotinib, a receptor tyrosine kinase inhibitor acting on the EGFR (Moyer et al., 1997), inhibited amphiregulin-induced *Spp1* upregulation in eosinophils without any obvious effects in the survival of eosinophils (Figures 6A, S6A, and S6B). Erlotinib also had no obvious effect on the survival and cytokine production of $ST2^{hi}$ memory Th2 cells (Figures S6C and S6D). However, Erlotinib treatment *in vivo* resulted in significant decreases in both collagen deposition and expression of fibrosis-related genes in inflamed lungs (Figures 6B and S6E–S6G). Osteopontin-positive eosinophils disappeared from the inflamed lungs of mice treated with Erlotinib (Figures 6C and 6D). Moreover, Erlotinib treatment after the induction of fibrotic changes by repetitive exposure to HDM resulted in ameliorated fibrosis accompanied by disappearance of osteopontin-positive eosinophils (Figures 6E–6G, S6H, and S6I). Thus, the amphiregulin-EGFR-osteopontin axis in eosinophils leads to fibrotic responses *in vivo*.

ECRS Polyps with Fibrotic Changes Exhibit Selective Amphiregulin Production by Memory $CD4^+$ T Cells and Osteopontin Expression by Eosinophils

We sought to determine whether the observed mechanisms were relevant to inflammatory lesions of human chronic allergic diseases. Eosinophilic chronic rhinosinusitis (ECRS) is a chronic upper airway inflammatory disease that often presents with nasal polyps infiltrated with eosinophils (Nakayama et al., 2011). Fibronectin deposition was significantly elevated in the polyps of patient with ECRS as compared to the normal nasal mucosa (Figure 7A). The expression of fibrosis-related genes such as *SPP1*, *TNC*, *COL1A1*, *ACTA2*, and *FN1* was significantly increased in ECRS polyps as compared to normal nasal mucosa tissue (Figure 7B). The expression of *AREG*, *IL33*, *IL1RL1*, and Th2 cytokines was also significantly higher in the ECRS polyps (Figures 7C and S7A). These results prompted us to characterize amphiregulin-producing cell population(s) in local inflammatory sites. Flow cytometry analysis of infiltrating mononuclear cells from ECRS polyps revealed amphiregulin production coming mainly from $CD45RO^+$ memory-type $CD4^+$ T cells, with a minor contribution from innate lymphoid cells (ILCs) (Figures S7B–S7D). Moreover, among polyp-infiltrating cells, ILCs produced significantly less amphiregulin than memory-type $CD4^+$ T cells (Figures 7D and S7E). Among nasal polyp-infiltrating memory-type $CD45RO^+CD4^+$ T cells, IL-5 and amphiregulin production was restricted to $CD161^{hi}CRTH2^{hi}$ cells (Figures 7E and

Figure 4. Amphiegulin Induced Transcriptional Reprogramming of Eosinophils

The global gene expression profiles of mouse bone marrow-derived eosinophils stimulated with or without amphiregulin for 72 hr were assessed by RNA-seq.

(A) Shown is a network visualization of Gene Ontology enrichment analysis. Node colors indicate GO terms that were significantly upregulated (red) or downregulated (blue) in eosinophils stimulated with amphiregulin compared to control eosinophils. Node sizes represent enrichment scores for each GO terms. Node connections were determined using overlap of the elemental gene products in the GO terms (Simpson coefficient $\geq$ 0.5).

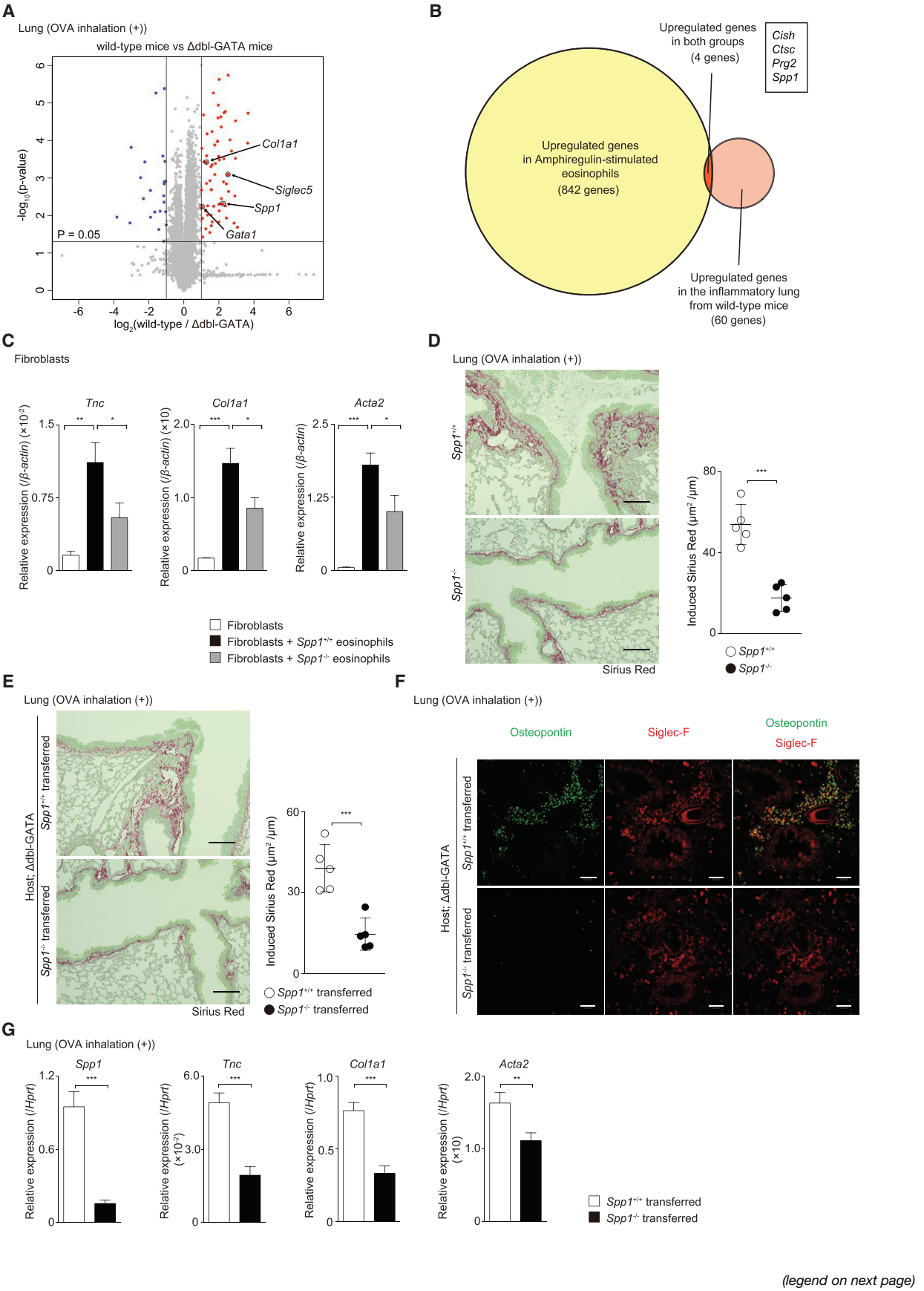
(B) CD101 expression and CD62L expression are shown by geometric mean channel fluorescence.

(C) Volcano plot depicts differential gene expression in eosinophils induced by amphiregulin compared to control. The arrow indicates *Spp1*.

(D) Heatmap of log2 expression values of fibrosis-related genes in eosinophils with or without amphiregulin stimulation.

(E) Quantitative RT-PCR analysis of *Spp1* in the indicated cells from lungs of wild-type mice stimulated with or without amphiregulin for 72 hr.

Data are the mean ± SD. **p < 0.01, ***p < 0.001, ****p < 0.0001; n.s., not significant; by unpaired t test or one-way analysis of variance (ANOVA). Please see also Figure S4.



(legend on next page)

S7F–S7H). However, distinct CD161^{hi}CRTH2^{hi} subpopulations were responsible for amphiregulin and IL-5 production (Figures 7E, S7F, and S7G). Histological analyses of ECRS nasal polyps revealed eosinophil infiltrates associated with dense osteopontin deposits (Figure 7F, lower panel). Eosinophils infiltrating ECRS polyps exhibited significantly elevated expression of *SPP1* as compared to circulating eosinophils in PBMCs obtained from the same patients (Figure 7G). The expression of *SPP1* was induced by amphiregulin in circulating eosinophils, and Erlotinib constrained the induction of *SPP1* (Figures 7H, S7I, and S7J). These results show that amphiregulin-producing memory-type CD4$^+$ T cells co-localize with ostepontin-expressing eosinophils in ECRS polyps where severe fibrotic responses were observed. Thus, we have identified an amphiregulin-producing memory-type CD4$^+$ T cell subpopulation that may direct tissue fibrotic responses via eosinophilic osteopontin in the nasal polyps of ECRS patients.

DISCUSSION

Herein, we have identified that amphiregulin produced by memory-type Th2 cells is a key molecule in the pathogenesis of fibrosis during eosinophilic inflammation. We found that amphiregulin reprogrammed eosinophils to adopt an inflammatory phenotype with enhanced osteopontin production. The genetic deletion of *Il33*, *Il1rl1*, *Areg*, or *Spp1* or the blockade of EGFR signaling *in vivo* attenuated fibrotic responses during eosinophilic inflammation in the lung. The analysis of ECRS polyps revealed severe fibrotic lesion infiltrated with osteopontin-expressing eosinophils and amphiregulin-producing CD161$^+$CRTH2$^+$ memory CD4$^+$ T cells. Amphiregulin-producing memory Th2 cells were distinct from IL-5-producing memory Th2 cells, and the co-operation of both pathogenic Th2 cell subpopulations appear to be critical for the induction of fibrosis in the airways of both mice and humans. Moreover, the blockade of EGFR signaling by Erlotinib resulted in decreased amphiregulin-induced upregulation of *SPP1* expression in eosinophils, indicating that the IL-33-amphiregulin-osteopontin axis could be a therapeutic target for treatment of fibrosis in chronic allergic inflammation.

IL-33 is associated with several fibrotic diseases such as hepatic fibrosis and bleomycin-induced pulmonary fibrosis via activation of type 2 innate lymphoid cells (ILC2s) and macrophages (Li et al., 2014; McHedlidze et al., 2013). The IL-33-ST2 axis plays a protective role in cardiac fibrosis (Sanada et al., 2007). By contrast, we demonstrated that IL-33 drove fibrotic responses in the inflamed lung through the activation of ST2^{hi} memory-type Th2 cells. Thus, IL-33 is a multifunctional cytokine and appears to exert distinct effects in different biological contexts. IL-33 stimulation resulted in selective production of amphiregulin by ST2^{hi} memory-type Th2 cells in models of allergen-induced allergic airway inflammation. Amphiregulin, encoded by *Areg*, belongs to the epidermal growth factor (EGF) family and signals through the EGFR system (Shoyab et al., 1989). Amphiregulin is known to promote tissue-protective epithelial responses in the intestine during helminth infection (Zaiss et al., 2006). Amphiregulin produced by regulatory T (Treg) cells, mast cells, and ILC2s has also been found to be involved in the process of tissue repair of muscle and lungs, thereby contributing to tissue homeostasis (Arpaia et al., 2015; Burzyn et al., 2013; Monticelli et al., 2011; Okumura et al., 2005; Zaiss et al., 2013). Although uncontrolled tissue repair due to chronic inflammation may cause fibrosis (Wick et al., 2013), until the current work the pathogenic role of amphiregulin in the induction of fibrosis had not been not established. In the present study, we have shown that genetic ablation of amphiregulin resulted in ameliorated fibrotic responses, which indicates that amphiregulin contributes to the pathogenesis of inflammation-associated fibrosis. Moreover, we found that ST2^{hi} memory-type Th2 cells were the major producer of amphiregulin in antigen-induced eosinophilic airway inflammation models and thus are key players in lung fibrotic responses. We also found that the majority of amphiregulin-producing ST2^{hi} memory-type Th2 cells did not produce IL-5. These results indicate functional heterogeneity of ST2^{hi} memory Th2 cell populations: IL-5-producing cells to recruit and activate eosinophils and amphiregulin-producing cells to induce fibrotic responses. A two-step interaction between eosinophils and distinct ST2^{hi} memory Th2 cell subpopulations producing either IL-5 or amphiregulin may underlie the establishment of pathological eosinophil-induced fibrotic changes.

Figure 5. Osteopontin Secretion by Eosinophils Is Required for Fibrotic Responses in the Lung

(A) OVA-specific memory Th2 cells (3 × 10^6 cells) were transferred i.v. into wild-type mice and ΔdbI-GATA mice that were subsequently challenged with OVA. Volcano plot depicts differential gene expression in the lungs of wild-type versus ΔdbI-GATA mice. Arrows indicate *Spp1*, *Col1a1*, *Gata1*, and *Siglec5*.

(B) Shown is a Venn diagram of upregulated genes in amphiregulin-stimulated eosinophils (842 genes) and upregulated genes in lungs from wild-type mice with OVA challenges (60 genes). The 4 overlapping genes are shown in a box.

(C) Quantitative RT-PCR analysis of the indicated genes in fibroblasts co-cultured with or without *Spp1*$^{+/+}$ and *Spp1*$^{-/-}$ eosinophils for 24 hr as indicated in Figure S5G. Three independent experiments were performed with similar results.

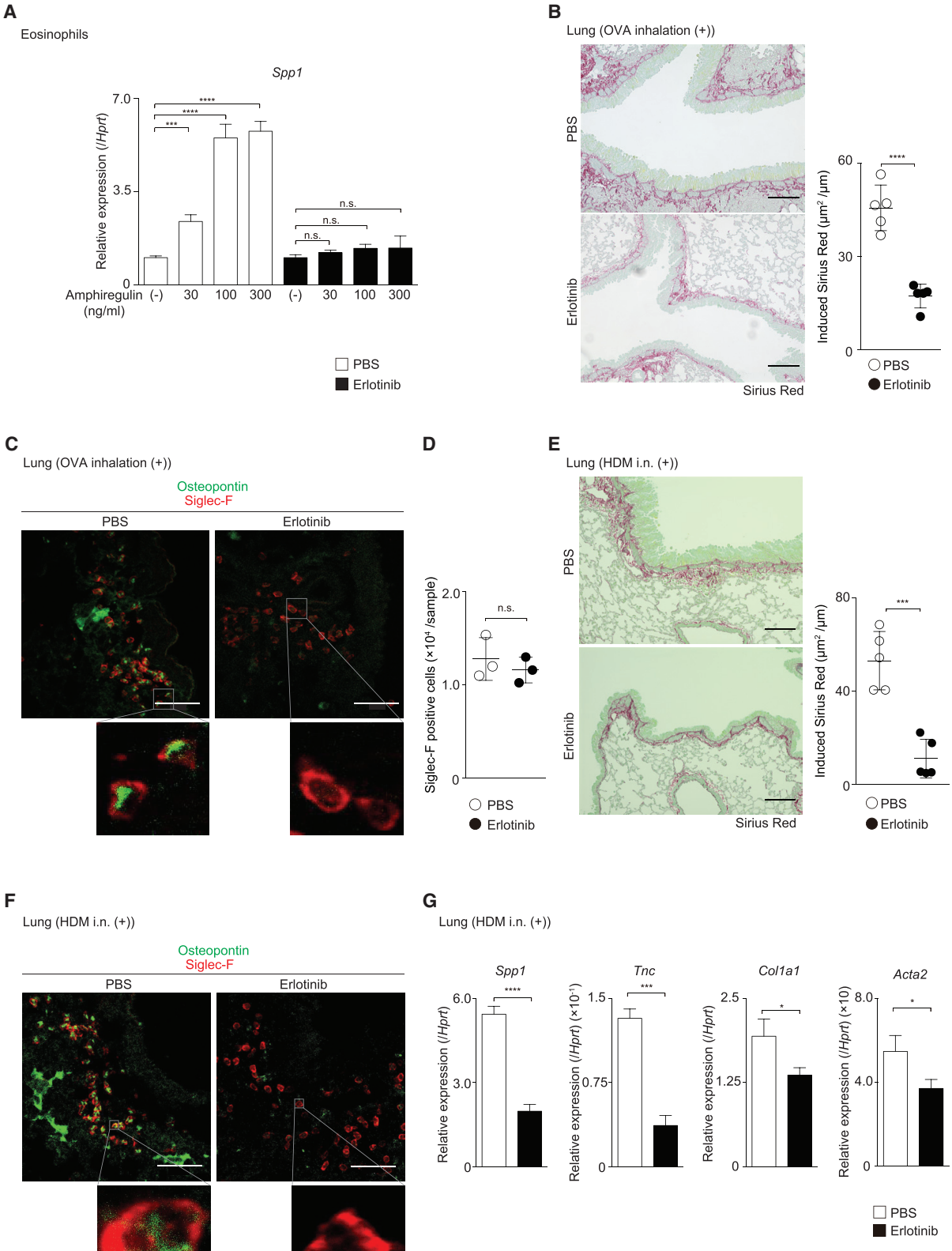
(D) *Spp1*$^{+/+}$ and *Spp1*$^{-/-}$ mice were immunized with OVA and Alum twice followed by a series of OVA inhalations. Shown is a representative confocal micrograph of lung tissue stained with Sirius red from a *Spp1*$^{+/+}$ and a *Spp1*$^{-/-}$ mouse (left) from three experiments. Scale bars represent 100 μm. Shown are ratios of areas of randomly selected regions stained with Sirius red surrounding bronchi versus the areas of associated basement membranes (right). More than three mice per group were analyzed.

(E) Memory Th2 cells (3 × 10^6 cells) were adoptively transferred i.v. into ΔdbI-GATA mice that were subsequently challenged with OVA and then adoptively transferred with *Spp1*$^{+/+}$ and *Spp1*$^{-/-}$ eosinophils (1 × 10^8 cells, i.v.) as indicated in Figure S5P. Shown is a representative confocal micrograph of lung tissue stained with Sirius red from recipients of *Spp1*$^{+/+}$ and *Spp1*$^{-/-}$ eosinophils (left) from two experiments. Scale bars represent 100 μm. Shown are ratios of areas of randomly selected regions stained with Sirius red surrounding bronchi versus the areas of associated basement membranes (right). More than three mice per group were analyzed.

(F) Shown is a representative confocal micrograph of the lungs stained with anti-Osteopontin (green) and Siglec-F (red) from recipients of *Spp1*$^{+/+}$ and *Spp1*$^{-/-}$ eosinophils from two experiments (scale bars represent 50 μm). Three independent experiments were performed with similar results.

(G) Quantitative RT-PCR analysis of the indicated genes in the lungs from recipients of *Spp1*$^{+/+}$ and *Spp1*$^{-/-}$ eosinophils (n = 3 mice per group).

Data are the mean ± SD. **p < 0.01, ***p < 0.001; by unpaired t test or one-way analysis of variance (ANOVA). Please see also Figure S5.



(legend on next page)

In the current study, we also identified eosinophils as critical target cells for amphiregulin in the process of inflammation-associated fibrosis. Amphiregulin is well known to stimulate lung epithelial cells to undergo proliferation and enhanced mucin production (Okumura et al., 2005; Zaiss et al., 2006). Amphiregulin also promotes the proliferation of lung fibroblasts (Al-Muhsen et al., 2011). Amphiregulin from tissue-resident Treg cells contributes to the downregulation of collagens from injured muscle cells (Burzyn et al., 2013). Other groups have reported that amphiregulin from cardiac Ly6C^{lo} macrophages is involved in the adaptive response to pressure overload in the heart (Fujiu et al., 2017). Our genome-wide analyses revealed that amphiregulin stimulation induced transcriptional reprogramming in eosinophils, marked by upregulation of inflammatory genes. One of the genes upregulated by amphiregulin stimulation in eosinophils was *Spp1*, a major component of noncollagenous ECM in fibrotic tissues and a contributor to the pathogenesis of fibrosis (Denhardt et al., 2001; Sabo-Attwood et al., 2011). Refractory asthma is often associated with tissue fibrosis leading to a decrease in lung function. Our findings indicate that eosinophils directly produce noncollagenous ECM and contribute to tissue fibrosis in allergic airway inflammation.

The analysis of ECRS polyps revealed significantly increased deposition of fibronectin and upregulation of various fibrosis-related genes. Previous work has shown that osteopontin is upregulated in nasal polys from patients with chronic rhinosinusitis with nasal polyps (CRSwNP) (Liu et al., 2015). Other work has shown that osteopontin is expressed in eosinophils from patients with atopic dermatitis and that expression of osteopontin is enhanced by GM-CSF and IL-5 (Puxeddu et al., 2010). In this study, we detected the accumulation of both amphiregulin-producing CD161^{hi}CRTH2^{hi} memory-type CD4^{+} T cells and osteopontin-producing eosinophils in ECRS polyps. But very limited numbers of ILC2s were detected in the nasal polyps of patients with ECRS. In particular, amphiregulin production was less than 1.0% in ILC2s as compared to T cells. Though perhaps unexpected given observations from previous publications (Bal et al., 2016; Ho et al., 2015), we provided a direct comparison of amphiregulin production among T cells and ILC2s. Our results show that in ECRS polyps, the major source of amphiregulin is a CD161^{hi}CRTH2^{hi} memory-type CD4^{+} T cell. Cells with this phenotype have been shown to produce large amounts of IL-5 and have been appreciated as ''pathogenic'' in various human allergic diseases, particularly in association with eosinophilic inflammation such as in eosinophilic esophagitis (Mitson-Salazar et al., 2016; Nakayama et al., 2017; Wambre et al., 2017). In the current study, similar to results from mouse systems, we detected both IL-5-producing and amphiregulin-producing subsets among CD161^{hi}CRTH2^{hi} memory-type CD4^{+} T cells infiltrating ECRS polyps. The majority of amphiregulin producers showed limited production of IL-5. Thus, the current study demonstrates functional heterogeneity of pathogenic memory Th2 cells in both mouse and human systems. Treatment with CRTH2 antagonist OC000459 causes reduction of extracellular deposits in patients with eosinophilic esophagitis (Straumann et al., 2013). Thus, the amphiregulin-osteopontin pathway could be a potential therapeutic target for patients with eosinophilic inflammatory disorders including ECRS that are refractory to corticosteroid treatment.

In summary, we have identified the cellular and molecular mechanisms that control the induction of airway fibrotic responses during chronic allergic inflammation. We have elucidated the critical role of the IL-33-amphiregulin-osteopontin axis in the interaction between ST2^{hi} memory-type pathogenic Th2 cells and eosinophils and how this shapes the pathology of fibrotic responses in allergic inflammation, and provides the molecular basis for the development of potential therapeutic strategies for intractable inflammation-associated fibrotic diseases.

STAR★METHODS

Detailed methods are provided in the online version of this paper and include the following:

- KEY RESOURCES TABLE
- CONTACT FOR REAGENT AND RESOURCE SHARING
- EXPERIMENTAL MODEL AND SUBJECT DETAILS
  - Mice
  - Human Samples

Figure 6. Inhibition of EGFR Signaling Ameliorates Fibrotic Responses *In Vivo*

(A) Quantitative RT-PCR analysis of *Spp1* in eosinophils. Eosinophils were cultured with amphiregulin (white) or amphiregulin plus Erlotinib (black) for 72 hr. Three independent experiments were performed and showed similar results.

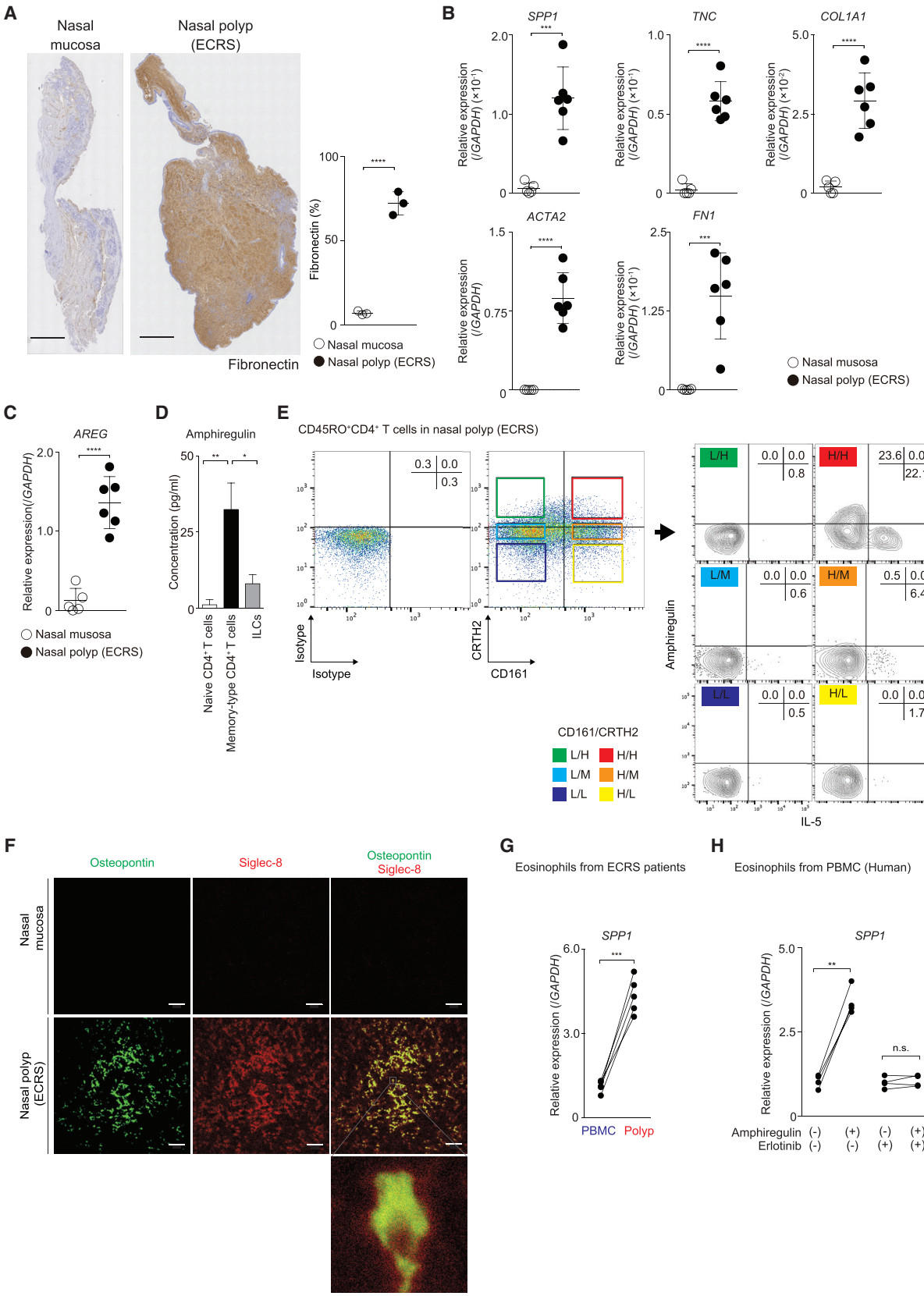
(B) Wild-type mice were OVA challenged with or without simultaneous Erlotinib treatment as indicated in Figure S6E. Shown is a representative confocal micrograph of lung tissue stained with Sirius red from mice treated with PBS (PBS) or Erlotinib (Erlotinib) (left) from three experiments. Scale bars represent 100 μm. Shown are ratios of areas of randomly selected regions stained with Sirius red surrounding bronchi versus the areas of associated basement membranes (right). More than three mice per group were analyzed.

(C and D) Shown is a representative confocal micrograph of the lung stained with anti-osteopontin (green) and anti-Siglec-F (red) from mice with or without simultaneous Erlotinib treatment from three experiments (C). Scale bars represent 50 μm. Three independent experiments were performed with similar results. Shown are the absolute number of Siglec-F-positive cells in randomly selected lung tissue slices. Three mice per group were analyzed (D).

(E) Wild-type mice were HDM challenged with or without subsequent Erlotinib treatment as indicated in Figure S6H. Shown is a representative confocal micrograph of lung tissue stained with Sirius red from mice treated with PBS (PBS) or Erlotinib (Erlotinib) (left) from two experiments. Scale bars represent 100 μm. Shown are ratios of areas of randomly selected regions stained with Sirius red surrounding bronchi versus the areas of associated basement membranes (right). More than three mice per group were analyzed.

(F) Shown is a representative confocal micrograph of the lung stained with anti-osteopontin (green) and anti-Siglec-F (red) from mice with or without subsequent Erlotinib treatment from two experiments. Scale bars represent 50 μm. Three independent experiments were performed with similar results.

(G) Quantitative RT-PCR analysis of the indicated genes in lungs from HDM-exposed mice with or without subsequent Erlotinib treatment (n = 3 mice per group). Data are the mean ± SD. *$p < 0.05$, ***$p < 0.001$, ****$p < 0.0001$; n.s., not significant; by unpaired t test or one-way analysis of variance (ANOVA). Please see also Figure S6.



(legend on next page)

- METHOD DETAILS
  - Histology and immunohistochemistry
  - The Generation and Culture of Effector and Memory Th2 Cells
  - Flow cytometry and sorting
  - Cell Viability Assay
  - ST2 Neutralizing Assay
  - Erlotinib Treatment
  - Quantitative Real-Time PCR
  - RNA Sequencing
  - ELISA for the Measurement of Amphiregulin Expression
  - BAL fluid Collecting
  - Exposure of HDM
  - Immunization and inhalation with OVA
  - Culture of Bone Marrow-Derived Eosinophils
  - *In vitro* treatment of Eosinophils with Amphiregulin
  - Adoptive Transfer of Eosinophils
  - Intratracheal Administration of IL-33
  - Co-culture of Eosinophils and Fibroblasts
  - Cell Isolation From Mouse Lungs
  - Nasal Polyp, Peripheral Blood Mononuclear Cell and Homogenate Preparation
- QUANTIFICATION AND STATISTICAL ANALYSIS
  - Statistical Analysis
  - Analysis and graphic display of RNA-seq data
  - Gene Ontology enrichment analysis
- DATA AND SOFTWARE AVAILABILITY

SUPPLEMENTAL INFORMATION

Supplemental Information includes seven figures and one table and can be found with this article online at https://doi.org/10.1016/j.immuni.2018.04.023.

ACKNOWLEDGMENTS

We are grateful for Drs. Mark Bix, Omid Akbari, and Yuka Kanno for their critical reading and providing valuable suggestions on the manuscript. We thank Toshihiro Ito, Kaoru Sugaya, and Miki Kato for their excellent technical assistance. This work was supported by the following grants: Ministry of Education, Culture, Sports, Science and Technology (MEXT Japan) Grants-in-Aid for Scientific Research (S) 26221305, (C) 17K08876 and 18K07164, and Young Scientists (B) 18K16830; AMED-CREST, AMED (no. JP16gm0410009); AMED-PRIME, AMED (no. JP18gm6110005); Practical Research Project for Allergic Diseases and Immunology (Research on Allergic Diseases and Immunology) from AMED (no. JP18ek0410030, JP18ek0410045); Takeda Science Foundation; and the Naito Foundation.

AUTHOR CONTRIBUTIONS

Y.M., K.H., and T.N. designed experiments. Y.M., K.H., M.K., T.W., T.K., M.O., and K.K. performed experiments. Y.M., K.H., T.I., A.O., D.S., Y.O., and T.N. analyzed and interpreted data. Y.M., K.H., Y.O., and T.N. wrote the paper.

DECLARATION OF INTERESTS

Y.M., K.H., Y.O., and T.N. are inventors of Japanese patent application 2017-176017, which is related to this work, and have assigned the application to Chiba University per the University's invention policy.

Received: July 4, 2017
Revised: March 12, 2018
Accepted: April 19, 2018
Published: June 26, 2018

REFERENCES

Adcock, I.M., Caramori, G., and Chung, K.F. (2008). New targets for drug development in asthma. Lancet *372*, 1073–1087.

Al-Muhsen, S., Johnson, J.R., and Hamid, Q. (2011). Remodeling in asthma. J. Allergy Clin. Immunol. *128*, 451–462, quiz 463–454.

Arpaia, N., Green, J.A., Moltedo, B., Arvey, A., Hemmers, S., Yuan, S., Treuting, P.M., and Rudensky, A.Y. (2015). A distinct function of regulatory T cells in tissue protection. Cell *162*, 1078–1089.

Bal, S.M., Bernink, J.H., Nagasawa, M., Groot, J., Shikhagaie, M.M., Golebski, K., van Drunen, C.M., Lutter, R., Jonkers, R.E., Hombrink, P., et al. (2016). IL-1β, IL-4 and IL-12 control the fate of group 2 innate lymphoid cells in human airway inflammation in the lungs. Nat. Immunol. *17*, 636–645.

Ball, S.L., Mann, D.A., Wilson, J.A., and Fisher, A.J. (2016). The role of the fibroblast in inflammatory upper airway conditions. Am. J. Pathol. *186*, 225–233.

Burzyn, D., Kuswanto, W., Kolodin, D., Shadrach, J.L., Cerletti, M., Jang, Y., Sefik, E., Tan, T.G., Wagers, A.J., Benoist, C., and Mathis, D. (2013). A special population of regulatory T cells potentiates muscle repair. Cell *155*, 1282–1295.

Busse, W.W., and Lemanske, R.F., Jr. (2001). Asthma. N. Engl. J. Med. *344*, 350–362.

Figure 7. Nasal Polyps of ECRS Patients Revealed Massive Deposition of SPP1 Accompanied by Amphiregulin-Producing Memory-type CD4$^+$ T Cells

(A) Representative confocal micrograph of the nasal mucosa from a healthy control subject (left) and a polyp from a patient with ECRS (middle) stained with anti-Fibronectin from three samples in each group (scale bars, 1 mm). The ratios of stained area versus the area of the whole tissue were measured in three samples from both groups (right).

(B) Quantitative RT-PCR analysis of the indicated genes in the nasal mucosa of healthy control subjects (control; n = 5) and in the polyps of patients with ECRS (ECRS; n = 6).

(C) Quantitative RT-PCR analysis of *AREG* in the nasal mucosa from healthy control subjects (control; n = 5) and in the polyps of patients with ECRS (ECRS; n = 6).

(D) Protein expression of amphiregulin from the indicated cells. Three independent experiments were performed with similar results.

(E) Shown is a representative flow cytometry plot of CD161 and CRTH2 surface expression in memory CD4$^+$ T cells from the polyp of a patient with ECRS with isotype controls (left) from 40 independent experiments (n = 40). Shown are representative flow cyometry plots of amphiregulin and IL-5 intracellular-staining for cells in each of the six quadrants of the CD161 and CRTH2 flow cytometry plot (right) from ten independent experiments (n = 10).

(F) Shown are representative confocal micrographs of the nasal mucosa from healthy control subjects (upper) and polyps of patients with ECRS (lower) stained with anti-SPP1 (green) and anti-Siglec-8 (red) from four independent experiments (n = 4) (scale bars represent 50 μm). More than three independent experiments were performed with similar results.

(G) Quantitative RT-PCR analysis of *SPP1* in eosinophils from patients with ECRS. Eosinophils from peripheral blood (PBMC) and polyps were sorted from individual patients (n = 5).

(H) Quantitative RT-PCR analysis of *SPP1* in eosinophils from healthy control subjects. Eosinophils were cultured with medium, amphiregulin, Erlotinib, or amphiregulin plus Erlotinib for 72 hr (n = 4 subjects).

Data are the mean ± SD. **p < 0.01, ***p < 0.001, ****p < 0.0001; n.s., not significant; by unpaired t test or paired t test. Please see also Figure S7.

Denhardt, D.T., Noda, M., O'Regan, A.W., Pavlin, D., and Berman, J.S. (2001). Osteopontin as a means to cope with environmental insults: regulation of inflammation, tissue remodeling, and cell survival. J. Clin. Invest. *107*, 1055–1061.

Doherty, T.A., Soroosh, P., Khorram, N., Fukuyama, S., Rosenthal, P., Cho, J.Y., Norris, P.S., Choi, H., Scheu, S., Pfeffer, K., et al. (2011). The tumor necrosis factor family member LIGHT is a target for asthmatic airway remodeling. Nat. Med. *17*, 596–603.

Durrani, S.R., Viswanathan, R.K., and Busse, W.W. (2011). What effect does asthma treatment have on airway remodeling? Current perspectives. J. Allergy Clin. Immunol. *128*, 439–448, quiz 449–450.

Endo, Y., Iwamura, C., Kuwahara, M., Suzuki, A., Sugaya, K., Tumes, D.J., Tokoyoda, K., Hosokawa, H., Yamashita, M., and Nakayama, T. (2011). Eomesodermin controls interleukin-5 production in memory T helper 2 cells through inhibition of activity of the transcription factor GATA3. Immunity *35*, 733–745.

Endo, Y., Hirahara, K., Iinuma, T., Shinoda, K., Tumes, D.J., Asou, H.K., Matsugae, N., Obata-Ninomiya, K., Yamamoto, H., Motohashi, S., et al. (2015). The interleukin-33-p38 kinase axis confers memory T helper 2 cell pathogenicity in the airway. Immunity *42*, 294–308.

Foster, P.S., Maltby, S., Rosenberg, H.F., Tay, H.L., Hogan, S.P., Collison, A.M., Yang, M., Kaiko, G.E., Hansbro, P.M., Kumar, R.K., and Mattes, J. (2017). Modeling T_H 2 responses and airway inflammation to understand fundamental mechanisms regulating the pathogenesis of asthma. Immunol. Rev. *278*, 20–40.

Fujiu, K., Shibata, M., Nakayama, Y., Ogata, F., Matsumoto, S., Noshita, K., Iwami, S., Nakae, S., Komuro, I., Nagai, R., and Manabe, I. (2017). A heart-brain-kidney network controls adaptation to cardiac stress through tissue macrophage activation. Nat. Med. *23*, 611–622.

Gieseck, R.L., 3rd, Wilson, M.S., and Wynn, T.A. (2018). Type 2 immunity in tissue repair and fibrosis. Nat. Rev. Immunol. *18*, 62–76.

Hamilos, D.L. (2015). Drivers of chronic rhinosinusitis: Inflammation versus infection. J. Allergy Clin. Immunol. *136*, 1454–1459.

Hansbro, P.M., Kim, R.Y., Starkey, M.R., Donovan, C., Dua, K., Mayall, J.R., Liu, G., Hansbro, N.G., Simpson, J.L., Wood, L.G., et al. (2017). Mechanisms and treatments for severe, steroid-resistant allergic airway disease and asthma. Immunol. Rev. *278*, 41–62.

Hirahara, K., Yamashita, M., Iwamura, C., Shinoda, K., Hasegawa, A., Yoshizawa, H., Koseki, H., Gejyo, F., and Nakayama, T. (2008). Repressor of GATA regulates TH2-driven allergic airway inflammation and airway hyperresponsiveness. J. Allergy Clin. Immunol. *122*, 512–520, e511.

Ho, J., Bailey, M., Zaunders, J., Mrad, N., Sacks, R., Sewell, W., and Harvey, R.J. (2015). Group 2 innate lymphoid cells (ILC2s) are increased in chronic rhinosinusitis with nasal polyps or eosinophilia. Clin. Exp. Allergy *45*, 394–403.

Humbles, A.A., Lloyd, C.M., McMillan, S.J., Friend, D.S., Xanthou, G., McKenna, E.E., Ghiran, S., Gerard, N.P., Yu, C., Orkin, S.H., and Gerard, C. (2004). A critical role for eosinophils in allergic airways remodeling. Science *305*, 1776–1779.

Islam, S.A., Chang, D.S., Colvin, R.A., Byrne, M.H., McCully, M.L., Moser, B., Lira, S.A., Charo, I.F., and Luster, A.D. (2011). Mouse CCL8, a CCR8 agonist, promotes atopic dermatitis by recruiting IL-5+ T(H)2 cells. Nat. Immunol. *12*, 167–177.

Kim, H.Y., DeKruyff, R.H., and Umetsu, D.T. (2010). The many paths to asthma: phenotype shaped by innate and adaptive immunity. Nat. Immunol. *11*, 577–584.

Kobayashi, Y., Asako, M., Ooka, H., Kanda, A., Tomoda, K., and Yasuba, H. (2015). Residual exhaled nitric oxide elevation in asthmatics is associated with eosinophilic chronic rhinosinusitis. J. Asthma *52*, 1060–1064.

Lambrecht, B.N., and Hammad, H. (2012). The airway epithelium in asthma. Nat. Med. *18*, 684–692.

Lambrecht, B.N., and Hammad, H. (2015). The immunology of asthma. Nat. Immunol. *16*, 45–56.

Li, D., Guabiraba, R., Besnard, A.G., Komai-Koma, M., Jabir, M.S., Zhang, L., Graham, G.J., Kurowska-Stolarska, M., Liew, F.Y., McSharry, C., and Xu, D. (2014). IL-33 promotes ST2-dependent lung fibrosis by the induction of alternatively activated macrophages and innate lymphoid cells in mice. J. Allergy Clin. Immunol. *134*, 1422–1432, e1411.

Liu, W.L., Zhang, H., Zheng, Y., Wang, H.T., Chen, F.H., Xu, L., Wei, Y., Sun, Y.Q., Shi, J.B., and Li, H.B. (2015). Expression and regulation of osteopontin in chronic rhinosinusitis with nasal polyps. Clin. Exp. Allergy *45*, 414–422.

Martinez, F.D., and Vercelli, D. (2013). Asthma. Lancet *382*, 1360–1372.

McHedlidze, T., Waldner, M., Zopf, S., Walker, J., Rankin, A.L., Schuchmann, M., Voehringer, D., McKenzie, A.N., Neurath, M.F., Pflanz, S., and Wirtz, S. (2013). Interleukin-33-dependent innate lymphoid cells mediate hepatic fibrosis. Immunity *39*, 357–371.

Mesnil, C., Raulier, S., Paulissen, G., Xiao, X., Birrell, M.A., Pirottin, D., Janss, T., Starkl, P., Ramery, E., Henket, M., et al. (2016). Lung-resident eosinophils represent a distinct regulatory eosinophil subset. J. Clin. Invest. *126*, 3279–3295.

Mitson-Salazar, A., Yin, Y., Wansley, D.L., Young, M., Bolan, H., Arceo, S., Ho, N., Koh, C., Milner, J.D., Stone, K.D., et al. (2016). Hematopoietic prostaglandin D synthase defines a proeosinophilic pathogenic effector human T(H)2 cell subpopulation with enhanced function. J. Allergy Clin. Immunol *137*, 907–918, e909.

Monticelli, L.A., Sonnenberg, G.F., Abt, M.C., Alenghat, T., Ziegler, C.G., Doering, T.A., Angelosanto, J.M., Laidlaw, B.J., Yang, C.Y., Sathaliyawala, T., et al. (2011). Innate lymphoid cells promote lung-tissue homeostasis after infection with influenza virus. Nat. Immunol. *12*, 1045–1054.

Moyer, J.D., Barbacci, E.G., Iwata, K.K., Arnold, L., Boman, B., Cunningham, A., DiOrio, C., Doty, J., Morin, M.J., Moyer, M.P., et al. (1997). Induction of apoptosis and cell cycle arrest by CP-358,774, an inhibitor of epidermal growth factor receptor tyrosine kinase. Cancer Res. *57*, 4838–4848.

Nakayama, T., Yoshikawa, M., Asaka, D., Okushi, T., Matsuwaki, Y., Otori, N., Hama, T., and Moriyama, H. (2011). Mucosal eosinophilia and recurrence of nasal polyps - new classification of chronic rhinosinusitis. Rhinology *49*, 392–396.

Nakayama, T., Hirahara, K., Onodera, A., Endo, Y., Hosokawa, H., Shinoda, K., Tumes, D.J., and Okamoto, Y. (2017). Th2 Cells in Health and Disease. Annu. Rev. Immunol. *35*, 53–84.

Oboki, K., Ohno, T., Kajiwara, N., Arae, K., Morita, H., Ishii, A., Nambu, A., Abe, T., Kiyonari, H., Matsumoto, K., et al. (2010). IL-33 is a crucial amplifier of innate rather than acquired immunity. Proc. Natl. Acad. Sci. USA *107*, 18581–18586.

Okumura, S., Sagara, H., Fukuda, T., Saito, H., and Okayama, Y. (2005). FcepsilonRI-mediated amphiregulin production by human mast cells increases mucin gene expression in epithelial cells. J. Allergy Clin. Immunol. *115*, 272–279.

Onodera, A., Tumes, D.J., Watanabe, Y., Hirahara, K., Kaneda, A., Sugiyama, F., Suzuki, Y., and Nakayama, T. (2015). Spatial interplay between Polycomb and Trithorax complexes controls transcriptional activity in T lymphocytes. Mol. Cell. Biol. *35*, 3841–3853.

Pawankar, R., and Nonaka, M. (2007). Inflammatory mechanisms and remodeling in chronic rhinosinusitis and nasal polyps. Curr. Allergy Asthma Rep. *7*, 202–208.

Puxeddu, I., Berkman, N., Ribatti, D., Bader, R., Haitchi, H.M., Davies, D.E., Howarth, P.H., and Levi-Schaffer, F. (2010). Osteopontin is expressed and functional in human eosinophils. Allergy *65*, 168–174.

Rosenberg, H.F., Dyer, K.D., and Foster, P.S. (2013). Eosinophils: changing perspectives in health and disease. Nat. Rev. Immunol. *13*, 9–22.

Rothenberg, M.E., and Hogan, S.P. (2006). The eosinophil. Annu. Rev. Immunol. *24*, 147–174.

Sabo-Attwood, T., Ramos-Nino, M.E., Eugenia-Ariza, M., Macpherson, M.B., Butnor, K.J., Vacek, P.C., McGee, S.P., Clark, J.C., Steele, C., and Mossman, B.T. (2011). Osteopontin modulates inflammation, mucin production, and gene expression signatures after inhalation of asbestos in a murine model of fibrosis. Am. J. Pathol. *178*, 1975–1985.

Sanada, S., Hakuno, D., Higgins, L.J., Schreiter, E.R., McKenzie, A.N., and Lee, R.T. (2007). IL-33 and ST2 comprise a critical biomechanically induced and cardioprotective signaling system. J. Clin. Invest. *117*, 1538–1549.

Seumois, G., Zapardiel-Gonzalo, J., White, B., Singh, D., Schulten, V., Dillon, M., Hinz, D., Broide, D.H., Sette, A., Peters, B., and Vijayanand, P. (2016). Transcriptional profiling of Th2 cells identifies pathogenic features associated with asthma. J. Immunol. *197*, 655–664.

Shinoda, K., Hirahara, K., Iinuma, T., Ichikawa, T., Suzuki, A.S., Sugaya, K., Tumes, D.J., Yamamoto, H., Hara, T., Tani-Ichi, S., et al. (2016). Thy1+IL-7+ lymphatic endothelial cells in iBALT provide a survival niche for memory T-helper cells in allergic airway inflammation. Proc. Natl. Acad. Sci. USA *113*, E2842–E2851.

Shoyab, M., Plowman, G.D., McDonald, V.L., Bradley, J.G., and Todaro, G.J. (1989). Structure and function of human amphiregulin: a member of the epidermal growth factor family. Science *243*, 1074–1076.

Stoll, S., Garner, W., and Elder, J. (1997). Heparin-binding ligands mediate autocrine epidermal growth factor receptor activation In skin organ culture. J. Clin. Invest. *100*, 1271–1281.

Straumann, A., Hoesli, S., Bussmann, Ch., Stuck, M., Perkins, M., Collins, L.P., Payton, M., Pettipher, R., Hunter, M., Steiner, J., and Simon, H.U. (2013). Anti-eosinophil activity and clinical efficacy of the CRTH2 antagonist OC000459 in eosinophilic esophagitis. Allergy *68*, 375–385.

Valladao, A.C., Frevert, C.W., Koch, L.K., Campbell, D.J., and Ziegler, S.F. (2016). STAT6 regulates the development of eosinophilic versus neutrophilic asthma in response to *Alternaria alternata*. J. Immunol. *197*, 4541–4551.

Wambre, E., Bajzik, V., DeLong, J.H., O'Brien, K., Nguyen, Q.A., Speake, C., Gersuk, V.H., DeBerg, H.A., Whalen, E., Ni, C., et al. (2017). A phenotypically and functionally distinct human T_H2 cell subpopulation is associated with allergic disorders. Sci. Transl. Med. *9*, https://doi.org/10.1126/scitranslmed.aam9171.

Wick, G., Grundtman, C., Mayerl, C., Wimpissinger, T.F., Feichtinger, J., Zelger, B., Sgonc, R., and Wolfram, D. (2013). The immunology of fibrosis. Annu. Rev. Immunol. *31*, 107–135.

Yamamoto, H., Okamoto, Y., Horiguchi, S., Kunii, N., Yonekura, S., and Nakayama, T. (2007). Detection of natural killer T cells in the sinus mucosa from asthmatics with chronic sinusitis. Allergy *62*, 1451–1455.

Zaiss, D.M., Yang, L., Shah, P.R., Kobie, J.J., Urban, J.F., and Mosmann, T.R. (2006). Amphiregulin, a TH2 cytokine enhancing resistance to nematodes. Science *314*, 1746.

Zaiss, D.M., van Loosdregt, J., Gorlani, A., Bekker, C.P., Gröne, A., Sibilia, M., van Bergen en Henegouwen, P.M., Roovers, R.C., Coffer, P.J., and Sijts, A.J. (2013). Amphiregulin enhances regulatory T cell-suppressive function via the epidermal growth factor receptor. Immunity *38*, 275–284.

STAR★METHODS

KEY RESOURCES TABLE

REAGENT or RESOURCE	SOURCE	IDENTIFIER
Antibodies		
Mouse Osteopontin/OPN Antibody	R&D systems	Cat#AF808; RRID: AB_2194992
Rat Anti-Mouse Siglec-F	BD Biosciences	Cat#552125; RRID: AB_394340
Anti-Human/Mouse CD11b	TONBO biosciences	Cat#70-0112; RRID: AB_2621483
CD45R (B220) Monoclonal Antibody	eBioscience	Cat#14-0452-81; RRID: AB_467253
Human Osteopontin/OPN Antibody	R&D systems	Cat#MAB1433; RRID: AB_2194981
Human Siglec-8 Antibody	R&D systems	Cat#MAB7975
Fibronectin Antibody	Santa Cruz Biotechnology	Cat#sc-8422; RRID: AB_627598
TCR DO11.10 Monoclonal Antibody	eBioscience	Cat#13-5808-81; RRID: AB_466677
anti–IFN-γ monoclonal antibody	Homemade	N/A
Brilliant Violet 421 anti-mouse IL-33Rα (IL1RL1, ST2) Antibody	BioLegend	Cat#145309; RRID: AB_2565634
Mouse Amphiregulin Antibody	R&D systems	Cat#206220; RRID: AB_2060661
PE anti-mouse/human IL-5 Antibody	BioLegend	Cat#504304; RRID: AB_315328
Brilliant Violet 421 anti-mouse/human IL-5 Antibody	BioLegend	Cat#504311; RRID: AB_2563161
PE/Cy7 anti-mouse IL-4 Antibody	BioLegend	Cat#504118; RRID: AB_10898116
IL-13 Monoclonal Antibody, Alexa Fluor 488	eBioscience	Cat#53-7133-80; RRID: AB_2016639
PE Rat Anti-Mouse Siglec-F	BD Biosciences	Cat#552126; RRID: AB_394341
Mouse CCR3 Alexa Fluor 647-conjugated Antibody	R&D systems	Cat#FAB729R
CD101 Monoclonal Antibody, PE	eBioscience	Cat#12-1011-82; RRID: AB_1210728
APC anti-mouse CD62L Antibody	BioLegend	Cat#104412; RRID: AB_313099
PE/Cy7 anti-human CD4 Antibody	BioLegend	Cat#317414; RRID: AB_571959
Brilliant Violet 421 anti-human CD45RO Antibody	BioLegend	Cat#304224; RRID: AB_2563817
PE anti-human CD161 Antibody	BioLegend	Cat#339904; RRID: AB_1501083
FITC anti-human CD294 (CRTH2) Antibody	BioLegend	Cat#350108; RRID: AB_11204086
Brilliant Violet 510 anti-human Lineage Cocktail	BioLegend	Cat#348807
Brilliant Violet 421 anti-human CD127	BioLegend	Cat#351310; RRID: AB_10960140
Human Amphiregulin Antibody	R&D systems	Cat#MAB262; RRID: AB_2060676
FITC anti-human IFN-γ Antibody	BioLegend	Cat#502506; RRID: AB_315231
Mouse ST2/IL-33 R Antibody	R&D systems	Cat#AF1004; RRID: AB_354527
Biotin Rat Anti-Mouse CD4	BD Biosciences	Cat#553044; RRID: AB_394580
Biotin anti-mouse CD326 (Ep-CAM) Antibody	BioLegend	Cat#118203; RRID: AB_1134174
Biotin Rat Anti-Mouse CD8a	BD Biosciences	Cat#553028; RRID: AB_394566
CD45R (B220) Monoclonal Antibody, Biotin	eBioscience	Cat#13-0452-86; RRID: AB_466451
Biotin Hamster Anti-Mouse CD11c	BD Biosciences	Cat#553800; RRID: AB_395059
Biotin Anti-Human/Mouse CD11b	TONBO biosciences	Cat#30-0112; RRID: AB_2621639
PE Rat Anti-Mouse Siglec-F	BD Biosciences	Cat#552126; RRID: AB_394341
Biotin anti-mouse Lineage Panel	BioLegend	Cat#133307; RRID: AB_11124348
Biotin anti-mouse CD90.2 Antibody	BioLegend	Cat#105304; RRID: AB_313175
Chemicals, Peptides, and Recombinant Proteins		
Recombinant Murine IL-2 Protein	Homemade	N/A
Recombinant Murine IL-4 Protein	PEPROTECH	Cat#214-14

(*Continued on next page*)

Continued

REAGENT or RESOURCE	SOURCE	IDENTIFIER
Recombinant Mouse IL-33 Protein	R&D systems	Cat#3626-ML
Recombinant Mouse IL-17E Protein	R&D systems	Cat#1399-IL
Recombinant Mouse TSLP Protein	R&D systems	Cat#555-TS
DAPI Fluoromount-G	SouthernBiotech	Cat#0100-20
Phorbol 12-myristate 13-acetate	Sigma-Aldrich	Cat#P1585
Ionomycin	Sigma-Aldrich	Cat#I0634
Monensin sodium salt	Sigma-Aldrich	Cat#M5273
Erlotinib HCl	Selleck	Cat#S1023
TRIzol	Invitrogen	Cat#15596026
Mite, House Dust (*Dermatophagoides pteronyssinus*)	Greer Laboratories Inc.	Cat#B84
Albumin from chicken egg white	Sigma-Aldrich	Cat#A5503
Imject Alum Adjuvant	Thermo Fisher Scientific	Cat#77161
Recombinant Mouse SCF Protein	R&D systems	Cat#455-MC
Recombinant Mouse Flt-3 Ligand Protein	R&D systems	Cat#427-FL
Recombinant Mouse IL-5 Protein	R&D systems	Cat#405-ML
Recombinant Mouse IL-33 Protein, CF	R&D systems	Cat#3626-ML/CF
Collagenase from *Clostridium histolyticum*	Sigma-Aldrich	Cat#C5138
Deoxyribonuclease I from bovine pancreas	Sigma-Aldrich	Cat#DN25
Hyaluronidase from sheep testes	Sigma-Aldrich	Cat#H6254
Critical Commercial Assays		
Alexa Fluor 488 Antibody Labeling Kit	Thermo Fisher Scientific	Cat#A20181
Alexa Fluor 555 Antibody Labeling Kit	Thermo Fisher Scientific	Cat#A20187
Alexa Fluor 647 Antibody Labeling Kit	Thermo Fisher Scientific	Cat#A20186
Alexa Fluor 680 Antibody Labeling Kit	Thermo Fisher Scientific	Cat#A20188
Pacific Blue Antibody Labeling Kit	Thermo Fisher Scientific	Cat#A30013
CD4+ T Cell Isolation Kit, mouse	Miltenyi Biotec	Cat#130-104-454
CD62L MicroBeads, mouse	Miltenyi Biotec	Cat#130-049-701
Eosinophil Isolation Kit, human	Miltenyi Biotec	Cat#130-092-010
FITC Annexin V Apoptosis Detection Kit I	BD Biosciences	Cat#556547
TruSeq RNA Sample Prep Kit v2	Illumina	Cat#RS-122-2001
Mouse Amphiregulin DuoSet ELISA kit	R&D systems	Cat#DY989
Human Amphiregulin DuoSet ELISA kit	R&D systems	Cat#DY262
Diff-Quik stain Kit	sysmex	Cat#16920
6.5mm Transwell with 0.4μm Pore Polycarbonate Membrane Insert, Sterile	Corning	Cat#3413
Deposited Data		
Raw and analyzed data	This paper	GEO: GSE114921
Software and Algorithms		
Photoshop	Adobe Systems Inc.	https://www.adobe.com/products/photoshop.html
Illustrator	Adobe Systems Inc.	https://www.adobe.com/products/illustrator.html
Bowtie 2	SOURCEFORGE	https://sourceforge.net/projects/bowtie-bio/files/bowtie2/2.0.0-beta7/
TopHat	Center for Computational Biology at Johns Hopkins University	https://ccb.jhu.edu/software/tophat/index.shtml
Cufflinks	Cole Trapnell	http://cole-trapnell-lab.github.io/cufflinks/
Prism	GraphPad	https://www.graphpad.com/scientific-software/prism/

(*Continued on next page*)

Continued

REAGENT or RESOURCE	SOURCE	IDENTIFIER
R	R Foundation	https://www.r-project.org/
Julia	NumFocus	https://julialang.org
Cytoscape	National Resource for Network Biology	http://www.cytoscape.org/
FlowJo	Tree Star, Inc.	https://www.flowjo.com/
Image J	NIH	https://imagej.nih.gov/ij/
Other		
BIOREVO	KEYENCE	https://www.keyence.com/ss/products/microscope/bz-x700/
autoMACS Pro Separator	Miltenyi Biotec	https://www.miltenyibiotec.com/JP-en/products/macs-cell-separation/instruments/automacs-pro-separator.html
BD FACSAria II Cell Sorter	BD Biosciences	N/A
BD FACSVerse 6 color Flow Cytometer	BD Biosciences	http://www.bdbiosciences.com/us/instruments/research/cell-analyzers/bd-facsverse/bd-facsverse-system/bd-facsverse-6-color-flow-cytometer/p/651154
Illumina HiSeq 1500 System	Illumina	N/A
Supersonic Nebulizer NE-U07	Omron	N/A

CONTACT FOR REAGENT AND RESOURCE SHARING

Further information and requests for resources and reagents should be directed to and will be fulfilled by the Lead Contact, Toshinori Nakayama (tnakayama@faculty.chiba-u.jp).

EXPERIMENTAL MODEL AND SUBJECT DETAILS

Mice

The animals used in this study were backcrossed to C57BL/6 or BALB/c mice more than ten times. *Areg*$^{-/-}$ mice were kindly provided by Dr. David C. Lee (University of Geogia, GA, USA). Anti-OVA-specific TCR-αβ (DO11.10) transgenic(Tg) mice were provided by Dr. D. Loh (Washington University School of Medicine, St. Louis). For antigen specific activation of CD4^{+} T cells mice expressing the OT-II-TCRαβ specific for residues 323-339 of OVA were also used. *Il33*$^{-/-}$ mice were generated as previously described (Oboki et al., 2010). *Il1rl1*$^{-/-}$ mice were kindly provided by Dr. Andrew N.J. McKenzie (Medical Research Council, Cambridge). *Spp1*$^{-/-}$ mice were kindly provided by Dr. David T. Denhardt (Rutgers University, Greensboro). All mice were used at 6-8 weeks old and were maintained under specific-pathogen-free conditions. Δdbl-GATA mice were purchased from The Jackson laboratory (Bar Harbor, ME, USA). Ly5.1 mice were purchased from Sankyo Laboratory (Tokyo, Japan). BALB/c, BALB/c nu/nu, and C57BL/6 mice were purchased from CLEA Japan (Tokyo, Japan). All of animals used in this study were female. The littermates of the same sex were randomly assigned to experimental groups. The research proposals were reviewed by the ethics committee for animals at Chiba University (registration number: 29-98, 29-99).

Human Samples

All participants with ECRS fulfilled the diagnostic criteria for ECRS prescribed by the Ministry of Health, Labor and Welfare, Japan. All participants as healthy controls did not have ECRS, asthma, other allergic diseases and any diseases that could affect their immune systems. The participants for this study were both male and female aged 20 to 68. The research proposals were reviewed by the ethics committee at Chiba University (registration number: 677). Informed consent was obtained from all participants.

METHOD DETAILS

Histology and immunohistochemistry

Pathological changes were evaluated by Haematoxylin & Eosin (H&E), Giemsa staining, Sirius-Red staining and immunofluororescent staining as previously described (Hirahara et al., 2008; Shinoda et al., 2016). Anti-Osteopontin (AF808, R&D Systems), anti-Siglec-F (E50-2440, BD Biosciences), anti-CD11b (M1/70, TONBO biosciences), anti-B220 (RA3-6B2, eBioscience) and DAPI Fluoromount-G® (SouthernBiotech) were used for immunofluorescent staining for mouse samples. Anti-Osteopontin (190312, R&D Systems) and anti-Siglec-8 (837535, R&D Systems) were used for immunofluorescent staining for human samples. Anti-Fibronectin

(EP5, Santa Cruz Biotechnology) was used for immunohistochemistry staining for human samples. The area of peribronchial Sirius Red staining in a paraffin-embedded lung was outlined and quantified using a light microscope (BIOREVO; KEYENCE Corp., Osaka, Japan) attached to an image-analysis system (Photoshop; Adobe Systems Inc., San Jose, California, USA). Results are expressed as the area of Sirius Red staining per micrometer length of basement membrane of bronchioles with 100 μm internal diameter. At least five bronchioles were counted in each slide. Basement membrane thickening was assessed as basement membrane per micrometer length of bronchus epithelium as previously reported (Valladao et al., 2016). At least five bronchioles were counted in each slide. Histological scores were determined based on the presence of the following: perivascular eosinophils (0–2), alveolar eosinophils (0–2), perivascular mononuclear cells (0–2), alveolar mononuclear cells (0–2), epithelial desquamation (normal = 0; elongation/distortion = 1; elongation, infolding, and narrowing = 2; loss of cells with broken airways = 3).

The Generation and Culture of Effector and Memory Th2 Cells

Splenic $CD62L^{+}CD44^{-}KJ1^{+}CD4^{+}$ T cells from DO11.10 OVA-specific TCR Tg mice were stimulated with an OVA peptide (Loh15, 1 μM) plus antigen-presenting cells (irradiated splenocytes) under Th2-cell-culture conditions (25 U/ml IL-2, 10 U/ml IL-4, and anti-IFN-γ monoclonal antibody) for 6 days *in vitro*. The effector Th2 cells (3×10^{7}) were transferred intravenously into BALB/c *nu/nu* or BALB/c recipient mice. Five weeks after cell transfer, $KJ1^{+}CD4^{+}$ T cells in the spleen were purified by autoMACS Sorter (Miltenyi Biotec, Bergisch Gladbach, Germany) and cell sorting (BD Aria II) and used as memory Th2 cells. Unless otherwise specifically noted, cells were stimulated with IL-33 at a concentration of 10 ng/ml for 72 hours. In some experiments, cells were stimulated with IL-25 (10 ng/ml) or TSLP (10 ng/ml).

Flow cytometry and sorting

Mouse memory Th2 cells were stained with anti-IL1rL1(ST2) (DIH9, BioLegend), and two subpopulations ($ST2^{low}$, $ST2^{high}$) were purified by FACS. Memory Th2 cells were stimulated with immobilized anti-TCRβ for 4 hours. Anti-Amphiregulin (206220, R&D Systems) was conjugated by ourselves using an Antibody Labeling Kit (Thermo Fisher Scientific) and used for intracellular staining of mouse samples. Anti-IL-5 (TRFK5, BioLegend), Anti-IL-4 (11B11, BioLegend) and Anti-IL-13 (eBio13A, eBioscience) were used for intracellular staining of mouse samples.

Anti-Siglec-F (E50-2440, BD Biosciences), Anti-CCR3 (83101, R&D Systems), Anti-CD101 (Moushi101, eBioscience) and Anti-CD62L (MEL-14, BioLegend) were used for cell surface staining of mouse samples.

T cells from PBMC and dissociated cells from the ECRS polyps were stained with anti-CD4 (OKT4, BioLegend), anti-CD45RO (UCHL1, BioLegend), anti-CD161 (HP-3G10, BioLegend), anti-CRTH2 (BM16, BioLegend), anti-Lineage Cocktails (BioLegend) and anti-CD127 (A019D5, BioLegend). Anti-Amphiregulin (31221, R&D Systems) was conjugated by ourselves using an Antibody Labeling Kit (Thermo Fisher Scientific) and used for intracellular staining for human samples. Anti-IL-5 (TRFK5, BioLegend) and anti-IFNγ (4S.B3, BioLegend) were used for intracellular staining of human samples.

Cell Viability Assay

Experiments were performed by using a FITC Annexin V Apoptosis Detection Kit I (BD Biosciences). Cells were washed, re-suspended in 100 μL 1X Binding Buffer, treated with 5 μL of FITC Annexin V and 5 μL PI, incubated for 15 min at RT in the dark, supplemented with 400 μL of 1X Binding Buffer and finally analyzed by flow cytometry.

ST2 Neutralizing Assay

Cells were incubated in the presence or absence of either anti-ST2 antibody (R&D Systems) or an isotype control antibody at a concentration of 1 μg/ml for 24 hours. After washing, cells were stimulated with IL-33 at a concentration of 10 ng/ml for 3 days.

Erlotinib Treatment

Erlotinib (Selleck, Houston, TX, USA) was dissolved in DMSO as described in the product manual. For *in vitro* experiments, Erlotinib was used to treat cells at a concentration of 100 nM and an equal amount of DMSO was used as a control. For *in vivo* experiments, Erlotinib was diluted with PBS and administered intraperitoneally at 12.5 mg/kg/day and an equal amount of DMSO diluted with PBS was administered intraperitoneally as a control.

Quantitative Real-Time PCR

Total RNA isolation, cDNA synthesis, and Quantitative real-time PCR was described previously (Endo et al., 2015). Primers and Roche Universal probes were purchased from Sigma and Roche, respectively. Primers and TaqMan probes were purchased from Applied Biosystems. Gene expression was normalized with the *Hprt* and *β-actin* mRNA signals and *GAPDH* (Human) mRNA signals.

RNA Sequencing

RNA-seq was carried out as previously described (Onodera et al., 2015). Total cellular RNA was extracted with TRIzol reagent (Invitrogen). For cDNA library construction, we used TruSeq RNA Sample Prep Kit v2 (Illumina) according to the manufacturer's protocol. Sequencing library fragments was performed on the HiSeq 1500 System. For data analysis, read sequences (50 bp) were

aligned to the mm10 mouse reference genome (University of California, Santa Cruz (UCSC) December 2011) using Bowtie 2 (version 2.0.0) and TopHat (version 1.3.2). Fragments per kilobase of exon per million mapped reads (FPKM) for each gene were calculated using Cufflinks (version 2.0.2).

ELISA for the Measurement of Amphiregulin Expression

Cells were stimulated with immobilized anti-TCR (10 μg/ml) in 48-well flat bottom plates (1.0×10^5 cells/well) for 24 hours at 37°C. The production of Amphiregulin was evaluated with a Mouse Amphiregulin DuoSet® ELISA kit (R&D systems) for mouse samples and with a Human Amphiregulin DuoSet® ELISA kit (R&D systems) for human samples according to the manufacturer's protocol.

BAL fluid Collecting

The trachea was exposed and lavaged with 1 mL PBS using a 20-gauge catheter. The collected cells in BAL fluid were sprayed on a glass slide, fixed, and stained with May-Giemsa staining using Diff-Quik stain. Cells on the slide glass were counted using a microscope.

Exposure of HDM

Dermatophagoides pteronyssinus extracts (Greer Laboratories Inc.) were administered to mice intranasaly: 200 μg on day 0, 100 μg on days 7 and 14, and then 50 μg of HDM was given twice per week for 4 weeks as reported previously (Doherty et al., 2011).

Immunization and inhalation with OVA

Mice were immunized i.p. with 250 μg of OVA (chicken egg albumin from Sigma-Aldrich) in 4 mg of aluminum hydroxide gel (Alum) on days 1 and 8. Mice were treated with aerosolized 1% OVA in saline for 30 min using a supersonic nebulizer (model NE-U07; Omron) on days 30, 33, 35, 37, 40 and 42. On day 43, various assays were performed.

For adoptive transfer experiments, OVA specific memory Th2 cells (3×10^6 cells) were transferred into mice, and then challenged with aerosolized 1% OVA on days 1, 3, 8 and 10. On day 11, various assays were performed.

Culture of Bone Marrow-Derived Eosinophils

Isolated bone marrow cells from BALB/c were stimulated with 100 ng/ml SCF (R & D Systems) plus 100 ng/ml FLT3 ligand (R & D Systems) for 4 days *in vitro*. After 4 days of culture, expanded cells were stimulated with 10 ng/ml IL-5 (R & D Systems) for 10 days.

In vitro treatment of Eosinophils with Amphiregulin

Eosinophils (1×10^6) from BALB/c bone marrow were stimulated with graded doses of Amphiregulin (0, 30, 100 and 300 ng/ml) in the presence or absence of Erlotinib (100 nM) for 72 hours. Unless otherwise specifically noted, eosinophils were cultured with Amphiregulin at a concentration of 100 ng/ml for 72 hours.

Adoptive Transfer of Eosinophils

OVA specific memory Th2 cells were transferred to mice on day 0. On days 1, 3, 8 and 10 bone marrow-derived eosinophils from *Spp1*$^{+/+}$ or *Spp1*$^{-/-}$ (1×10^8 in 200 μL saline) were injected intravenously into ΔdbI-GATA mice and finally exposed to aerosolized 1% OVA.

Intratracheal Administration of IL-33

On day 0, *Il33*$^{-/-}$ mice received recombinant mouse IL-33 (5cμg dissolved in 50cμl sterile saline; R&D Systems, Minneapolis, MN, USA) or control saline intratrachealy followed by adoptive transfer of OVA specific memory Th2 cells (3×10^6 cells). On days 1, 3, 8 and 10 mice were challenged with aerosolized 1% OVA.

Co-culture of Eosinophils and Fibroblasts

Experiments were performed with Transwell plates (0.4-mm pores; Corning, NY, USA). Fibroblasts in DMEM (with 10% FCS and Penicillin/Streptomycin) were cultured to confluence in 24-well tissue culture plates. Transwell inserts containing eosinophils (5×10^5) in RPMI complete media were co-cultured with the confluent fibroblasts at 37°C for 24 hours before fibroblasts were collected using Trypsin-EDTA.

Cell Isolation From Mouse Lungs

Epithelial cells, CD4$^+$ cells, CD8$^+$ cells, B220$^+$ cells, dendritic cells, macrophages, eosinophils and ILC2s were purified by autoMACS (Miltenyi Biotec, Bergisch Gladbach, Germany) from the lungs of mice. The following antibodies were used to identify each cell population; anti-EpCAM (G8.8, BioLegend), anti-CD4 (RM4-5, BD Biosciences), anti-CD8 (53-6.7, BD Biosciences), anti-B220 (RA3-6B2, eBioscience), anti-CD11c (HL3, BD Biosciences), anti-CD11b (M1/70, TONBO biosciences), anti-Siglec-F (E50-2440, BD Biosciences), anti-Lineage Cocktails (BioLegend) and anti-CD90.2 (30-H12, BioLegend). For the collection of fibroblasts, dissociated cells from lungs were seeded on 10 cm culture dish in DMEM including 10% FCS and Penicillin/Streptomycin and cultured at 37°C for 24 hours. After aspiration of supernatants, adherent fibroblasts were collected using Trypsin-EDTA.

Nasal Polyp, Peripheral Blood Mononuclear Cell and Homogenate Preparation

Nasal polyp mononuclear cells (NPMCs) were obtained as previously described (Yamamoto et al., 2007). In brief, freshly obtained nasal polyps were immediately minced and incubated in RPMI 1640 medium containing 1 mg/ml collagenase, 0.5 mg/ml hyaluronidase, and 0.2 mg/ml DNase I (Sigma-Aldrich). After incubation, NPMCs were purified by Ficoll-Hypaque technique. A volume of 1 mL of PBS was added for every 100 mg of tissue and was supplemented with aprotinin and leupeptin (Roche). Peripheral blood mononuclear cells (PBMCs) were obtained similarly. Human eosinophils were purified by autoMACS from PBMC and from nasal polyps using the Eosinophil Isolation Kit (Miltenyi Biotec, Bergisch Gladbach, Germany). FACS cell sorting (BD Aria II) was used to purify naive $CD4^+$ T cells ($CD4^+CD45RO^-$), memory-type $CD4^+$ T cells ($CD4^+CD45RO^+$) and ILCs ($Lineage^-CD127^+$).

QUANTIFICATION AND STATISTICAL ANALYSIS

Statistical Analysis

Data were analyzed with GraphPad Prism software (version 6). Comparisons of two groups were calculated with unpaired t test. Comparison of more than three groups were calculated with one-way analysis of variance (ANOVA) with Tukey's test. Differences with *p*-values below 0.05 were considered significant.

Analysis and graphic display of RNA-seq data

10,899 genes in which maximum FPKM value of each gene was equal to or greater than 1.0 were used for further analysis. Principal component analysis (PCA, rgl package) was perform by R (https://www.r-project.org/). A volcano plot was constructed by R (https://www.r-project.org/). Julia (https://julialang.org/, PyPlot and seaborn package) was used for constructing heatmaps.

Gene Ontology enrichment analysis

Gene Ontology enrichment analysis was performed with 10,899 genes by R and GSA package and c5.all.v5.2.symbols.gmt as GO term database (http://software.broadinstitute.org/gsea/msigdb) with FDR < 0.10 and p value < 0.01 as the cutoff value. A network of enriched GO terms was generated by Julia. Connection of the nodes was determined with cutoff level of Simpson coefficient $\geq$ 0.5. The network graph was visualized using Cytoscape (http://www.cytoscape.org/) and the Force Directed Layout with Simpson coefficient as a weight for the length of the spring.

DATA AND SOFTWARE AVAILABILITY

Raw and analyzed data reported in this paper are available under accession number GEO: GSE114921.

Immunity, Volume *49*

Supplemental Information

Amphiregulin-Producing Pathogenic Memory T Helper 2 Cells Instruct Eosinophils to Secrete Osteopontin and Facilitate Airway Fibrosis

Yuki Morimoto, Kiyoshi Hirahara, Masahiro Kiuchi, Tomoko Wada, Tomomi Ichikawa, Toshio Kanno, Mikiko Okano, Kota Kokubo, Atsushi Onodera, Daiju Sakurai, Yoshitaka Okamoto, and Toshinori Nakayama

Supplementary Information

Amphiregulin-producing pathogenic memory T helper-2 cells instruct eosinophils to secrete Osteopontin and facilitate airway fibrosis

Yuki Morimoto, Kiyoshi Hirahara, Masahiro Kiuchi, Tomoko Wada, Tomomi Ichikawa, Toshio Kanno, Mikiko Okano, Kota Kokubo, Atsushi Onodera, Daijyu Sakurai, Yoshitaka Okamoto, and Toshinori Nakayama

Figures and Figure Legends S1-S7

Figure S1

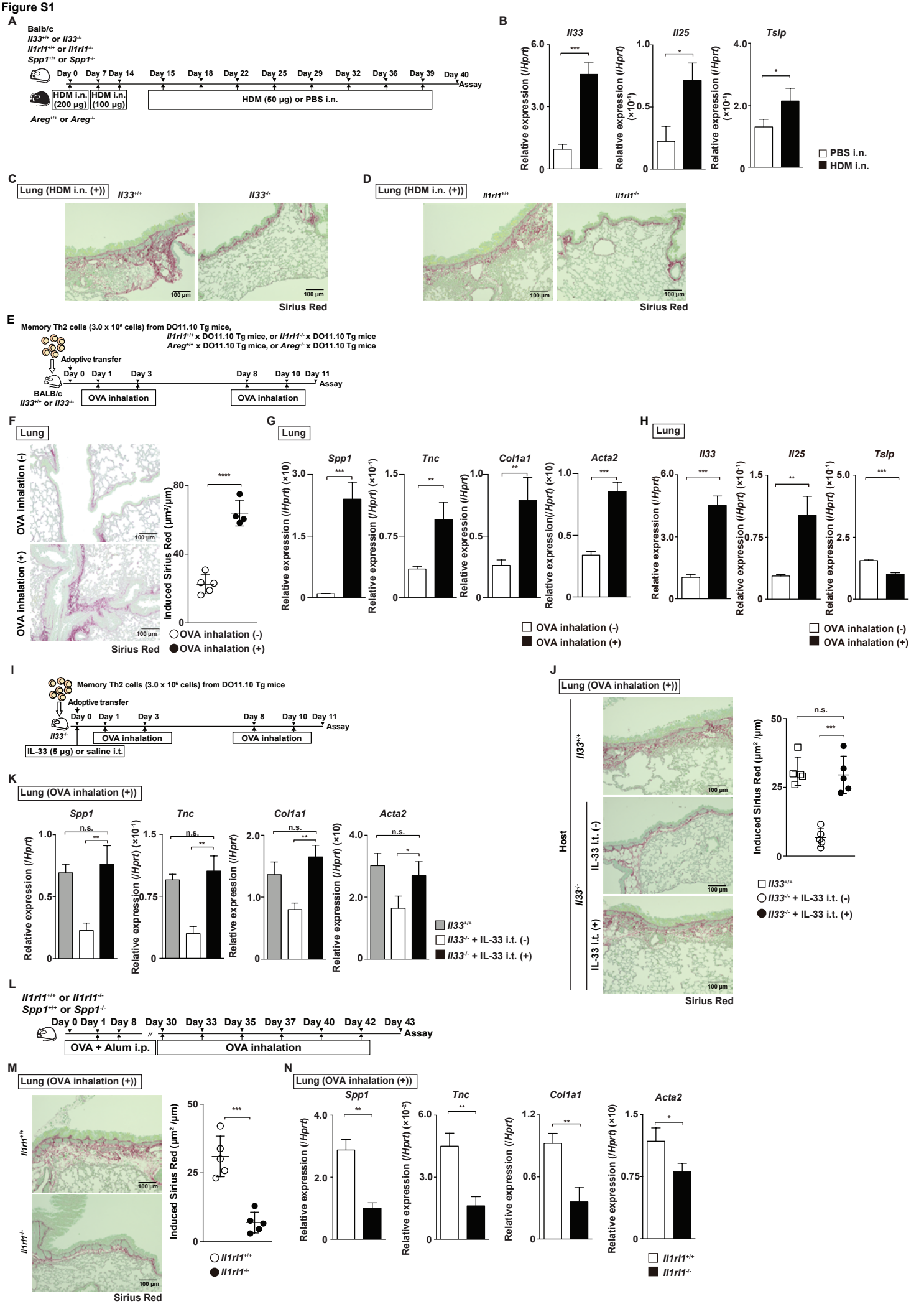

A
Balb/c
Il33+/+ or Il33-/-
Il1rl1+/+ or Il1rl1-/-
Spp1+/+ or Spp1-/-
Day 0 Day 7 Day 14 Day 15 Day 18 Day 22 Day 25 Day 29 Day 32 Day 36 Day 39 Day 40 Assay
HDM i.n. (200 μg)
HDM i.n. (100 μg)
HDM (50 μg) or PBS i.n.
Areg+/+ or Areg-/-
B
Il33
Il25
Tslp
Relative expression (/Hprt)
PBS i.n.
HDM i.n.
C
Lung (HDM i.n. (+))
Il33+/+
Il33-/-
100 μm
Sirius Red
D
Lung (HDM i.n. (+))
Il1rl1+/+
Il1rl1-/-
100 μm
Sirius Red
E
Memory Th2 cells (3.0 x 10^6 cells) from DO11.10 Tg mice,
Il1rl1+/+ x DO11.10 Tg mice, or Il1rl1-/- x DO11.10 Tg mice
Areg+/+ x DO11.10 Tg mice, or Areg-/- x DO11.10 Tg mice
Adoptive transfer
Day 0 Day 1 Day 3 Day 8 Day 10 Day 11 Assay
BALB/c
Il33+/+ or Il33-/-
OVA inhalation
OVA inhalation
F
Lung
OVA inhalation (-)
OVA inhalation (+)
100 μm
Induced Sirius Red (μm²/μm)
OVA inhalation (-)
OVA inhalation (+)
Sirius Red
G
Lung
Spp1
Tnc
Col1a1
Acta2
Relative expression (/Hprt)
OVA inhalation (-)
OVA inhalation (+)
H
Lung
Il33
Il25
Tslp
Relative expression (/Hprt)
OVA inhalation (-)
OVA inhalation (+)
I
Memory Th2 cells (3.0 x 10^6 cells) from DO11.10 Tg mice
Adoptive transfer
Day 0 Day 1 Day 3 Day 8 Day 10 Day 11 Assay
Il33-/-
OVA inhalation
OVA inhalation
IL-33 (5 μg) or saline i.t.
J
Lung (OVA inhalation (+))
Host
Il33+/+
Il33-/-
IL-33 i.t. (-)
IL-33 i.t. (+)
100 μm
Sirius Red
Induced Sirius Red (μm² /μm)
n.s.
Il33+/+
Il33-/- + IL-33 i.t. (-)
Il33-/- + IL-33 i.t. (+)
K
Lung (OVA inhalation (+))
Spp1
Tnc
Col1a1
Acta2
Relative expression (/Hprt)
n.s.
Il33+/+
Il33-/- + IL-33 i.t. (-)
Il33-/- + IL-33 i.t. (+)
L
Il1rl1+/+ or Il1rl1-/-
Spp1+/+ or Spp1-/-
Day 0 Day 1 Day 8 Day 30 Day 33 Day 35 Day 37 Day 40 Day 42 Day 43 Assay
OVA + Alum i.p.
OVA inhalation
M
Lung (OVA inhalation (+))
Il1rl1+/+
Il1rl1-/-
100 μm
Induced Sirius Red (μm² /μm)
Il1rl1+/+
Il1rl1-/-
Sirius Red
N
Lung (OVA inhalation (+))
Spp1
Tnc
Col1a1
Acta2
Relative expression (/Hprt)
Il1rl1+/+
Il1rl1-/-

Figure S1. Related to Figure 1. Antigen dependent airway inflammation causes lung fibrotic responses via the IL-33-ST2 axis.

(**A**) Experimental protocol for an airway inflammation mouse model using repetitive intranasal exposure to HDM. (**B**) Quantitative RT-PCR analysis of the indicated genes in lungs of mice with or without HDM exposure (n = 3 mice per group). Three independent experiments were performed with similar results. (**C**) Representative histology of lungs of *Il33*$^{+/+}$ and *Il33*$^{-/-}$ mice with HDM exposure as indicated in Figure **S1A**, fixed and stained with Sirius Red. Scale bars, 100 μm. More than 3 mice per group were analyzed. (**D**) Representative histology of lungs of *Il1rl1*$^{+/+}$ and *Il1rl1*$^{-/-}$ mice with HDM exposure as indicated in Figure S1**A**, fixed and stained with Sirius Red. Scale bars, 100 μm. More than 3 mice per group were analyzed. (**E**) Experimental protocol for Th2 cell-dependent allergic inflammation mouse model employing adoptive transfer of memory Th2 cells. (**F**) Representative histology of lungs of mice with or without OVA inhalation, fixed and stained with Sirius Red (left). Scale bars, 100 μm. Shown are ratios of areas of randomly selected regions stained with Sirius Red surrounding bronchi versus the areas of associated basement membranes (right). More than 3 mice per group were analyzed. (**G**) Quantitative RT-PCR analysis of the indicated genes in lung of mice with or without OVA inhalation (n = 3 mice per group). Three independent experiments were performed with similar results. (**H**) Quantitative RT-PCR analysis of the indicated genes in lungs of mice with or without OVA inhalation (n = 3 mice per group). Three independent experiments were performed with similar results. (**I**) Experimental protocol for an allergic inflammation mouse model employing adoptive transfer of memory Th2 cells followed by intratracheal (i.t.) administration of recombinant IL-33. (**J**) Representative histology of lungs of *Il33*$^{+/+}$ and *Il33*$^{-/-}$ mice with or without administration of IL-33 or saline followed by OVA inhalation, fixed and stained with Sirius Red (left). Scale bars, 100 μm. Shown are ratios of areas of randomly selected regions stained with Sirius Red surrounding bronchi versus areas of associated basement membranes (right). More than 3 mice per group were analyzed. (**K**) Quantitative RT-PCR analysis of the indicated genes in lungs of *Il33*$^{+/+}$ and *Il33*$^{-/-}$ mice with or without administration of IL-33 or saline followed by OVA inhalation (n = 3 mice per group). Three independent experiments were performed with similar results. Data are the mean ± SD. **P* < 0.05, ***P* < 0.01, ****P* < 0.001; n.s., not significant; by unpaired t test or one-way analysis of variance (ANOVA). (**L**) Experimental protocol for an allergic airway inflammation mouse model using intraperitoneal (i.p.) immunization with OVA and aluminum hydroxide gel (Alum) followed by OVA inhalation. (**M**) Representative histology of lungs of *Il1rl1*$^{+/+}$ and *Il1rl1*$^{-/-}$ mice challenged with OVA as indicated in Figure **S1L**, fixed and stained with Sirius Red (left). Scale bars, 100 μm. Shown are ratios of areas of randomly selected regions stained with Sirius Red surrounding bronchi versus areas of associated basement membranes (right). More than 3 mice per group were analyzed. (**N**) Quantitative RT-PCR analysis of the indicated genes in *Il1rl1*$^{+/+}$ and *Il1rl1*$^{-/-}$ mice challenged with OVA as indicated in Figure **S1L** (n = 3 mice per group). Three independent experiments were performed with similar results. Data are the mean ± SD. **P* < 0.05, ***P* < 0.01, ****P* < 0.001; n.s., not significant; by unpaired t test or one-way analysis of variance (ANOVA).

Figure S2

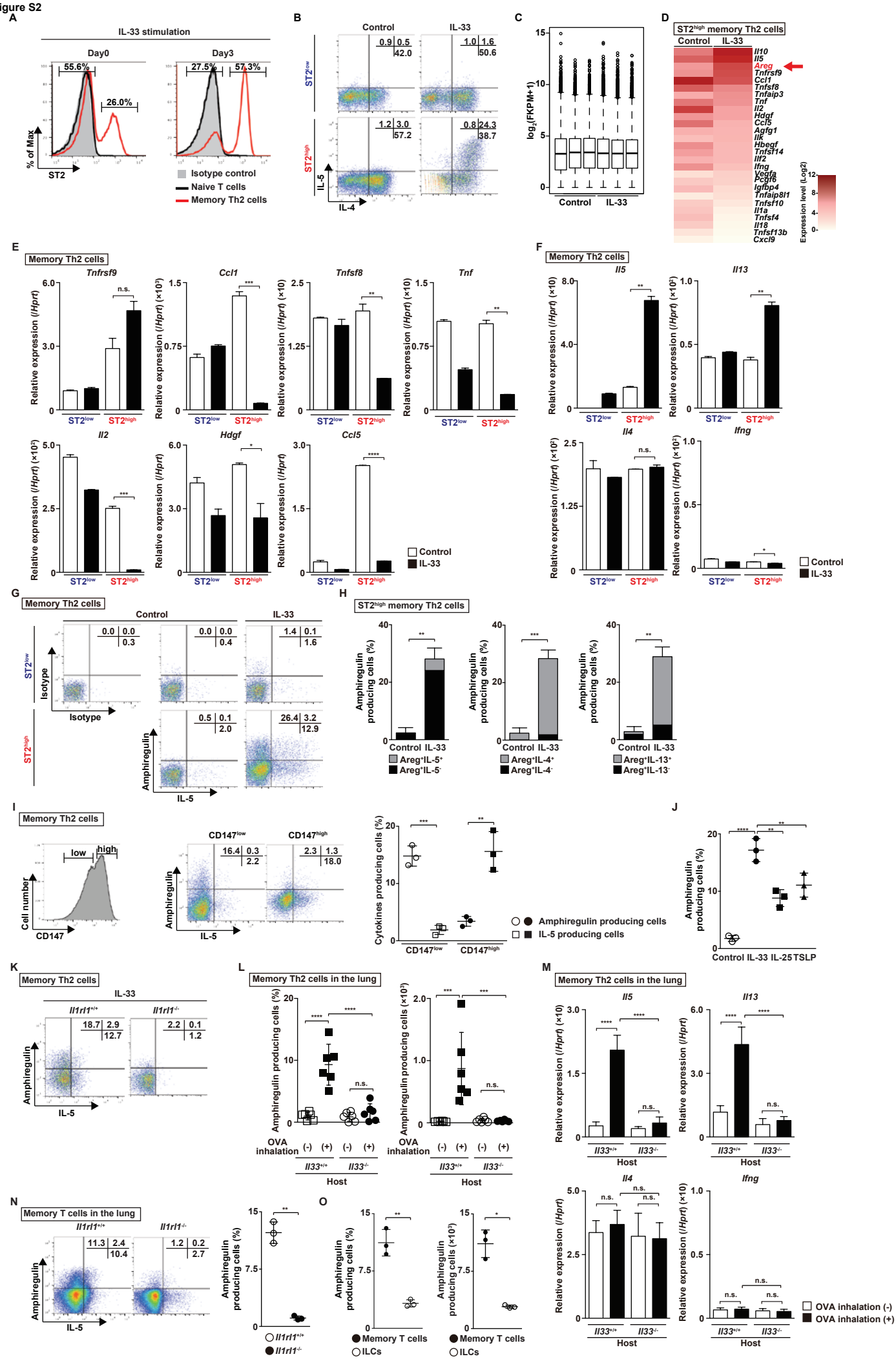

A
IL-33 stimulation
Day0
Day3
55.6%
26.0%
27.5%
57.3%
% of Max
ST2
Isotype control
Naive T cells
Memory Th2 cells
B
Control
IL-33
ST2low
ST2high
IL-5
IL-4
C
log2(FKPM+1)
Control
IL-33
D
ST2high memory Th2 cells
Control
IL-33
Il10
Il5
Areg
Tnfrsf9
Ccl1
Tnfsf8
Tnfaip3
Tnf
Il2
Hdgf
Ccl5
Agfg1
Ilk
Hbegf
Tnfsf14
Il1f2
Ifng
Vegfa
Pc3f6
Igfbp4
Tnfaip8l1
Tnfsf10
Il1a
Tnfsf4
Il18
Tnfsf13b
Cxcl9
Expression level (Log2)
E
Memory Th2 cells
Tnfrsf9
Ccl1
Tnfsf8
Tnf
Il2
Hdgf
Ccl5
Relative expression (/Hprt)
n.s.
ST2low
ST2high
Control
IL-33
F
Memory Th2 cells
Il5
Il13
Il4
Ifng
G
Memory Th2 cells
Control
IL-33
Isotype
Amphiregulin
IL-5
H
ST2high memory Th2 cells
Amphiregulin producing cells (%)
Areg+IL-5+
Areg+IL-5-
Areg+IL-4+
Areg+IL-4-
Areg+IL-13+
Areg+IL-13-
I
Memory Th2 cells
low
high
Cell number
CD147
CD147low
CD147high
Cytokines producing cells (%)
Amphiregulin producing cells
IL-5 producing cells
J
Amphiregulin producing cells (%)
Control
IL-33
IL-25
TSLP
K
Memory Th2 cells
IL-33
Il1rl1+/+
Il1rl1-/-
L
Memory Th2 cells in the lung
Amphiregulin producing cells (%)
Amphiregulin producing cells (×10³)
OVA inhalation
Il33+/+
Il33-/-
Host
M
Memory Th2 cells in the lung
Il5
Il13
Il4
Ifng
N
Memory T cells in the lung
O
Memory T cells
ILCs
OVA inhalation (-)
OVA inhalation (+)

Figure S2. Related to Figure 2. IL-33 stimulation induces production of Amphiregulin and type 2 cytokines in ST2^{hi} memory Th2 cells both *in vitro* and *in vivo*.

(**A**) Shown are cell surface-staining profiles of ST2 in naïve and memory Th2 cells before (left panel) and after (right) IL-33 stimulation. (**B**) Shown are intracellular-staining profiles of IL-4 and IL-5 in naïve and memory Th2 cells with or without IL-33 stimulation. (**C**) Shown are box plots of RNA-Seq data from ST2^{hi} memory Th2 cells stimulated with or without IL-33. (**D**) ST2^{hi} memory Th2 cells were cultured with or without IL-33 for 72 hours. Shown is a heatmap depicting humoral factor genes with statistically significant changes between IL-33 treated or untreated samples. (**E**, **F**) Shown are plots of quantitative RT-PCR analyses of the indicated genes in ST2^{low} or ST2^{hi} memory Th2 cells. Four independent experiments were performed with similar results. (**G**) Shown are FACS plots of intracellular Amphiregulin and IL-5 with isotype controls. (**H**) Shown is percentage of Amphiregulin-producing ST2^{hi} memory Th2 cells among ST2^{hi} memory Th2 cells with or without IL33 stimulation. Amphiregulin only-producing ST2^{hi} memory Th2 cells (Areg^{+}IL-5^{-}, Areg^{+}IL-4^{-} and Areg^{+}IL-13^{-}) are shown in black, and ST2^{hi} memory Th2 cells producing Amphiregulin with the indicated cytokines (Areg^{+}IL-5^{+}, Areg^{+}IL-4^{+} and Areg^{+}IL-13^{+}) are shown in gray. Data are the mean ± SD. **P* < 0.05, ***P* < 0.01, ****P* < 0.001, *****P* < 0.0001; n.s., not significant; by unpaired t test or one-way analysis of variance (ANOVA). (**I**) Shown is a cell surface-staining profile of CD147 in memory Th2 cells (left panel). Shown are FACS plots of intracellular Amphiregulin and IL-5 expression in CD147^{low} memory Th2 cells and CD147^{high} memory Th2 cells (middle panel). Shown are the percentages of Amphiregulin producing cells (circle) and IL-5 producing cells (square) in CD147^{low} memory Th2 cells (white) or CD147^{high} memory Th2 cells (black) (right panel). Data are the mean ± SD. ***P* < 0.01, ****P* < 0.001; by unpaired t test. (**J**) Shown are the percentage of Amphiregulin-producing memory Th2 cells among memory Th2 cells stimulated with the indicated cytokines for 72 hours. (**K**) Shown are FACS plots of intracellular Amphiregulin and IL-5 in *Il1rl1*$^{+/+}$ and *Il1rl1*$^{-/-}$ memory Th2 cells stimulated with IL-33 for 72 hours. (**L**) Shown are the ratios of Amphiregulin producing memory Th2 cells in whole memory Th2 cells (left) and absolute numbers of them (right) in the lungs from *Il33*$^{+/+}$ and *Il33*$^{-/-}$ recipients with or without OVA challenges. (**M**) Shown are quantitative RT-PCR analyses of the indicated genes in lung memory Th2 cells from *Il33*$^{+/+}$ and *Il33*$^{-/-}$ recipients (n = 6). (**N**) Shown are FACS plots of intracellular Amphiregulin and IL-5 in lung memory T cells from *Il1rl1*$^{+/+}$ and *Il1rl1*$^{-/-}$ mice treated with OVA and Alum twice followed by a series of OVA inhalations (left). Shown is the percentage of Amphiregulin-producing memory T cells among memory T cells from the lungs of *Il1rl1*$^{+/+}$ and *Il1rl1*$^{-/-}$ mice (right). (**O**) Shown is the percentage of Amphiregulin-producing cells among memory T cells or ILCs (left), and the absolute numbers of Amphiregulin-producing memory T cells and ILCs (right) in the lungs of mice challenged with OVA as indicated in Figure **S1L**. Data are the mean ± SD. **P* < 0.05, ***P* < 0.01, ****P* < 0.001, *****P* < 0.0001; n.s., not significant; by unpaired t test or one-way analysis of variance (ANOVA).

Figure S3

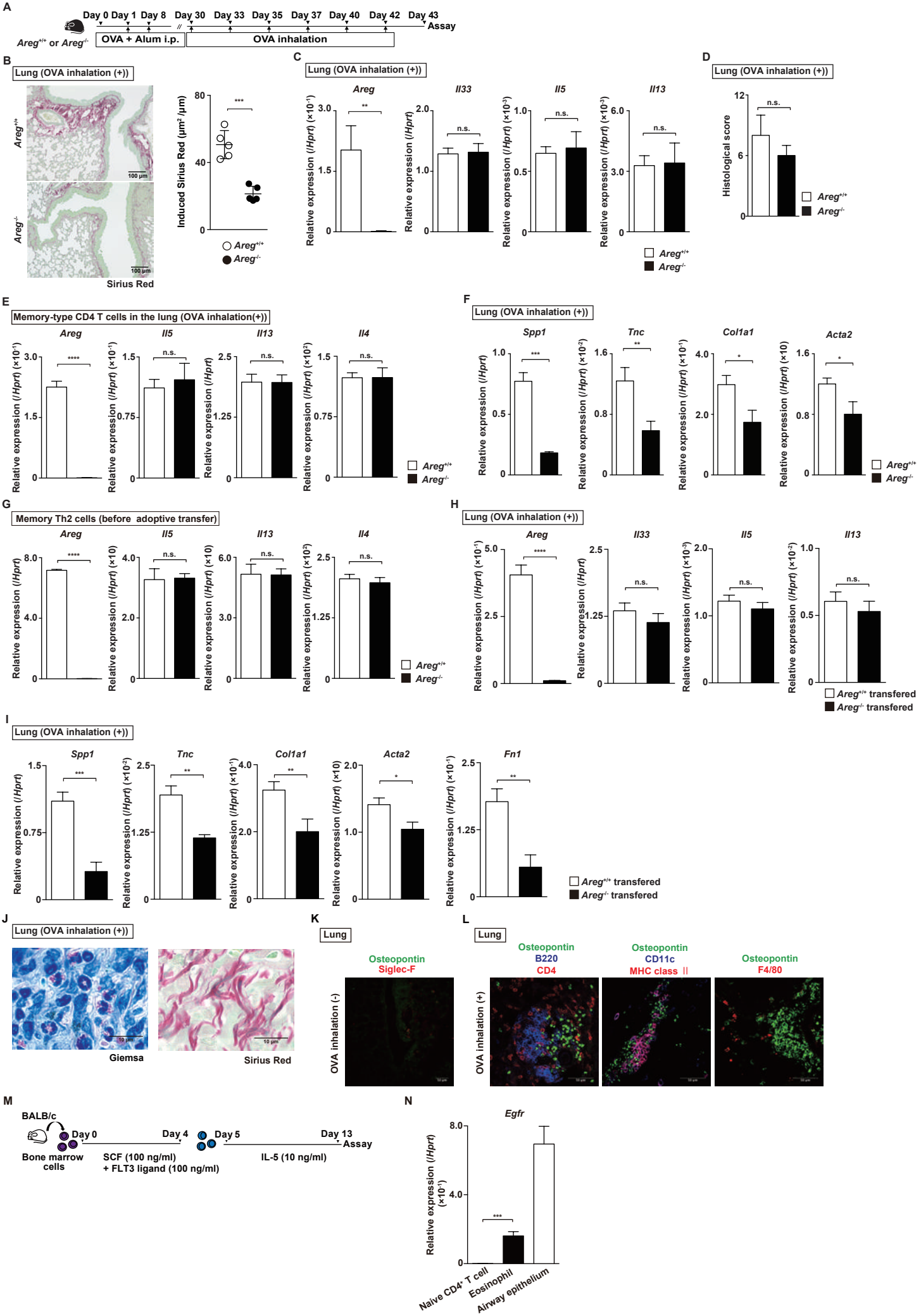

A
Day 0 Day 1 Day 8 Day 30 Day 33 Day 35 Day 37 Day 40 Day 42 Day 43
Assay
Areg+/+ or Areg-/-
OVA + Alum i.p.
OVA inhalation
B
Lung (OVA inhalation (+))
Areg+/+
Areg-/-
100 μm
Induced Sirius Red (μm2 /μm)
***
Areg+/+
Areg-/-
Sirius Red
C
Lung (OVA inhalation (+))
Areg
Il33
Il5
Il13
Relative expression (/Hprt)
**
n.s.
Areg+/+
Areg-/-
D
Lung (OVA inhalation (+))
Histological score
n.s.
Areg+/+
Areg-/-
E
Memory-type CD4 T cells in the lung (OVA inhalation(+))
Areg
Il5
Il13
Il4
Relative expression (/Hprt)
****
n.s.
Areg+/+
Areg-/-
F
Lung (OVA inhalation (+))
Spp1
Tnc
Col1a1
Acta2
Relative expression (/Hprt)
***
**
*
Areg+/+
Areg-/-
G
Memory Th2 cells (before adoptive transfer)
Areg
Il5
Il13
Il4
Relative expression (/Hprt)
****
n.s.
Areg+/+
Areg-/-
H
Lung (OVA inhalation (+))
Areg
Il33
Il5
Il13
Relative expression (/Hprt)
****
n.s.
Areg+/+ transfered
Areg-/- transfered
I
Lung (OVA inhalation (+))
Spp1
Tnc
Col1a1
Acta2
Fn1
Relative expression (/Hprt)
***
**
*
Areg+/+ transfered
Areg-/- transfered
J
Lung (OVA inhalation (+))
10 μm
Giemsa
Sirius Red
K
Lung
Osteopontin
Siglec-F
OVA inhalation (-)
L
Lung
Osteopontin
B220
CD4
Osteopontin
CD11c
MHC class II
Osteopontin
F4/80
OVA inhalation (+)
M
BALB/c
Day 0
Day 4
Day 5
Day 13
Assay
Bone marrow cells
SCF (100 ng/ml) + FLT3 ligand (100 ng/ml)
IL-5 (10 ng/ml)
N
Egfr
Relative expression (/Hprt) (×10-1)
***
Naive CD4+ T cell
Eosinophil
Airway epithelium

Figure S3. Related to Figure 3. OVA challenge induces fibrotic changes by Amphiregulin produced from memory Th2 cells and production of Osteopontin from eosinophils in the asthmatic lung.

(**A**) Experimental protocol for an allergic airway inflammation mouse model using intraperitoneal (i.p.) OVA and aluminum hydroxide gel (Alum) treatment. (**B**) *Areg*$^{+/+}$ and *Areg*$^{-/-}$ mice were challenged with OVA as indicated in Figure **S3A**. Shown is a representative confocal micrograph of lung tissue stained with Sirius Red from an *Areg*$^{+/+}$ and an *Areg*$^{-/-}$ mouse (left). Scale bars represent 100 μm. Shown are ratios of areas of randomly selected regions stained with Sirius Red surrounding bronchi versus the areas of associated basement membranes (right). More than 3 mice per group were analyzed. (**C**) Shown are quantitative RT-PCR analyses of the indicated genes in the lungs of *Areg*$^{+/+}$ and *Areg*$^{-/-}$ mice challenged with OVA inhalation (n = 3 mice per group). Three independent experiments were performed with similar results. (**D**) Shown are the histological scores of H & E-stained lung sections from *Areg*$^{+/+}$ and *Areg*$^{-/-}$ mice. Histological scores were calculated according to the criteria indicated in STAR Methods (n = 3). (**E**) Shown are quantitative RT-PCR analyses of the indicated genes in lung memory Th2 cells from *Areg*$^{+/+}$ or *Areg*$^{-/-}$ mice (n = 3). (**F**) Quantitative RT-PCR analysis of the indicated genes in the lungs of *Areg*$^{+/+}$ and *Areg*$^{-/-}$ mice with OVA inhalation (n = 3 mice per group). (**G**) Shown are quantitative RT-PCR analyses of the indicated genes in memory Th2 cells from *Areg*$^{+/+}$ or *Areg*$^{-/-}$ mice (n = 3) prior to adoptive transfer. (**H**) Shown are quantitative RT-PCR analyses of the indicated genes in lungs from recipients of *Areg*$^{+/+}$ or *Areg*$^{-/-}$ memory Th2 cells (n = 3 mice per group). (**I**) Shown are quantitative RT-PCR analyses of the indicated genes in lungs from recipients of *Areg*$^{+/+}$ or *Areg*$^{-/-}$ memory Th2 cells (n = 3 mice per group). Data are the mean ± SD. $*P < 0.05$, $**P < 0.01$, $***P < 0.001$, $****P < 0.0001$; n.s., not significant; by unpaired t test or one-way analysis of variance (ANOVA). (**J**) Shown is a representative histological analysis of lungs from mice fixed and stained with Giemsa (left) and Sirius Red (right). Scale bars represent 10 μm. Three independent experiments were performed with similar results. (**K**) Shown are representative confocal micrographs of lungs stained with anti-Osteopontin (green) and anti-Siglec-F (red) from mice without OVA inhalation. Scale bars represent 50 μm. (**L**) Shown are representative confocal micrographs of mouse lungs stained with anti-CD4 (red), anti- Osteopontin (green), and anti-B220 (blue) (left), anti-MHC class II (red), anti-Osteopontin (green), and anti-CD11c (blue) (middle), anti- Osteopontin (green), and anti-F4/80 (red). Scale bars represent 50 μm. Three independent experiments were performed with similar results. (**M**) Experimental protocol for differentiation of mouse bone marrow derived eosinophils. (**N**) Shown is a quantitative RT-PCR analysis of *Egfr* in the indicated cell types. Bone marrow-derived eosinophils were cultured with or without Amphiregulin for 72 hours. Data are the mean ± SD. $***P < 0.001$; by one-way analysis of variance (ANOVA).

Figure S4

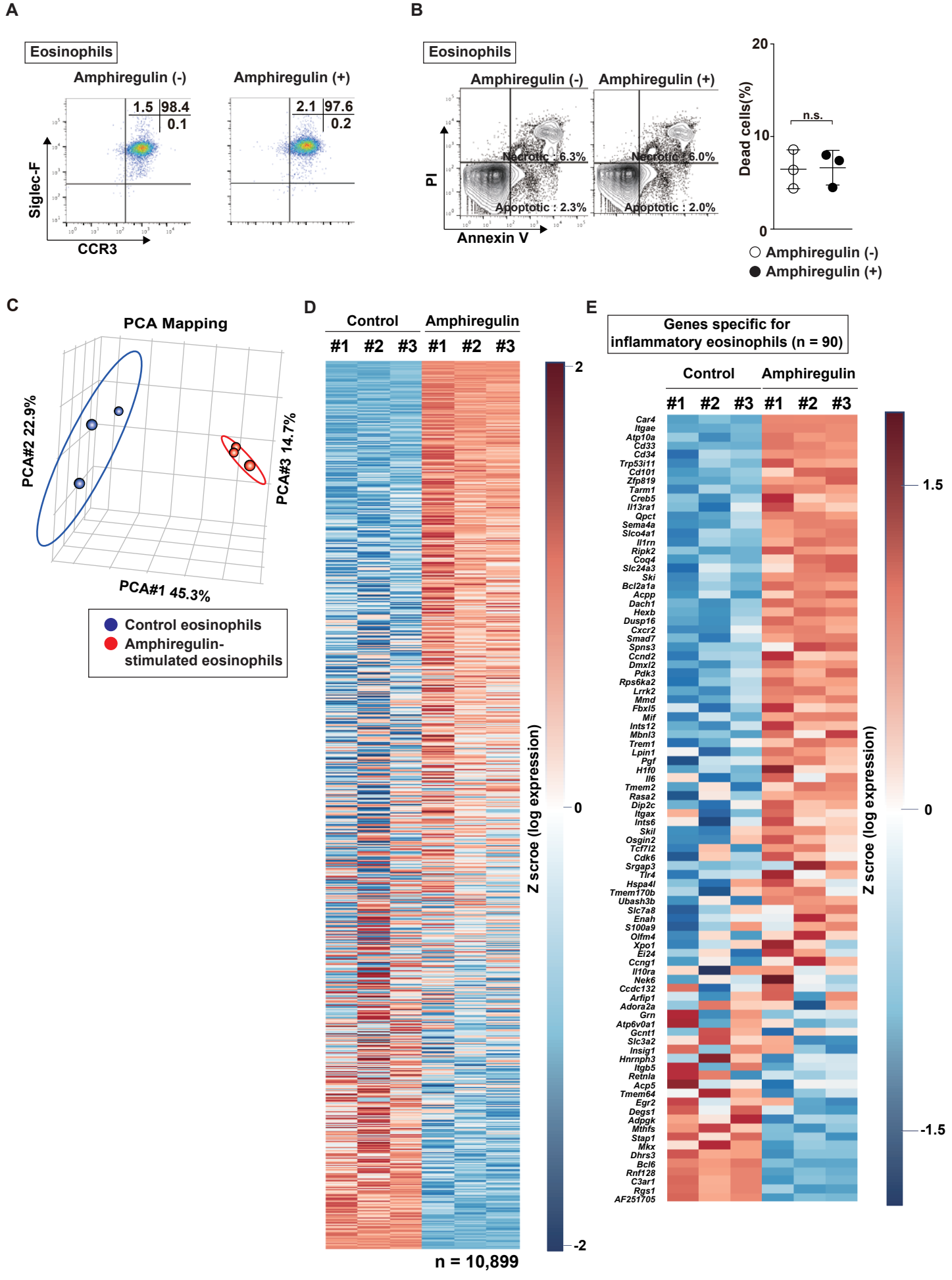

A
Eosinophils
Amphiregulin (-)
Amphiregulin (+)
1.5
98.4
0.1
2.1
97.6
0.2
Siglec-F
CCR3
B
Eosinophils
Amphiregulin (-)
Amphiregulin (+)
Necrotic : 6.3%
Necrotic : 6.0%
Apoptotic : 2.3%
Apoptotic : 2.0%
PI
Annexin V
Dead cells(%)
20
10
0
n.s.
Amphiregulin (-)
Amphiregulin (+)
C
PCA Mapping
PCA#2 22.9%
PCA#3 14.7%
PCA#1 45.3%
Control eosinophils
Amphiregulin-stimulated eosinophils
D
Control
Amphiregulin
#1 #2 #3 #1 #2 #3
2
0
-2
Z scroe (log expression)
n = 10,899
E
Genes specific for inflammatory eosinophils (n = 90)
Control
Amphiregulin
#1 #2 #3 #1 #2 #3
Car4
Itgae
Atp10a
Cd33
Cd34
Trp53i11
Cd101
Zfp819
Tarm1
Creb5
Il13ra1
Qpct
Sema4a
Slco4a1
Il1rn
Ripk2
Coq4
Slc24a3
Ski
Bcl2a1a
Acpp
Dach1
Hexb
Dusp16
Cxcr2
Smad7
Spns3
Ccnd2
Dmxl2
Pdk3
Rps6ka2
Lrrk2
Mmd
Fbxl5
Mif
Ints12
Mbnl3
Trem1
Lpin1
Pgf
H1f0
Il6
Tmem2
Rasa2
Dip2c
Itgax
Ints6
Skil
Osgin2
Tcf7l2
Cdk6
Srgap3
Tlr4
Hspa4l
Tmem170b
Ubash3b
Slc7a8
Enah
S100a9
Olfm4
Xpo1
Ei24
Ccng1
Il10ra
Nek6
Ccdc132
Arfip1
Adora2a
Grn
Atp6v0a1
Gcnt1
Slc3a2
Insig1
Hnrnph3
Itgb5
Retnla
Acp5
Tmem64
Egr2
Degs1
Adpgk
Mthfs
Stap1
Mkx
Dhrs3
Bcl6
Rnf128
C3ar1
Rgs1
AF251705
1.5
0
-1.5
Z scroe (log expression)

Figure S4. Related to Figure 4. Amphiregulin stimulation induces Osteopontin production via EGFR signaling both *in vitro* and *in vivo*.

(**A**) Shown are FACS plots of CCR3 and Siglec-F expression in eosinophils with or without Amphiregulin stimulation for 72 hours. (**B**) Shown are FACS plots of PI and Annexin V expression in eosinophils with or without Amphiregulin stimulation for 72 hours as indicated in STAR Methods (left). Shown are the percentage of dead cells among total cells (right). (**C**) Shown is a PCA plot of RNA-Seq data from eosinophils stimulated with or without Amphiregulin. (**D**) Shown is a heatmap of the expression of 10,899 genes in eosinophils stimulated with Amphiregulin and in control unstimulated eosinophils (n = 3 per group). (**E**) Shown is a heat map of Log10 expression values of signature genes for inflammatory eosinophils (n = 90) [as defined in a previous report *(Mesnil et al, J Clin Invest, 2016;PMID:27548519)*], in eosinophils stimulated with or without Amphiregulin. Data are the mean ± SD. n.s., not significant; by unpaired t test.

Figure S5

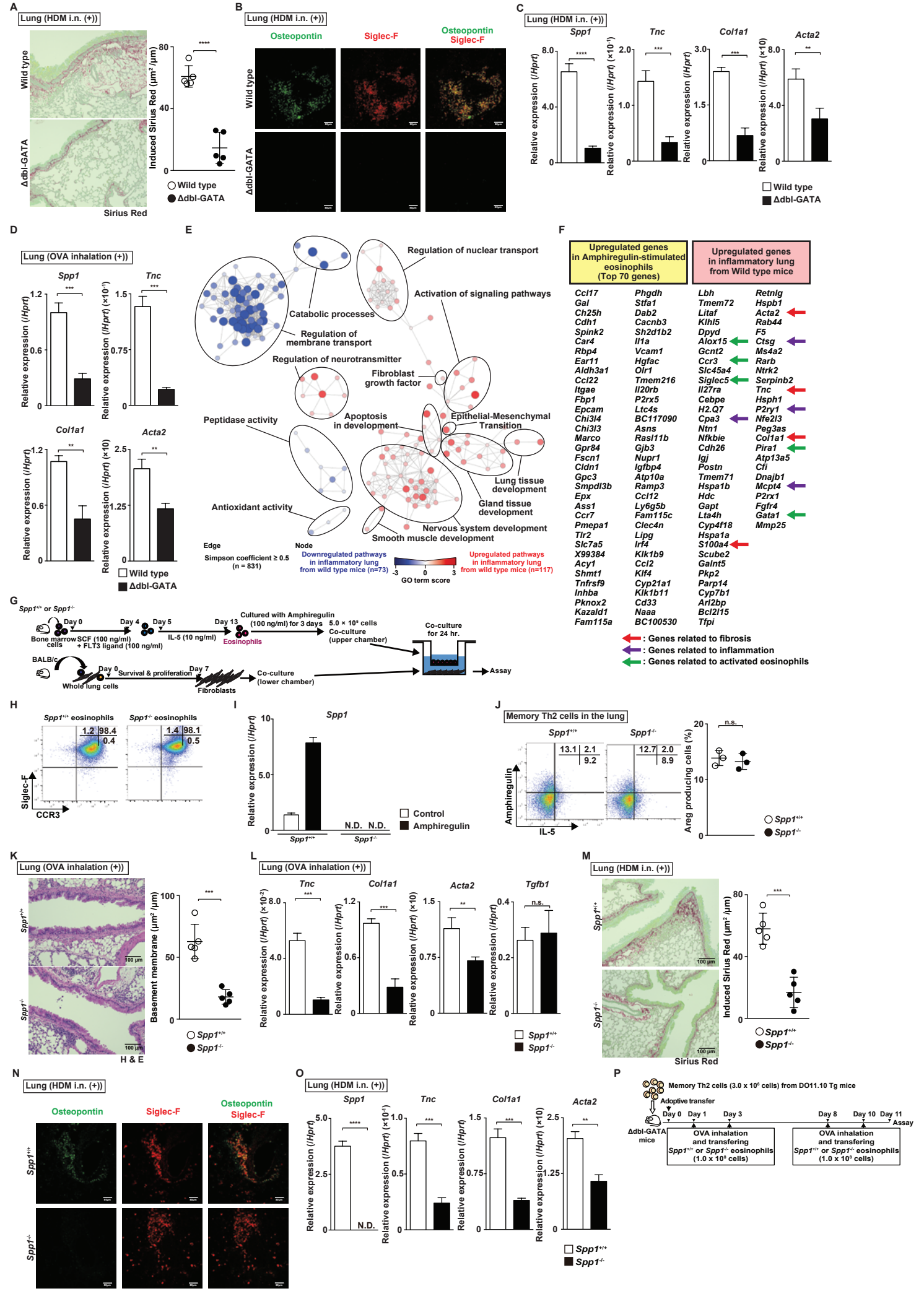

A
Lung (HDM i.n. (+))
Wild type
ΔdblGATA
Sirius Red
Induced Sirius Red (μm² /μm)
Wild type
ΔdblGATA
B
Lung (HDM i.n. (+))
Osteopontin
Siglec-F
Osteopontin Siglec-F
Wild type
ΔdblGATA
C
Lung (HDM i.n. (+))
Spp1
Tnc
Col1a1
Acta2
Relative expression (/Hprt)
Wild type
ΔdblGATA
D
Lung (OVA inhalation (+))
Spp1
Tnc
Col1a1
Acta2
Relative expression (/Hprt)
Wild type
ΔdblGATA
E
Regulation of nuclear transport
Activation of signaling pathways
Catabolic processes
Regulation of membrane transport
Regulation of neurotransmitter
Fibroblast growth factor
Peptidase activity
Apoptosis in development
Epithelial-Mesenchymal Transition
Lung tissue development
Gland tissue development
Antioxidant activity
Nervous system development
Smooth muscle development
Edge
Node
Simpson coefficient ≥ 0.5 (n = 831)
Downregulated pathways in inflammatory lung from wild type mice (n=73)
GO term score
Upregulated pathways in inflammatory lung from wild type mice (n=117)
F
Upregulated genes in Amphiregulin-stimulated eosinophils (Top 70 genes)
Upregulated genes in inflammatory lung from Wild type mice
Ccl17 Gal Ch25h Cdh1 Spink2 Car4 Rbp4 Ear11 Aldh3a1 Ccl22 Itgae Fbp1 Epcam Chi3l4 Chi3l3 Marco Gpr84 Fscn1 Cldn1 Gpc3 Smpdl3b Epx Ass1 Ccr7 Pmepa1 Tlr2 Slc7a5 X99384 Acy1 Shmt1 Tnfrsf9 Inhba Pknox2 Kazald1 Fam115a
Phgdh Stfa1 Dab2 Cacnb3 Sh2d1b2 Il1a Vcam1 Hgfac Olr1 Tmem216 Il20rb P2rx5 Ltc4s BC117090 Asns Rasl11b Gjb3 Nupr1 Igfbp4 Atp10a Ramp3 Ccl12 Ly6g5b Fam115c Clec4n Lipg Irf4 Klk1b9 Ccl2 Klf4 Cyp21a1 Klk1b11 Cd33 Naaa BC100530
Lbh Tmem72 Litaf Klhl5 Dpyd Alox15 Gcnt2 Ccr3 Slc45a4 Siglec5 Il27ra Cebpe H2.Q7 Cpa3 Ntn1 Nfkbie Cdh26 Igj Postn Tmem71 Hspa1b Hdc Gapt Lta4h Cyp4f18 Hspa1a S100a4 Scube2 Galnt5 Pkp2 Parp14 Cyp7b1 Arl2bp Bcl2l15 Tfpi
Retnlg Hspb1 Acta2 Rab44 F5 Ctsg Ms4a2 Rarb Ntrk2 Serpinb2 Tnc Hsph1 P2ry1 Nfe2l3 Peg3as Col1a1 Pira1 Atp13a5 Cfi Dnajb1 Mcpt4 P2rx1 Fgfr4 Gata1 Mmp25
: Genes related to fibrosis
: Genes related to inflammation
: Genes related to activated eosinophils
G
Spp1+/+ or Spp1-/-
Bone marrow cells
Day 0
SCF (100 ng/ml) + FLT3 ligand (100 ng/ml)
Day 4
Day 5
IL-5 (10 ng/ml)
Day 13
Eosinophils
Cultured with Amphiregulin (100 ng/ml) for 3 days
5.0 × 10⁵ cells Co-culture (upper chamber)
Co-culture for 24 hr.
Assay
BALB/c
Whole lung cells
Day 0
Survival & proliferation
Day 7
Fibroblasts
Co-culture (lower chamber)
H
Spp1+/+ eosinophils
Spp1-/- eosinophils
Siglec-F
CCR3
I
Spp1
Relative expression (/Hprt)
N.D.
Control
Amphiregulin
J
Memory Th2 cells in the lung
Spp1+/+
Spp1-/-
Amphiregulin
IL-5
Areg producing cells (%)
n.s.
K
Lung (OVA inhalation (+))
Spp1+/+
Spp1-/-
H & E
Basement membrane (μm² /μm)
L
Lung (OVA inhalation (+))
Tnc
Col1a1
Acta2
Tgfb1
Relative expression (/Hprt)
n.s.
M
Lung (HDM i.n. (+))
Spp1+/+
Spp1-/-
Sirius Red
Induced Sirius Red (μm² /μm)
N
Lung (HDM i.n. (+))
Osteopontin
Siglec-F
Osteopontin Siglec-F
Spp1+/+
Spp1-/-
O
Lung (HDM i.n. (+))
Spp1
Tnc
Col1a1
Acta2
Relative expression (/Hprt)
N.D.
P
Memory Th2 cells (3.0 x 10⁶ cells) from DO11.10 Tg mice
Adoptive transfer
ΔdblGATA mice
Day 0
Day 1
Day 3
Day 8
Day 10
Day 11
Assay
OVA inhalation and transfering Spp1+/+ or Spp1-/- eosinophils (1.0 x 10⁵ cells)
OVA inhalation and transfering Spp1+/+ or Spp1-/- eosinophils (1.0 x 10⁵ cells)

Figure S5. Related to Figure 5. Amphiregulin stimulation induces Osteopontin production via EGFR signaling both *in vitro* and *in vivo*.

(**A**) Wild type mice and Δdbl-GATA mice were exposed to HDM as indicated in Figure **S1A**. Shown is a representative confocal micrograph of lung tissue stained with Sirius Red from a wild type mouse and a Δdbl-GATA mouse (left). Scale bars represent 100 μm. Shown are ratios of areas of randomly selected regions stained with Sirius Red surrounding bronchi versus areas of associated basement membranes (right). More than 3 mice per group were analyzed. (**B**) Shown is a representative confocal micrograph of lungs stained with anti-Osteopontin (green) and Siglec-F (red) from wild type and Δdbl-GATA mice with HDM exposure (Scale bars represent 50 μm). Three independent experiments were performed with similar results. (**C**) Quantitative RT-PCR analysis of the indicated genes in the lungs from wild type mice and Δdbl-GATA mice with HDM exposure (n = 3 mice per group). (**D**) OVA specific memory Th2 cells (3 x 10^6 cells) were transferred i.v. into wild type and Δdbl-GATA mice that were subsequently challenged with OVA. Quantitative RT-PCR analysis of the indicated genes in the lungs of wild type and Δdbl-GATA mice challenged with OVA. (n = 3 mice per group). (**E**) Shown is a network visualization of Gene Ontology enrichment analysis. Node colors indicate GO terms that were significantly upregulated (red) or downregulated (blue) in the lungs of wild type mice challenged with OVA compared to Δdbl-GATA mice challenged with OVA. Node sizes are proportional to enrichment scores for each GO terms. Node connections were determined using overlap of the elemental gene products in the GO terms (Simpson coefficient ≥ 0.5). (**F**) Shown is a list of the top 70 upregulated genes in Amphiregulin-stimulated eosinophils and all upregulated genes in inflamed lungs from wild-type mice. Red arrows indicate genes related to fibrosis, purple arrows indicate genes related to inflammation and green arrows indicate genes related to activated eosinophils. (**G**) Experimental protocol for co-culture of eosinophils and fibroblasts as indicated in STAR Methods. (**H**) Shown are FACS plots of CCR3 and Siglec-F expression on *Spp1*$^{+/+}$ and *Spp1*$^{-/-}$ eosinophils. (**I**) Quantitative RT-PCR analysis of *Spp1* in *Spp1*$^{+/+}$ and *Spp1*$^{-/-}$ eosinophils treated with or without Amphiregulin for 72 hours (n = 3 samples per group). (**J**) *Spp1*$^{+/+}$ and *Spp1*$^{-/-}$ mice were challenged with OVA as indicated in Figure **S1L**. Shown are FACS plots of intracellular Amphiregulin and IL-5 in lung memory CD4$^+$ T cells from *Spp1*$^{+/+}$ and *Spp1*$^{-/-}$ mice (left). Shown is the percentage of Amphiregulin producing memory T cells among total memory T cells of lungs from *Spp1*$^{+/+}$ and *Spp1*$^{-/-}$ mice (right). (**K**) Shown is a representative confocal micrograph of H & E stained lung tissue from a *Spp1*$^{+/+}$ mouse and a *Spp1*$^{-/-}$ mouse (left). Scale bars represent 100 μm. Shown are ratios of areas of basement membranes surrounding bronchi versus length of bronchus epithelium (right). More than 3 mice per group were analyzed. (**L**) Quantitative RT-PCR analysis of the indicated genes in the lungs of *Spp1*$^{+/+}$ and *Spp1*$^{-/-}$ mice challenged with OVA. (n = 3 mice per group). Data are the mean ± SD. $^{**}P < 0.01$, $^{***}P < 0.001$, $^{****}P < 0.0001$; n.s., not significant; by unpaired t test. (**M**) *Spp1*$^{+/+}$ and *Spp1*$^{-/-}$ mice were exposed to HDM as indicated in Figure **S1A**. Shown is a representative confocal micrograph of lung tissue stained with Sirius Red from a *Spp1*$^{+/+}$ and a *Spp1*$^{-/-}$ mouse (left). Scale bars represent 100 μm. Shown are ratios of areas of randomly

selected regions stained with Sirius Red surrounding bronchi versus the areas of associated basement membranes (right). More than 3 mice per group were analyzed. (**N**) Shown is a representative confocal micrograph of the lungs stained with anti-Osteopontin (green) and Siglec-F (red) from *Spp1*$^{+/+}$ and *Spp1*$^{-/-}$ mice with HDM exposure (Scale bars represent 50 μm). Three independent experiments were performed with similar results. (**O**) Quantitative RT-PCR analysis of the indicated genes in the lungs from *Spp1*$^{+/+}$ and *Spp1*$^{-/-}$ mice with HDM exposure (n = 3 mice per group). (**P**) Experimental protocol for a Th2 cell-dependent allergic inflammation mouse model employing adoptive transfer of memory Th2 cells followed by the transfer of eosinophils from *Spp1*$^{+/+}$ or *Spp1*$^{-/-}$ mice as indicated in STAR Methods. Data are the mean ± SD. $^{**}P < 0.01$, $^{***}P < 0.001$; by unpaired t test.

Figure S6

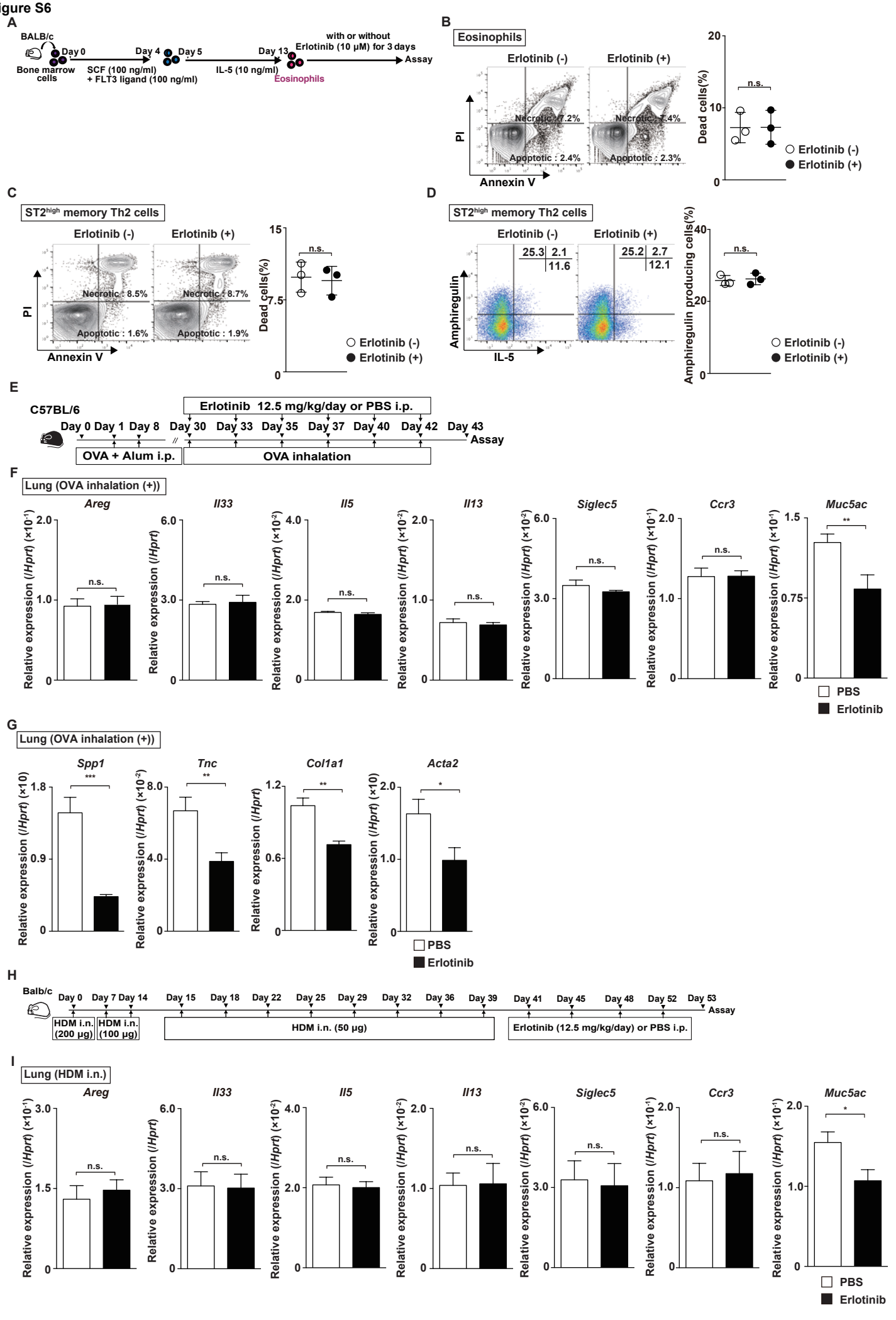

A
BALB/c
Day 0
Bone marrow cells
Day 4
SCF (100 ng/ml) + FLT3 ligand (100 ng/ml)
Day 5
Day 13
IL-5 (10 ng/ml)
Eosinophils
with or without Erlotinib (10 μM) for 3 days
Assay
B
Eosinophils
Erlotinib (-)
Erlotinib (+)
Necrotic : 7.2%
Necrotic : 7.4%
Apoptotic : 2.4%
Apoptotic : 2.3%
PI
Annexin V
Dead cells(%)
n.s.
Erlotinib (-)
Erlotinib (+)
C
ST2high memory Th2 cells
Erlotinib (-)
Erlotinib (+)
Necrotic : 8.5%
Necrotic : 8.7%
Apoptotic : 1.6%
Apoptotic : 1.9%
PI
Annexin V
Dead cells(%)
n.s.
Erlotinib (-)
Erlotinib (+)
D
ST2high memory Th2 cells
Erlotinib (-)
Erlotinib (+)
25.3
2.1
11.6
25.2
2.7
12.1
Amphiregulin
IL-5
Amphiregulin producing cells(%)
n.s.
Erlotinib (-)
Erlotinib (+)
E
C57BL/6
Erlotinib 12.5 mg/kg/day or PBS i.p.
Day 0 Day 1 Day 8 Day 30 Day 33 Day 35 Day 37 Day 40 Day 42 Day 43
Assay
OVA + Alum i.p.
OVA inhalation
F
Lung (OVA inhalation (+))
Areg
Il33
Il5
Il13
Siglec5
Ccr3
Muc5ac
Relative expression (/Hprt)
n.s.
**
PBS
Erlotinib
G
Lung (OVA inhalation (+))
Spp1
Tnc
Col1a1
Acta2
Relative expression (/Hprt)
***
**
*
PBS
Erlotinib
H
Balb/c
Day 0 Day 7 Day 14 Day 15 Day 18 Day 22 Day 25 Day 29 Day 32 Day 36 Day 39 Day 41 Day 45 Day 48 Day 52 Day 53
Assay
HDM i.n. (200 μg)
HDM i.n. (100 μg)
HDM i.n. (50 μg)
Erlotinib (12.5 mg/kg/day) or PBS i.p.
I
Lung (HDM i.n.)
Areg
Il33
Il5
Il13
Siglec5
Ccr3
Muc5ac
Relative expression (/Hprt)
n.s.
*
PBS
Erlotinib

Figure S6. Related to Figure 6. Inhibition of EGFR signaling ameliorates fibrotic responses *in vivo*. (**A**) Experimental protocol for the induction of bone marrow-derived eosinophils. The detailed protocol is in STAR Methods. (**B**) Shown are FACS plots of PI and Annexin V expression in eosinophils cultured with or without Erlotinib for 72 hours (left). Shown are the percentage of dead cells among total cells (right). (**C**) Shown are FACS plots of PI and Annexin V expression in $ST2^{hi}$ memory Th2 cells cultured with or without Erlotinib for 72 hours (left). Shown is percentage of dead cells among total cells (right). (**D**) Shown are FACS plots of intracellular Amphiregulin and IL-5 in $ST2^{hi}$ memory Th2 cells cultured with or without Erlotinib for 72 hours (left). Shown is the percentage of Amphiregulin-producing $ST2^{hi}$ memory Th2 cells among total $ST2^{hi}$ memory Th2 cells. (**E**) Experimental protocol for simultaneous Erlotinib treatment in an allergic airway inflammation mouse model using intraperitoneal (i.p.) OVA and aluminum hydroxide gel (Alum). C57BL/6 mice were sensitized by OVA and Alum i.p on days 1 and 8. Subsequently, mice were challenged with OVA inhalation and simultaneously treated with Erlotinib (12.5 mg/kg) or PBS i.p. on days 30, 33, 35, 37, 40 and 42. (**F**, **G**) Shown are quantitative RT-PCR analyses of the indicated genes in the lungs of OVA challenged mice simultaneously treated with PBS or Erlotinib (n = 3 mice per group). (**H**) Experimental protocol for subsequent Erlotinib treatment in an allergic inflammation mouse model with HDM exposure. BALB/c mice were exposed with HDM as indicated in STAR Methods. Subsequently, these mice were treated with Erlotinib (12.5 mg/kg) or PBS i.p. on days 41, 45, 48 and 52. (**I**) Shown are quantitative RT-PCR analyses of the indicated genes in the lungs of OVA challenged mice subsequently treated with PBS or Erlotinib (n = 3 mice per group). Data are the mean ± SD. $*P < 0.05$, $**P < 0.01$, $***P < 0.001$; n.s., not significant; by unpaired t test.

Figure S7

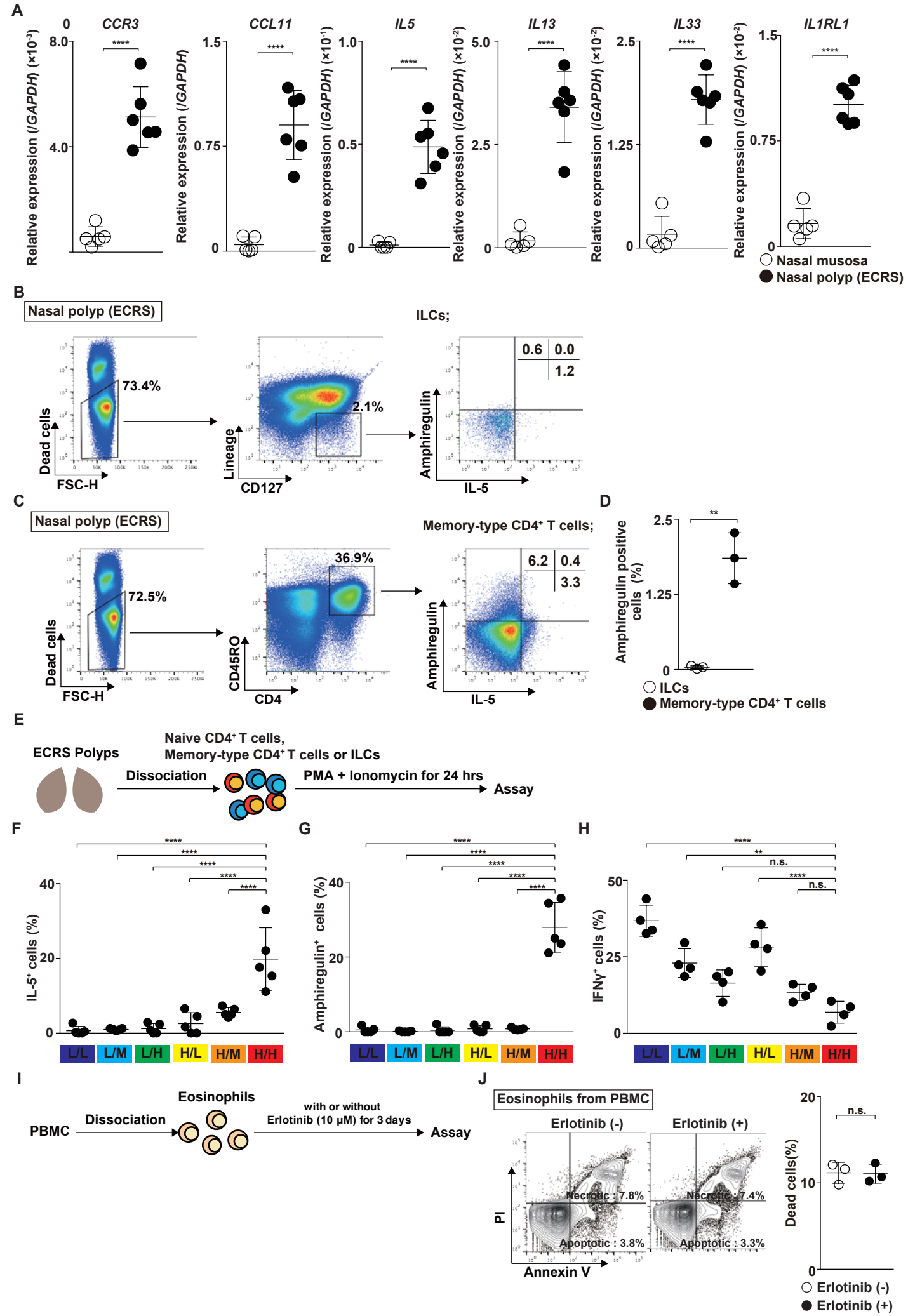

A
CCR3
CCL11
IL5
IL13
IL33
IL1RL1
Relative expression (/GAPDH)
Nasal musosa
Nasal polyp (ECRS)
B
Nasal polyp (ECRS)
ILCs;
73.4%
2.1%
0.6
0.0
1.2
Dead cells
FSC-H
Lineage
CD127
Amphiregulin
IL-5
C
Nasal polyp (ECRS)
Memory-type CD4⁺ T cells;
72.5%
36.9%
6.2
0.4
3.3
CD45RO
CD4
D
Amphiregulin positive cells (%)
ILCs
Memory-type CD4⁺ T cells
E
ECRS Polyps
Naive CD4⁺ T cells,
Memory-type CD4⁺ T cells or ILCs
Dissociation
PMA + Ionomycin for 24 hrs
Assay
F
IL-5⁺ cells (%)
G
Amphiregulin⁺ cells (%)
H
IFNγ⁺ cells (%)
n.s.
L/L
L/M
L/H
H/L
H/M
H/H
I
PBMC
Dissociation
Eosinophils
with or without
Erlotinib (10 μM) for 3 days
Assay
J
Eosinophils from PBMC
Erlotinib (-)
Erlotinib (+)
Necrotic : 7.8%
Necrotic : 7.4%
Apoptotic : 3.8%
Apoptotic : 3.3%
PI
Annexin V
Dead cells(%)

Figure S7. Related to Figure 7. Large numbers of Amphiregulin-producing memory-type CD4$^+$ T cells in the nasal polyps of ECRS patients.

(**A**) Shown are quantitative RT-PCR analyses of the indicated genes in the nasal mucosa of healthy control subjects (Control; n = 5) and in the polyps of patients with ECRS (ECRS; n = 6). (**B**) Shown are representative FACS plots of intracellular Amphiregulin and IL-5 expression by lineage$^-$ CD127$^+$ cells from a polyp of a patient with ECRS. (**C**) Shown are representative FACS plots of intracellular Amphiregulin and IL-5 in CD4$^+$ CD45RO$^+$ cells from a polyp of a patient with ECRS. (**D**) Shown is a comparison of the absolute numbers of ILCs and memory-type CD4$^+$ T cells that produce Amphiregulin. Three independent donors were analyzed. (**E**) Experimental protocol for the collection of the indicated cells from ECRS polyps followed by stimulation with PMA and Ionomycin for 24 hours. (**F**, **G**, **H**) Shown is pooled data from five (Amphiregulin and IL-5) or four (IFNγ) separate experiments depicting IL-5-producing cells (**F**) , Amphiregulin-producing cells (**G**) and IFNγ-producing cells (**H**) gated into 6 subpopulations by the expression of CD161 and CRTH2, as described in Figure 7E. (**I**) Experimental protocol for the collection of eosinophils from PBMC followed by stimulation with or without Erlotinib. (**J**) Shown are FACS plots of PI and Annexin V expression on eosinophils from PBMC cultured with or without Erlotinib for 72 hours as indicated in STAR Methods (left). Shown is the percentage of dead cells among total cells (right). Data are the mean ± SD. $^{**}P < 0.01$, $^{****}P < 0.0001$; n.s., not significant; by unpaired t test or one-way analysis of variance (ANOVA).